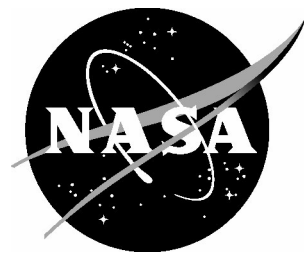NASA/TM-2012-4399: ;

Analysis of the Radiated Field in an Electromagnetic Reverberation Chamber as an Upset-Inducing Stimulus for Digital Systems

Wilfredo Torres-Pomales
Langley Research Center, Hampton, Virginia

December 2012

NASA STI Program . . . in Profile

Since its founding, NASA has been dedicated to the advancement of aeronautics and space science. The NASA scientific and technical information (STI) program plays a key part in helping NASA maintain this important role.

The NASA STI program operates under the auspices of the Agency Chief Information Officer. It collects, organizes, provides for archiving, and disseminates NASA's STI. The NASA STI program provides access to the NASA Aeronautics and Space Database and its public interface, the NASA Technical Report Server, thus providing one of the largest collections of aeronautical and space science STI in the world. Results are published in both non-NASA channels and by NASA in the NASA STI Report Series, which includes the following report types:

- TECHNICAL PUBLICATION. Reports of completed research or a major significant phase of research that present the results of NASA Programs and include extensive data or theoretical analysis. Includes compilations of significant scientific and technical data and information deemed to be of continuing reference value. NASA counterpart of peer-reviewed formal professional papers, but having less stringent limitations on manuscript length and extent of graphic presentations.

- TECHNICAL MEMORANDUM. Scientific and technical findings that are preliminary or of specialized interest, e.g., quick release reports, working papers, and bibliographies that contain minimal annotation. Does not contain extensive analysis.

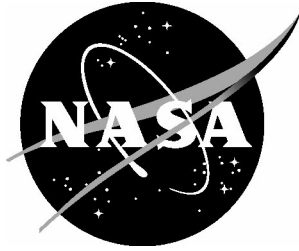- CONTRACTOR REPORT. Scientific and technical findings by NASA-sponsored contractors and grantees.

- CONFERENCE PUBLICATION. Collected papers from scientific and technical conferences, symposia, seminars, or other meetings sponsored or co-sponsored by NASA.

- SPECIAL PUBLICATION. Scientific, technical, or historical information from NASA programs, projects, and missions, often concerned with subjects having substantial public interest.

- TECHNICAL TRANSLATION. English-language translations of foreign scientific and technical material pertinent to NASA's mission.

Specialized services also include organizing and publishing research results, distributing specialized research announcements and feeds, providing information desk and personal search support, and enabling data exchange services.

For more information about the NASA STI program, see the following:

- Access the NASA STI program home page at *http://www.sti.nasa.gov*

- E-mail your question to help@sti.nasa.gov

- Fax your question to the NASA STI Information Desk at 443-757-5803

- Phone the NASA STI Information Desk at 443-757-5802

- Write to:
  STI Information Desk
  NASA Center for AeroSpace Information
  7115 Standard Drive
  Hanover, MD 21076-1320

Analysis of the Radiated Field in an Electromagnetic Reverberation Chamber as an Upset-Inducing Stimulus for Digital Systems

Wilfredo Torres-Pomales
Langley Research Center, Hampton, Virginia

Acknowledgement

Abstract

Preliminary data analysis for a physical fault injection experiment of a digital system exposed to High Intensity Radiated Fields (HIRF) in an electromagnetic reverberation chamber suggests a direct causal relation between the time profile of the field strength amplitude in the chamber and the severity of observed effects at the outputs of the radiated system. This report presents an analysis of the field strength modulation induced by the movement of the field stirrers in the reverberation chamber. The analysis is framed as a characterization of the discrete features of the field strength waveform responsible for the faults experienced by a radiated digital system. The results presented here will serve as a basis to refine the approach for a detailed analysis of HIRF-induced upsets observed during the radiation experiment. This work offers a novel perspective into the use of an electromagnetic reverberation chamber to generate upset-inducing stimili for the study of fault effects in digital systems.

Table of Contents

Abbreviations

AC	Alternating Current
ASIC	Application Specific Integrated Circuit
ASCII	American Standard Code for Information Interchange
BIU	Bus Interface Unit
CCP	Controller Coordination Protocol
COTS	Commercial Off-The-Shelf
CPU	Central Processing Unit
CW	Continuous Wave
DC	Direct Current
DUT	Device Under Test
EM	Electromagnetic
EMI	Electromagnetic Interference
Et	Overstroke Reference Level
FHSTC	Fine HIRF Susceptibility Threshold Characterization
FPGA	Field Programmable Gate Array
FSM	Finite State Machine
GPIB	General Purpose Instrumentation Bus
HC	Hardware Configuration
HEC	HIRF Effects Characterization
HFA	Hub Fault Analyzer
HIRF	High Intensity Radiated Field
HSTC	HIRF Susceptibility Threshold Characterization
IMA	Integrated Modular Architecture
IVHM	Integrated Vehicle Health Management
LUF	Lowest Usable Frequency
Mbps	Mega-bits per second
MHz	Megahertz
ms	Millisecond
NFA	Node Fault Analyzer
NIST	National Institute of Standards and Technology
OS	Overstroke
PE	Processing Element
RC	Reverberation Chamber
RF	Radio Frequency
RMS	Root Mean Square
RMU	Redundancy Management Unit
ROBUS	Robust Bus
RPP	ROBUS Protocol Processor
RSPP	Reconfigurable SPIDER Prototyping Platform
RTCA	Radio Technical Commission for Aeronautics
SD	Standard Deviation
SHM	System Health Monitor
SIM	Stirrer Induced Modulation
SPIDER	Scalable Processor-Independent Design for Extended Reliability
SUT	System Under Test
TCS	Test Control System
TDMA	Time Division Multiple Access
VHDL	VHSIC Hardware Description Language
VHSIC	Very High Speed Integrated Circuit
V/m	Volts per meter

1. Introduction

A physical fault injection experiment was conducted in which a prototype implementation of an onboard data network for safety-critical, real-time Integrated Modular Architectures (IMA) was exposed to a High Intensity Radiated Field (HIRF) environment in a mode-stirred electromagnetic reverberation chamber. The purpose of the experiment was to gain insight into the response of the system to a wide range of internal faults, including conditions that exceed the design safety margins [1, 2, 3]. There is special interest in examining the response to functional **upsets**, which are error modes that involve no permanent component damage, can simultaneously occur in multiple channels of a redundant distributed system and can cause unrecoverable distributed state error conditions [4, 5, 6].

The fault injection experiment was divided in two parts. The HIRF Susceptibility Threshold Characterization (HSTC) experiment was intended to identify and examine factors that determine the measured minimum HIRF field strength level at which a particular electronic System Under Test (SUT) begins to experience HIRF-induced interference to its internal operation (i.e., faults). The results and lessons learned in the execution of the HSTC experiment are described in report [3]. The HIRF Effects Characterization (HEC) experiment was intended to assess the SUT's response to functional system upsets. The analysis of the HEC data is ongoing.

The experiment was conducted at the NASA Langley Research Center's HIRF Laboratory using Reverberation Chamber A of the facility to generate the HIRF environment [1, 7]. Similar to a large microwave oven, a reverberation chamber operates as a cavity resonator in which the electromagnetic field generated by a transmitting antenna reflects off the metal walls forming complex three-dimensional electromagnetic field patterns with low energy loss. Rotating mechanical stirrers in the chamber with electrically conductive paddle surfaces spread the spatial energy distribution by changing the field structures, effectively producing a statistically uniform and isotropic electromagnetic environment. The diagram in Figure 1 shows the layout inside the chamber. The photos in Figures 2 and 3 show the inside of the chamber with the positions where SUTs could be placed on non-conductive foam blocks or tables.

When the HSTC experiment was initially designed, we thought that the amplitude profile of the field experienced by an SUT in the chamber would be determined mainly by the signal driving the transmitting antenna. For example, it was expected that a constant amplitude input signal would result in constant amplitude radiation. However, during the experiment it was observed that the field strength amplitude was actually time varying even when the input to the chamber was an unmodulated constant wave (CW) signal. Figure 4 shows an oscilloscope trace of the field strength amplitude during a radiation burst measured at the output of a field-monitoring antenna in the chamber. The duration of the burst was determined by the input signal, which was a pulse of CW with duration much larger than the chamber time constant [1, 7, 8]. This means that the time varying field strength amplitude of the radiation burst is not due to transient effects in the chamber when the input pulse is applied because the duration of the pulse is much larger than the time required for the field strength to reach steady state. Instead, the observed time varying field strength amplitude is presumed to be due to changes in the boundary conditions in the chamber (i.e., the spatial positioning of electromagnetically reflective surfaces) as the stirrers rotate. In Figure 4 it can be seen that this Stirrer-Induced Modulation (SIM) has a strong influence on the field strength amplitude inside in the chamber. Based on this, we believe that the SIM is also a critical factor in the characteristics of physical faults generated by the HIRF environment and, consequently, on the observed system responses in the HEC experiment. This is the motivation for the stirrer induced modulation test and analysis presented in this report.
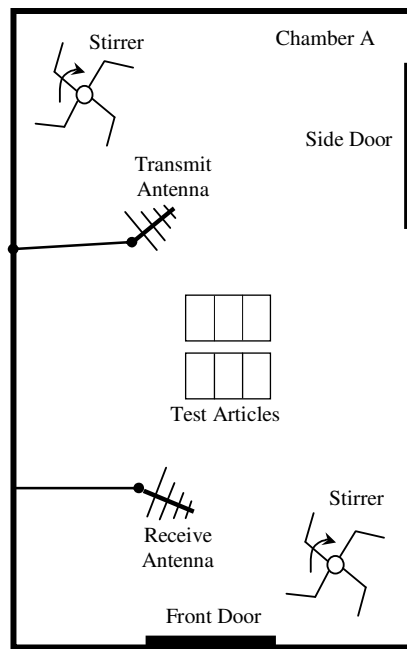
Figure 1: Basic layout of reverberation chamber A for a HIRF experiment

Figure 2: Photo of Reverberation Chamber A taken from the back of the chamber (Also shows SUT test articles placed on foam blocks and tables.)

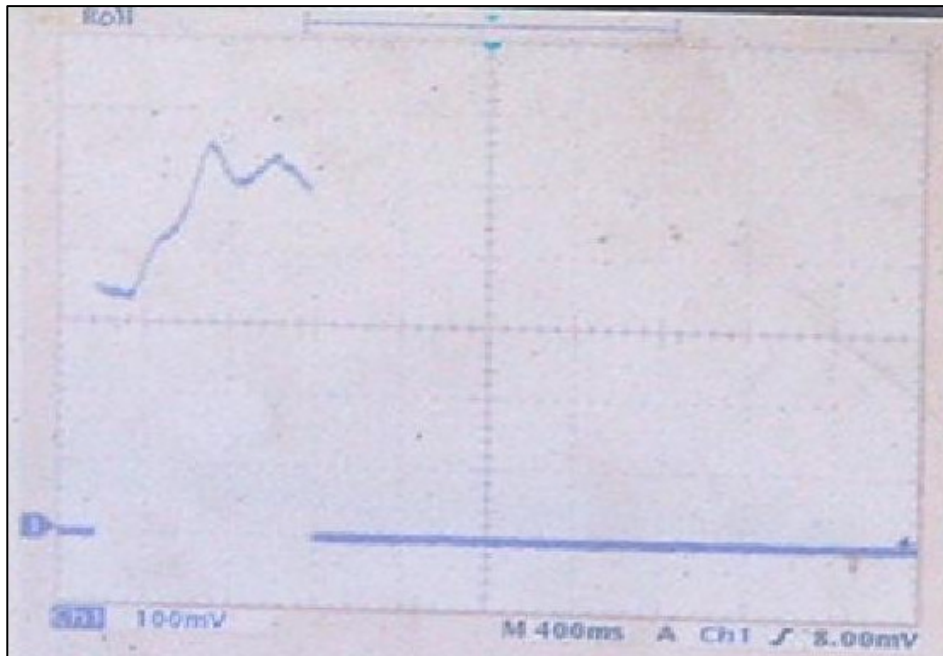Figure 3: Photo of Reverberation Chamber A taken from the front of the chamber

Figure 4: Oscilloscope trace of the field strength amplitude during a radiation pulse measured at the output of a field-monitoring antenna in the reverberation chamber

The purpose of the analysis presented here is to understand the relation between the radiated electromagnetic field in the reverberation chamber and the faults experienced by SUTs. We expect the results to be a critical component in the analysis of the HEC experiment data. We intend to leverage the relation described in Section 3 between the field strength characteristics and the error bursts at the output of a radiated digital device. That relation will be the basis for a high-level functional (i.e., black box) stimulus-response analysis to assess the severity of the effects caused by the HIRF environment on the radiated digital devices and to rank the devices based on the relative resilience to the environment. This will be followed by detailed analyses of upset events to identify the low-level physical components directly affected by the HIRF environment and the error propagation paths from the faulty components to the outputs of the radiated devices and on to the outputs of the prototype onboard data network. This will then be used to identify error containment and recovery weaknesses in the network and propose ways to strengthen the design. That work is ongoing and will be the presented in future reports [11].

The content of the report is as follows. The next section describes the test performed in Chamber A of the HIRF Lab to gather SIM data suitable for a meaningful characterization. This is followed by a description of a useful insight about the error generation process in the HIRF environment learned during preliminary analysis of the HEC data. This insight is applied in the definition of the approach to analyze the stirrer-induced modulation. The data analysis results are presented after that. The report concludes with final remarks about what has been accomplished and describes how results presented here will be used in the analysis of the HEC experiment data. The appendices present a subset of the SIM waveforms measured during the test, as well as additional plots of SIM features not included in the main body of the report.

2. Stirrer-Induced Modulation Test

A test was carried out using Chamber A of the HIRF Lab to gather data suitable for a characterization of the SIM waveforms in the chamber. Figure 5 illustrates the test setup. A computer, labeled Test Controller in Figure 5, was programmed to control the chamber using a GPIB bus to interact with the instrumentation. A signal generator drove a power amplifier which produced the input signal to the transmit antenna in the chamber. Only CW signals were used in this test to provide a constant input power while the stirrers were rotating. The calibration procedure described in report [1], Section 4, was used to determine the input power to the chamber. The stirrers were driven by motors set to rotate at 5.0 seconds per revolution. The field in the chamber was measured with a receive antenna connected to a spectrum analyzer. The collected data consisted of field strength measurement traces, each composed of 800 sample points uniformly spaced over a time interval of 5.05 seconds to ensure full coverage of a stirrer revolution. At each test frequency, 11 field strength traces were collected with a period of approximately 30 seconds timed by the Test Controller. The variable "**revolution**" is used to refer to the field-strength traces and the relative time at the beginning of a trace identifies individual revolutions: 0 sec, 30 sec, etc. Table 1 lists the 14 test frequencies selected for this test. These frequencies were a subset of the ones used in the HSTC experiment and included only those for which HIRF susceptibility was observed at no higher than 300 V/m calibrated field strength [1, 3]. The rotational angular offset of the stirrers, illustrated in Figure 6, was changed in 45-degree increments from 0 to 315 degrees for a total of 8 test values. Overall, 1232 traces were collected (= 8 angular offsets x 14 test frequencies x 11 revolutions). Figure 7 shows a field strength trace at 110.07 MHz with a 45-degree stirrer angular offset.

4

Table 1: Test frequencies for the Stirrer-Induced Modulation Test

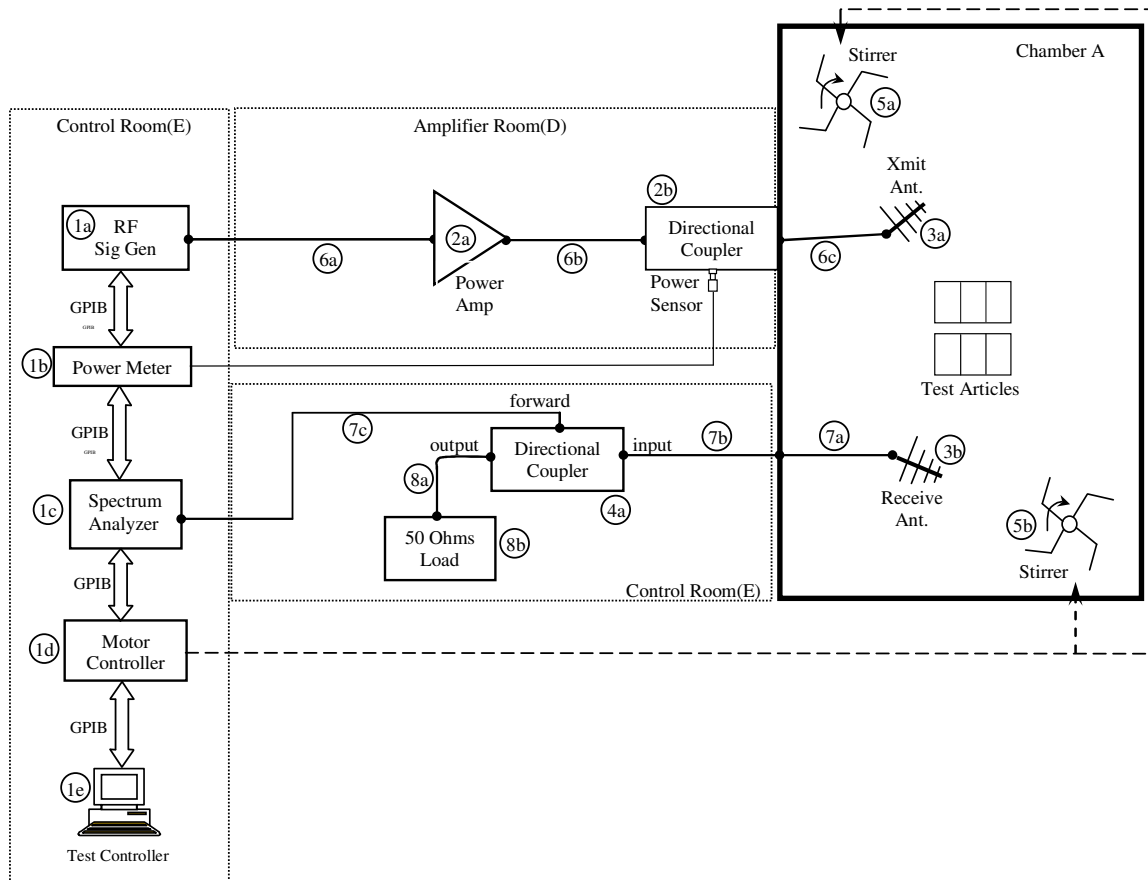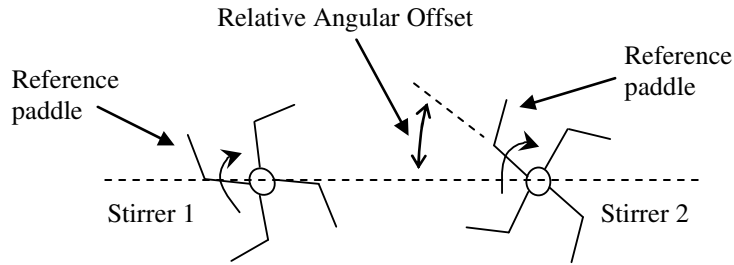| Test Frequency (MHz)	Test Frequency (MHz)
100.00	195.73
110.07	316.23
121.15	383.12
133.35	421.70
146.78	510.90
161.56	562.34
177.83	908.52

Figure 5: Setup for stirrer induced modulation test using Chamber A

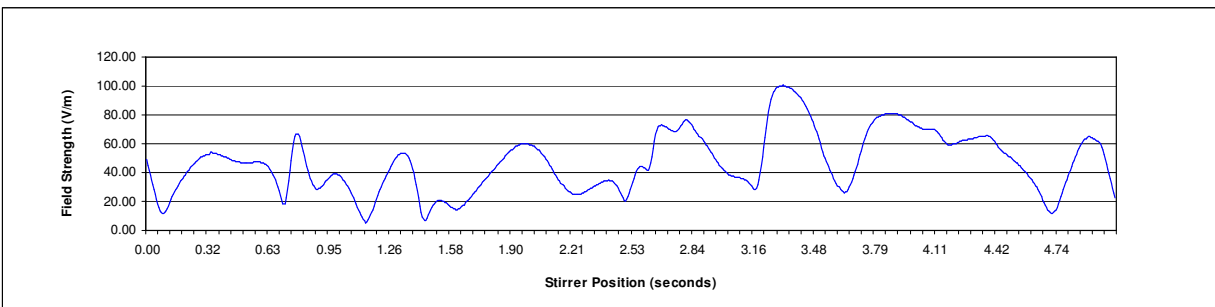Figure 6: Illustration of the relative rotational angular offset for field stirrers rotating at the same speed

Figure 7: Sample field strength trace at 110.07 MHz and 45-degree stirrer angular offset

3. Insight into the Error Generation Mechanism in a HIRF Environment

In the HEC experiment, the SUTs were exposed to a series of 5-second radiation bursts at nominal calibrated peak field strengths of 0, 10 and 20 V/m above the susceptibility threshold of the SUT at each test frequency. A radiation burst is called a **strike**, a series of strikes is called a **round**, and the field strength above the susceptibility threshold of an SUT is called the **over-strength** of the radiation. The field stirrers were set to rotate at a rate of 5 seconds per revolution such that for each strike an SUT was exposed to the time varying field strength pattern induced by the stirrers in one full revolution.

The plots in Figures 8 to 10 were generated during a preliminary analysis of the response of an SUT in the HEC experiment. These plots show the output error rate of the SUT (i.e., number of output errors per time unit) during radiation strikes with nominal over-strengths of 0, 10, and 20 V/m. Each error rate surge delimited by error-free intervals is called an **error burst**. Notice that the error bursts increase in amplitude and duration as the over-strength increases, but their relative positions in time remain constant. In addition, a higher over-strength generates more error bursts. Another interesting feature seen on the three largest error bursts in Figure 10 is the saturation in the error rate, which indicates that the SUT was completely overwhelmed by the HIRF environment.
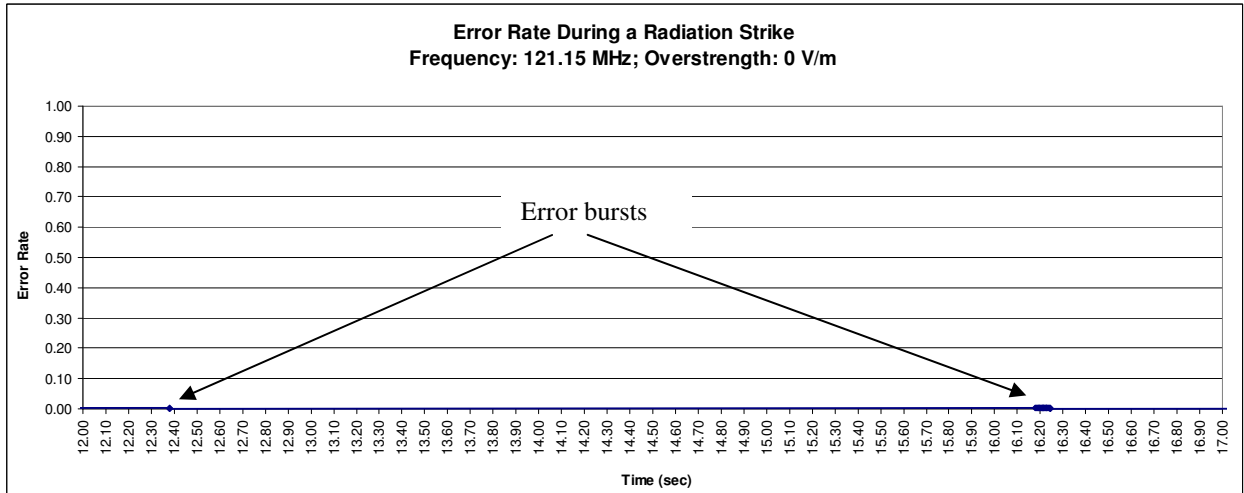
6

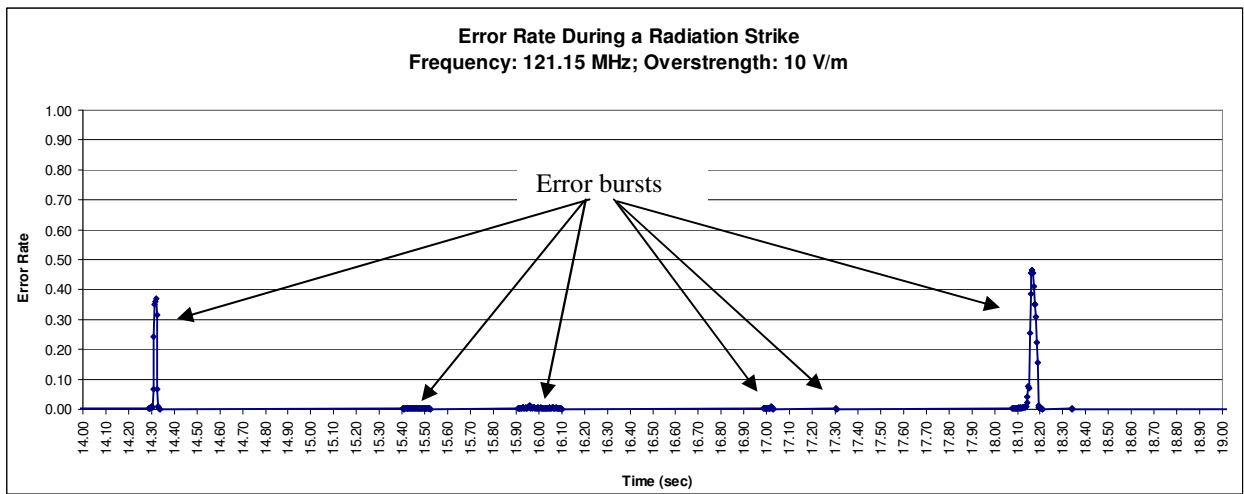Figure 8: Output error rate of an SUT at 0 V/m nominal over-strength

Figure 9: Output error rate of an SUT at 10 V/m nominal over-strength
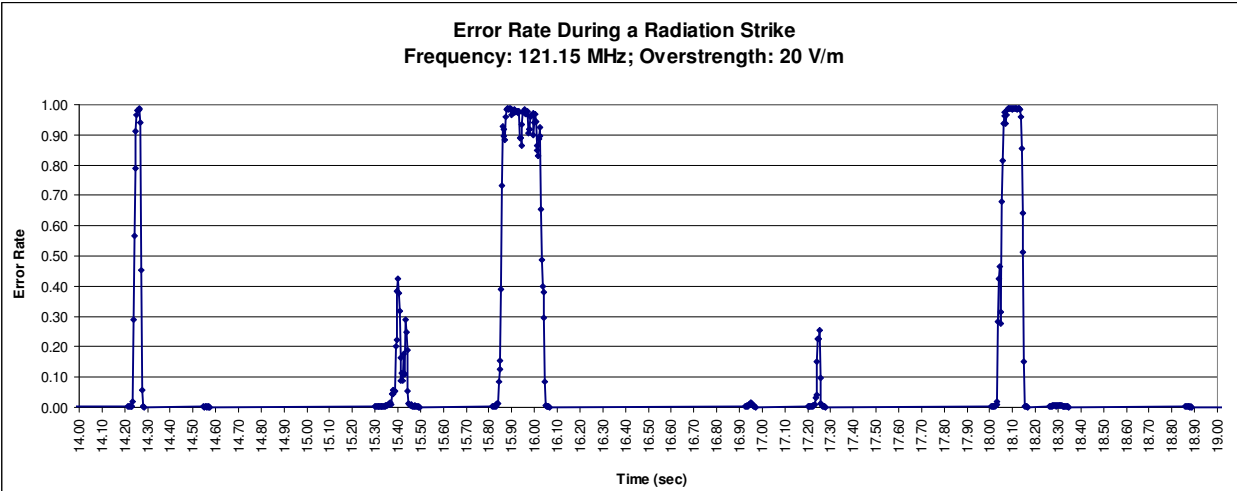
Figure 10: Output error rate of an SUT at 20 V/m nominal over-strength

Now consider the field strength trace shown in Figure 11, which was generated with a constant-amplitude CW input signal to the reverberation chamber. (Note that the trace in Figure 11 was taken with no SUTs in the chamber, and in particular, the field strength measured in Figure 11 was not the field strength at the time the error-rate data in Figure 8 to 10 was taken.) The amplitude of the trace in Figure 11 has been normalized as we are interested in the shape of the waveform rather than its actual amplitude. A higher power CW input signal should simply cause an increase in the amplitude of the waveform, but the shape of the waveform should remain unchanged. The HIRF susceptibility threshold of an SUT at a particular test frequency is the minimum field strength at which the HIRF environment interferes with the operation of the SUT. In general, it is expected that as long as the field strength experienced by an SUT is greater than the susceptibility threshold, the operation of the SUT will be impaired. Therefore, for example, if an SUT were exposed to a field strength with the profile in Figure 11 and the susceptibility threshold of the SUT were at the level indicated by the red line, we would expect the SUT to malfunction at least for the duration of each of the two field strength excursions above the threshold. These excursions of the field strength above the susceptibility threshold are called **overstrokes**. Figures 12 to 14 show the overstrokes for the waveform in Figure 11 with susceptibility threshold levels of 0.85, 0.75, and 0.65, respectively. A reduction of the susceptibility threshold level (also called the overstroke **reference level**) on an amplitude-normalized trace corresponds to an increase in the peak field strength in the non-normalized waveform. Notice that the amplitude and duration of the overstrokes, as well as the number of overstrokes, all increase as the reference level decreases (i.e., as the field strength increases). Also, notice that the relative position of the overstrokes is unchanged as the reference level decreases.

Comparing Figures 8 to 10 with Figures 12 to 14, we notice similar trends for error-rate bursts and overstrokes as the over-strength increases: the amplitude and duration of the bursts and overstrokes increase, and the number of bursts and overstrokes also increase. Based on this, we conjecture that error bursts are caused by overstrokes and that the amplitude of an error-rate burst is directly related to the amplitude of the overstroke experienced by the SUT.

This insight into the error generation process in the HIRF environment will be leveraged in the definition of the approach to analyze the stirrer-induced modulation traces.
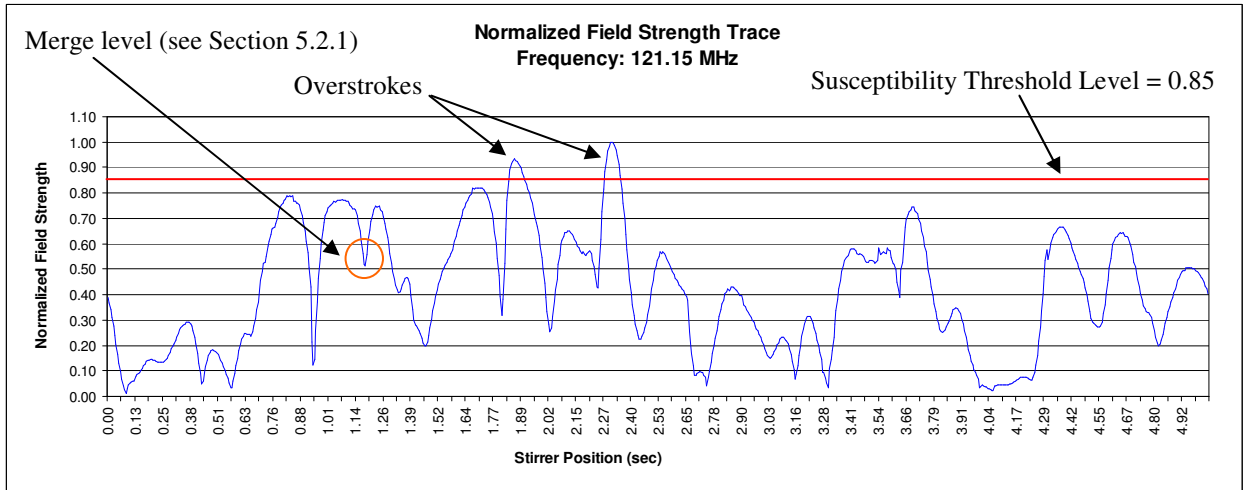
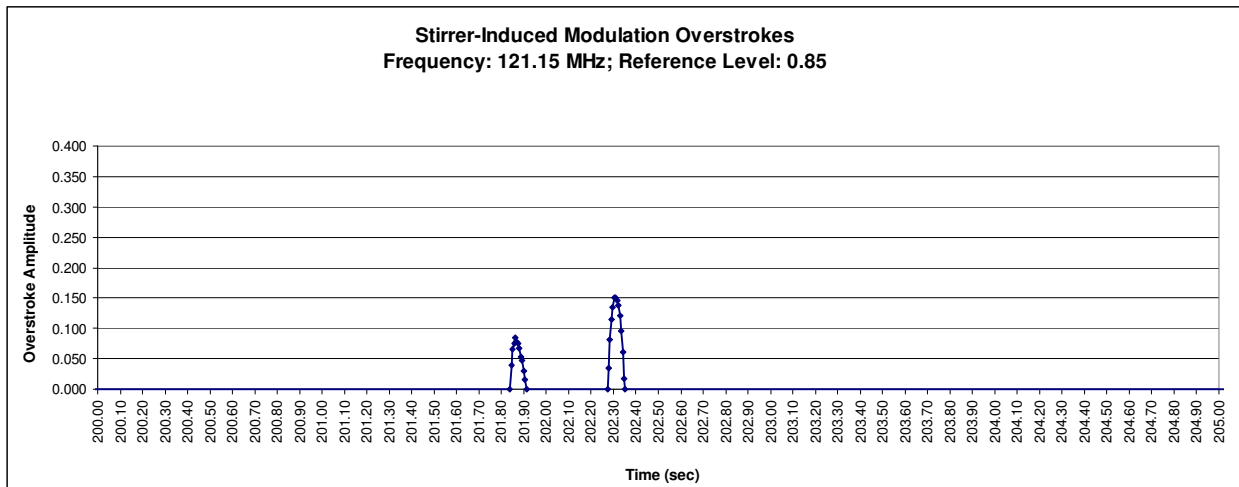Figure 11: Amplitude-normalized field strength trace
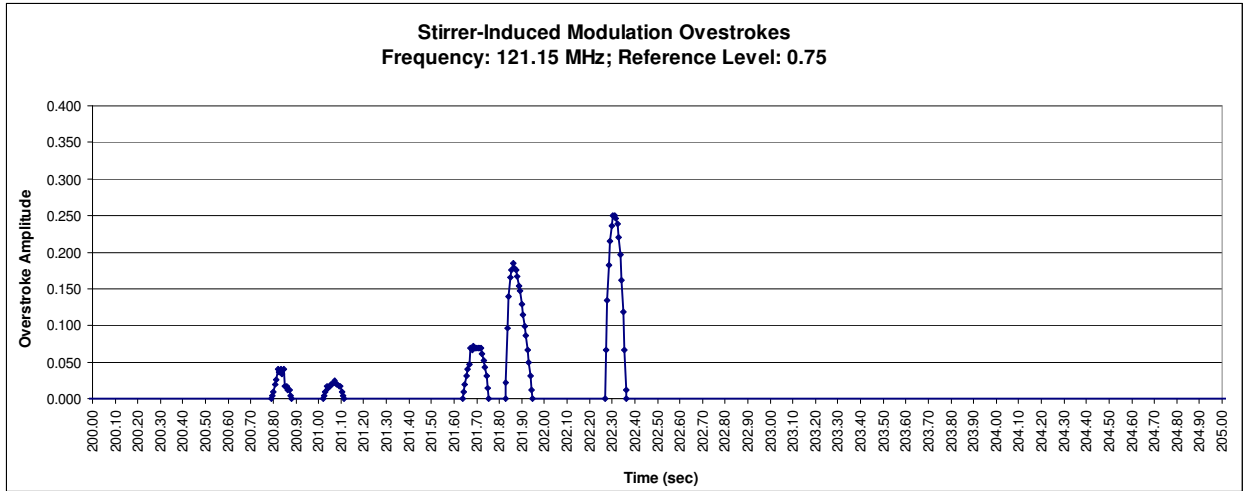

Figure 12: SIM overstrokes at reference level 0.85

Figure 13: SIM overstrokes at reference level 0.75
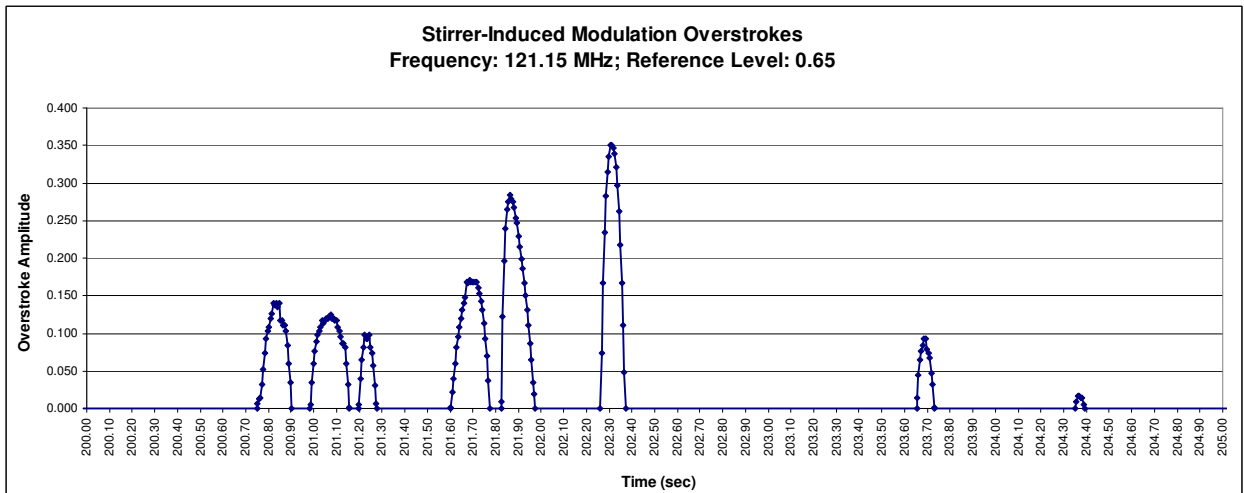

Figure 14: SIM overstrokes at reference level 0.65

4. Approach to the Analysis of Stirrer-Induced Modulation

The purpose of the SIM data analysis is not to describe this electromagnetic phenomenon per se. The SIM characterization is valuable only to the extent that it enables a meaningful analysis of observed HIRF effects in the HEC experiment. Given our insight into how the HIRF environment causes error bursts in the SUTs, the SIM characterization should be viewed as an upset stimulus characterization. The existing detailed knowledge of the internal operation of the SUTs [2, 9, 10] should make it possible to identify causal relations between internal faults and observed responses at the interface. The SIM characterization will enable the study of complete sequences of events in the HEC experiment beginning with the applied external stimulus of HIRF overstrokes that cause faults in an SUT, which then propagate internally through the SUT until reaching the external interface and produce the observed responses.

The first part of the SIM characterization consists of a qualitative examination of SIM waveform features relative to the test controlled variables of stirrer revolution, angular offset, and test carrier frequency. Here we are simply trying to gain a high-level understanding of the effects of the controlled variables on the shape of the SIM waveforms.

The second part of the SIM characterization is a quantitative analysis of SIM overstrokes with respect to the stirrer revolution, stirrer angular offset, test frequency and overstroke reference level. For simplicity, only two basic size features of an overstroke are measured, peak amplitude (**p**) and duration (**d**), as these are related to the error rate and duration of faults in SUTs. A more detailed overstroke model may be developed in future work if needed for a proper analysis of observed HEC responses. We are also interested in the relation between peak and duration, for which we define two composite measures: peak multiplied by duration (**p•d**) and peak divided by duration (**p/d**). For sets of overstrokes defined in terms of particular ranges of the controlled test variables, we use scatter plots and averages (i.e., mean, standard deviation and root-mean-squared) to study the spread and trends in distributions. We also analyze the variability of these set metrics across the range of stirrer angular offsets in order to estimate a bound for the difference of stimulus applied to different SUTs in the HEC experiment, where the angular offset was neither specified in the plan nor controlled during the experiment.

In addition, we study overstroke sets with reference level profiles based on the measured susceptibility thresholds from the HSTC experiment. These overstroke sets represent the effective HIRF environment as experienced by SUTs in the HEC experiment.

5. Results and Analysis

The following three subsections present the SIM characterization results.

5.1. Stirrer-Induced Modulation Waveforms

We first examine the SIM waveforms relative to the controlled test variables of stirrer revolution, stirrer rotational angular offset and carrier frequency.

5.1.1. Periodicity

Figure 15 shows field strength traces taken 150 seconds apart for a carrier frequency of 110.07 MHz and stirrer angular offset of 0 degrees. The waveforms follow no discernible patterns and appear to be completely different. They are continuous but have sharp transitions and large amplitude ranges of over 100 V/m. Recall that both field stirrers in the reverberation chamber were set to rotate at 5.0 seconds per revolution. If the large field-strength amplitude variations in Figure 15 were caused by the rotation of the stirrers, we would expect the traces to be periodic with period equal to the time for the stirrers to complete one revolution (i.e., 5.0 seconds). To check this, a computer program was developed to "synchronize" the traces by finding the circularly shifted version of one of the traces that returned the minimum sum of squared differences between the traces. Figure 16 shows the traces after synchronization. This shows that the waveforms are actually nearly identical and supports the hypothesis that the field-strength waveform is periodic and caused by the rotation of the stirrers.
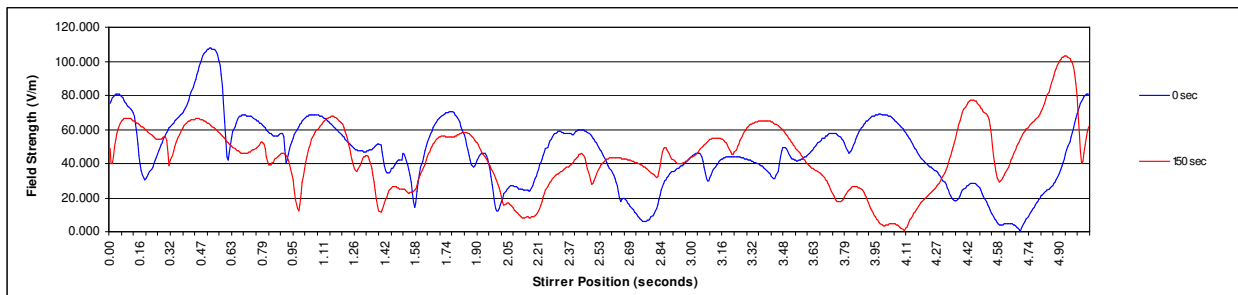
Figure 15: Field strength traces at 110.07 MHz and 0-degree stirrer angular offset
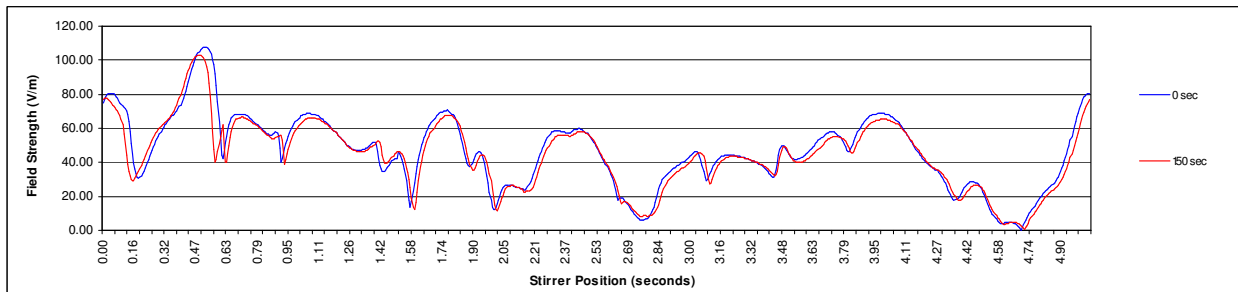
Figure 16: Synchronized field strength traces at 110.07 MHz and 0-degree stirrer angular offset

As stated previously, we are interested in working with amplitude-normalized traces to focus the analysis on the shape of the waveforms regardless of their real amplitudes. To compare multiple traces we need to use a common normalizing amplitude value, but as seen in Figure 16, the peak amplitude of the field strength can vary slightly between periods. To handle this situation for a set of traces, we chose the median peak amplitude as the normalizing amplitude. The median was preferred over the mean because the median is not affected by extreme high or low values.

Figure 17 shows the synchronized and amplitude-normalized field-strength traces for 110.07 MHz and 0-degree stirrer angular offset. This figure shows that the stirrer-induced modulation remains stable in time, but there are slight amplitude differences that appear randomly and have variable duration. Given the strong evidence that the SIM waveform is caused by the rotation of the stirrers, it was suspected that the amplitude variations were due to irregular operation of the stirrers' drive mechanism. Indeed, an

inspection revealed that parts of the mechanism had degraded from normal wear after years of service. It is believed that the worn parts were increasing the friction in the drive mechanism, which caused random variations in the rotational speed of the stirrers. Replacement of the worn parts improved the operation of the stirrers. An unexpected outcome of this analysis is the realization that the SIM waveform could be used as an indirect means of checking the operating status of the stirrers.
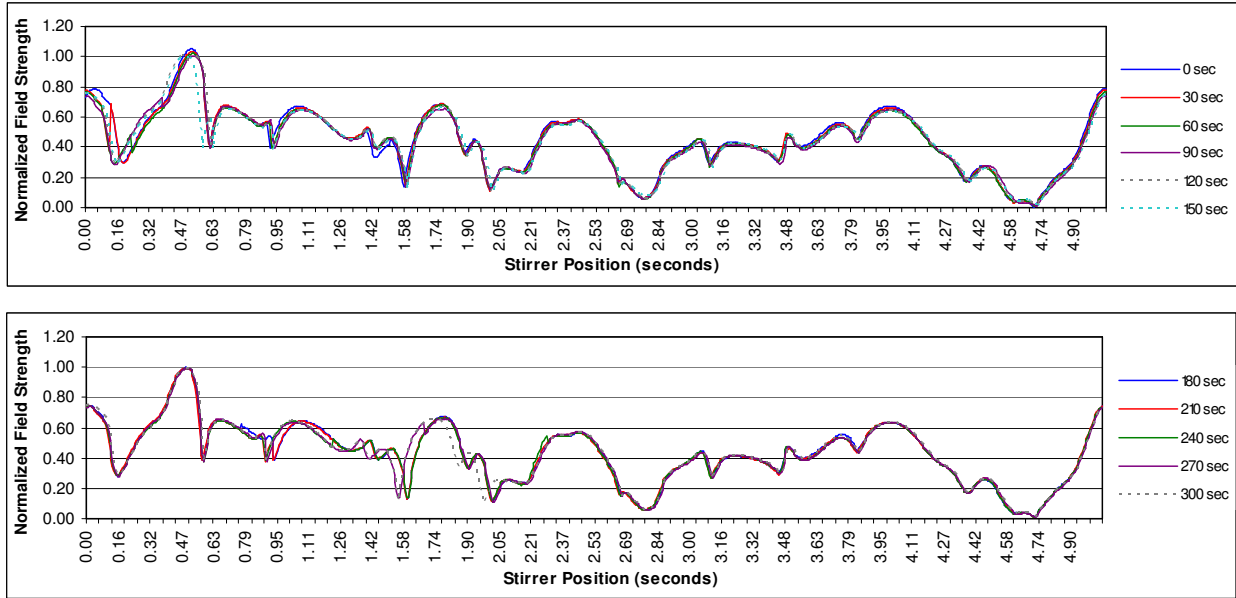

Figure 17: Normalized and synchronized field strength traces at 110.07 MHz and 0-degree stirrer angular offset

5.1.2. Effect of stirrer angular offset

Figure 18 shows SIM traces for various stirrer angular offsets at 110.07 MHz. These waveforms are different from each other and cannot be synchronized as described above. This is true in general: a change in the stirrer angular offset changes the SIM waveform. However, a closer examination of the waveform features, like the shape, number and time distribution of the peaks and valleys, suggests that the waveforms are the result of a common generation process that imposes local constrains on the shapes of the features but allows the waveforms to have an arbitrary global pattern, albeit constrained to be periodic due to the rotation of the stirrers. It is believed that this behavior is an effect of the spatial field patterns determined by the frequency-dependent resonance modes in the reverberation chamber. With respect to the generation of faults in radiated systems, it is of interest to bound the differences in the fault sets experienced by systems tested with different stirrer angular offsets as this was not a controlled variable in the HEC experiment. This is addressed in a later section covering the analysis of SIM overstrokes.

5.1.3. Effect of frequency

Figure 19 shows example SIM traces for test frequencies at 110.07, 316.23 and 908.52 MHz. The trend as the frequency increases is that the waveforms have faster transitions, the peaks have shorter duration and there are more peaks and valleys per trace. This is consistent with a decrease in the wavelength of the radiation at higher frequency, where the chamber accommodates a larger number of resonance modes [7].
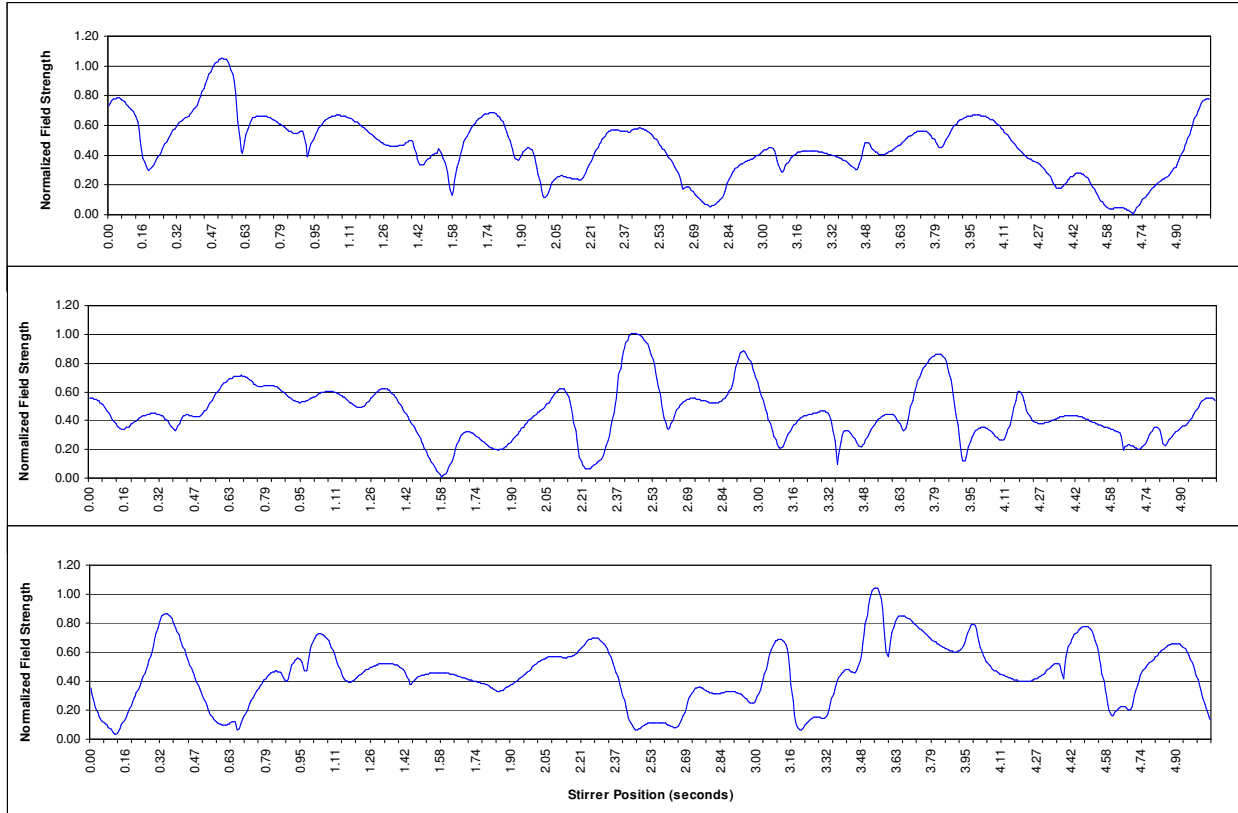
13

Figure 18: SIM traces for different stirrer angular offsets at 110.07 MHz

5.2. Overstrokes

In this section, we perform a quantitative examination of the SIM traces using the overstroke concept. The analysis centers on the relation between the independent controlled variables and the features of the generated overstrokes. The test-controlled variables are the frequency, stirrer angular offset and stirrer revolution, with the chamber input power set to achieve a desired electric field strength level (see [1] Section 4.3). For the analysis presented here, the overstroke reference level is another independently controlled variable. The basic overstroke features of interest include the peak (i.e., maximum) amplitude (p) and duration (d). We are also interested in the relation between the peak amplitude and the duration, and for this, we define the two additional overstroke metrics of peak multiplied by duration (p·d) and peak divided by duration (p/d).

The population of overstrokes derived from the set of available SIM traces can be subdivided based on the values of the controlled variables. In the first part of the analysis in Sections 5.2.2 and 5.2.3, we divide the overstroke set only by frequency and overstroke reference level, and aggregate the overstrokes over the ranges of stirrer angular offset and revolution. Later in Section 5.2.4, we examine the effect of the stirrer angular offset with overstroke aggregation only for the stirrer revolution variable.

14
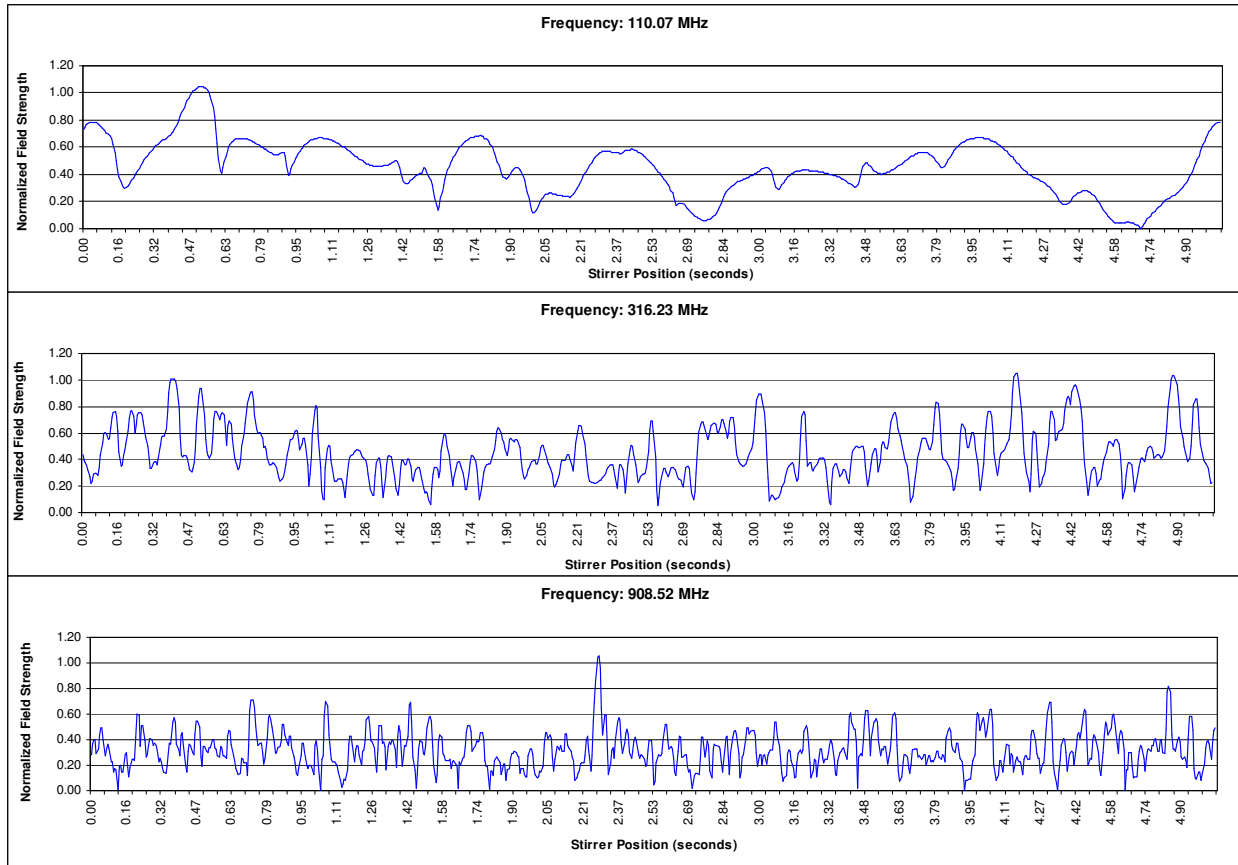
Figure 19: Examples of SIM traces for different test carrier frequencies

5.2.1. Population Spread

Figure 20 shows how the number of overstrokes at various frequencies varies as the reference level decreases. The overstrokes were generated for amplitude-normalized but unsynchronized field-strength traces. As expected from inspection of Figure 19, at each frequency the trend is that the number of overstrokes increases as the reference level decreases. Interestingly, the number of overstrokes at a particular reference level is not always larger for higher frequencies. In particular, notice how at 908.52 MHz the rate of increase in the overstroke count starts slow and grows very quickly as the reference level decreases. Given that this data is for aggregated sets over the stirrer angular offsets and revolutions, it appears that the SIM profile in Figure 19 for 908.52 MHz is generally valid at this frequency. That is, at 908.52 MHz, there are very few SIM waveform peaks approaching the maximum normalizing amplitude and almost all of the peaks have amplitude lower than 60% of the maximum. Another way of looking at the trend in Figure 20 is that, as the reference level decreases, it is more likely (i.e., there are fewer exceptions to the pattern) that the number of overstrokes is larger at higher frequencies.
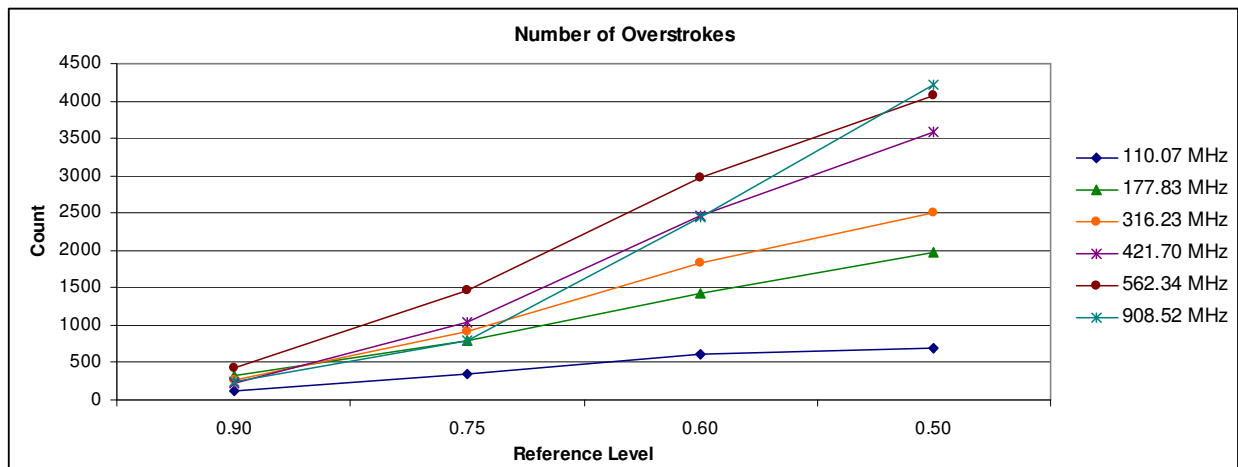
Figure 20: Number of overstrokes as the reference level decreases for various test frequencies

Figures 21 to 23 show scatter plots of the overstroke populations for 110.07, 316.23, and 908.52 MHz at reference levels of 0.90, 0.75, and 0.60. The clustering effect of some points, especially at 110.07 MHz, is probably due in part on the periodicity of SIM traces with the same frequency and angular offset but different stirrer revolutions. In Figure 21 at reference level 0.60, the overstrokes with duration between 700 and 800 ms are probably the result of the merging of overstrokes when the reference level drops below the lowest value of the gap separating them. This can be visualized, for example, by considering the overstrokes in Figure 11 at around 1.14 seconds if the reference level (indicated by the red reference line) drops below 0.50, at which point the overstrokes on either side of the gap become a single overstroke of large duration.

From Figure 20, we know that, in general, at a particular reference level there are more overstrokes at higher frequency. However, from Figures 21 to 23 we see that at lower frequencies the features of the overstrokes vary much more than at higher frequencies. For example, at reference level 0.60, the overstrokes with 0.2 peak amplitude vary in duration over a duration interval of about 600 ms at 110.07 MHz, 100 ms at 316.23 MHz, and 70 ms at 908.52 MHz.

Also, notice in Figures 22 and 23 that each frequency appears to impose a constraint on the maximum ratio of overstroke peak to duration as indicated by the crowding of points along a boundary line on the left hand side of the populated areas. This apparent peak-to-duration ratio constraint is larger at higher frequencies, which means that the overstrokes can have a more acute (i.e., pointy) profile. This trend can also be inferred from examination of the SIM traces in Figure 19.

The significance of these scatter plots is that, based on the conjectured relation between overstrokes and error bursts experienced by an SUT as described in Section 3, each point in Figures 21 to 23 corresponds to a possible error burst that could be injected by the reverberation chamber into a radiated SUT.
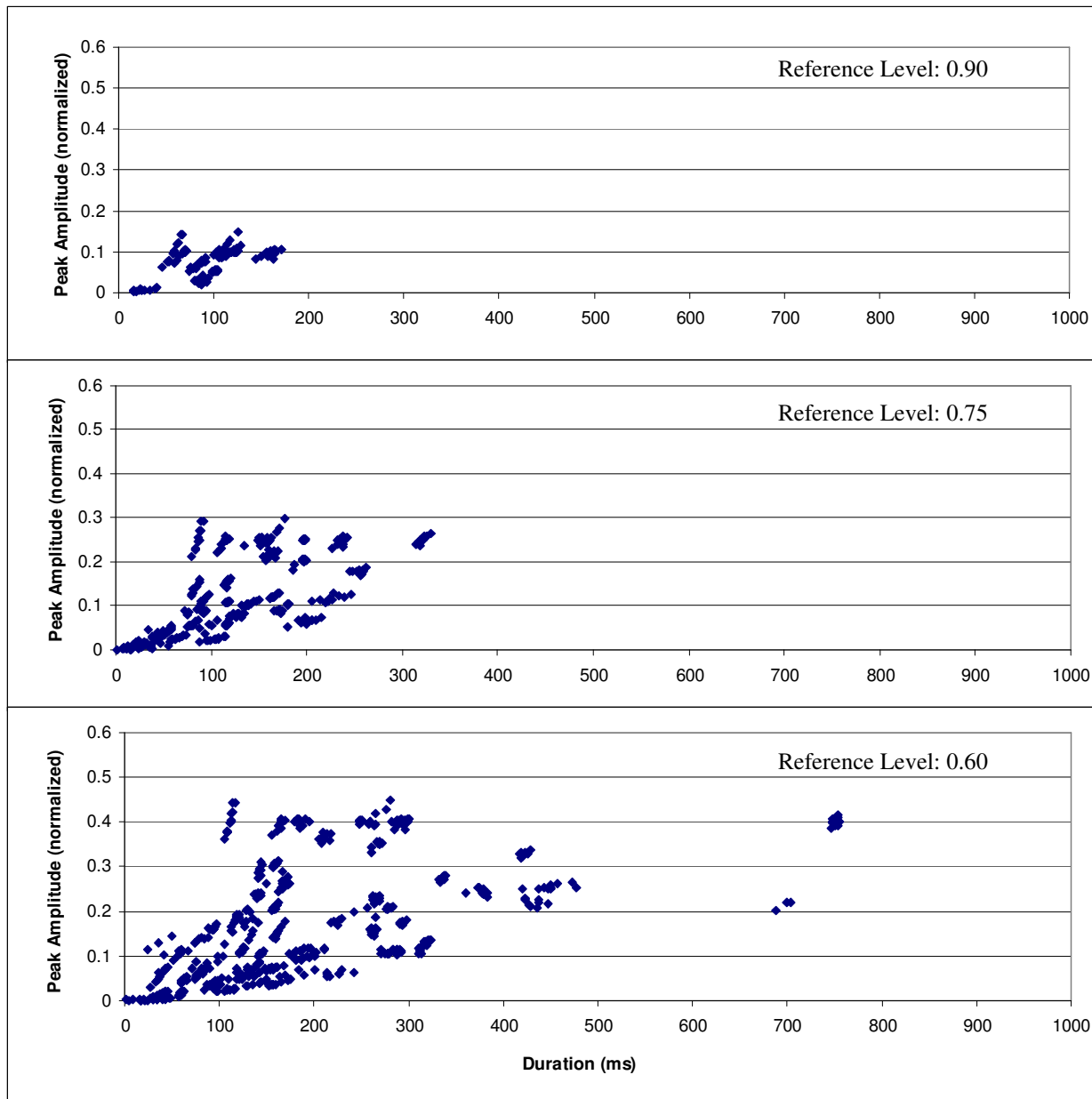
Figure 21: Scatter plots of overstroke peak amplitude versus duration at 110.07 MHz
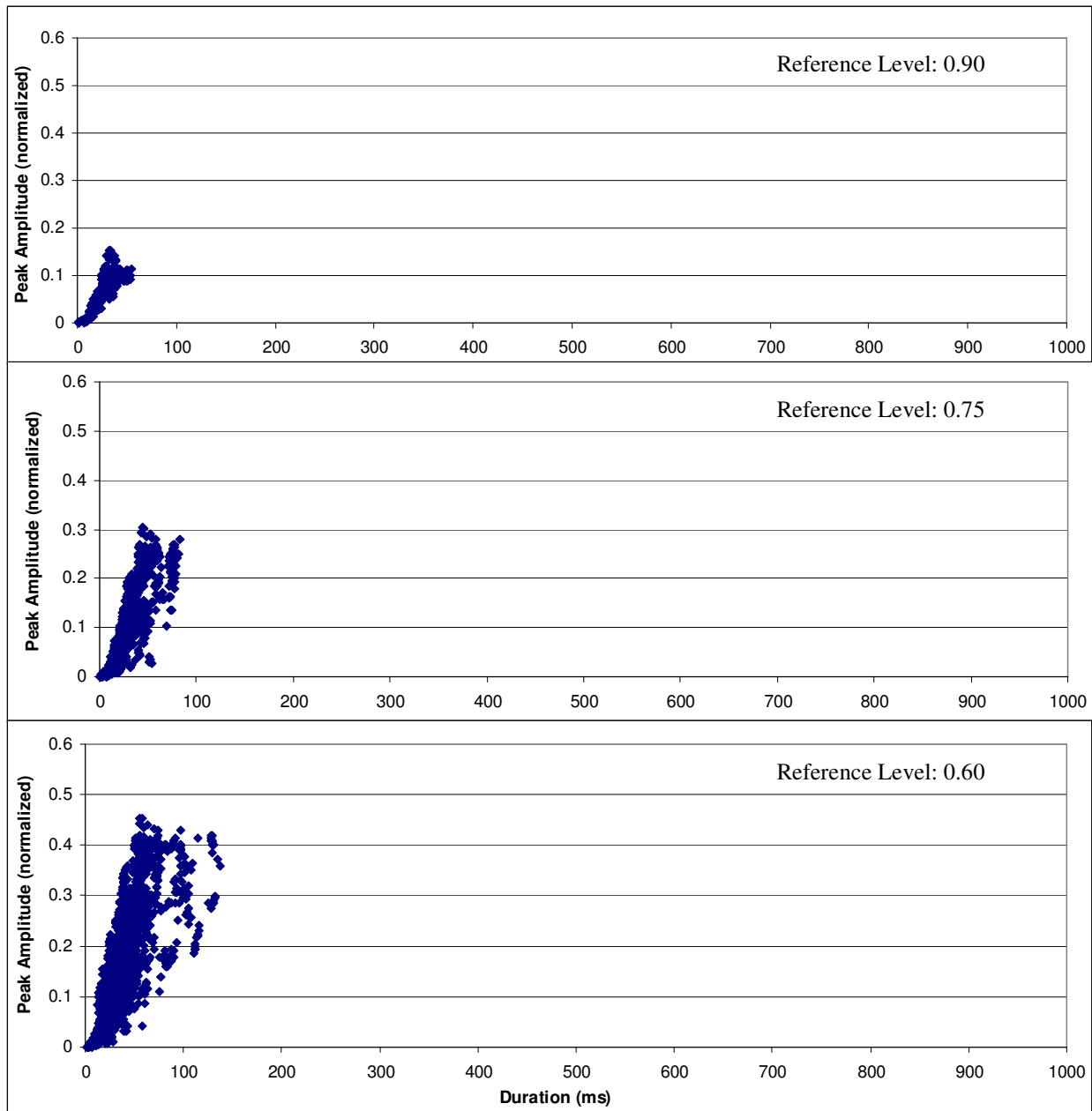
Figure 22: Scatter plots of overstroke peak amplitude versus duration at 316.23 MHz
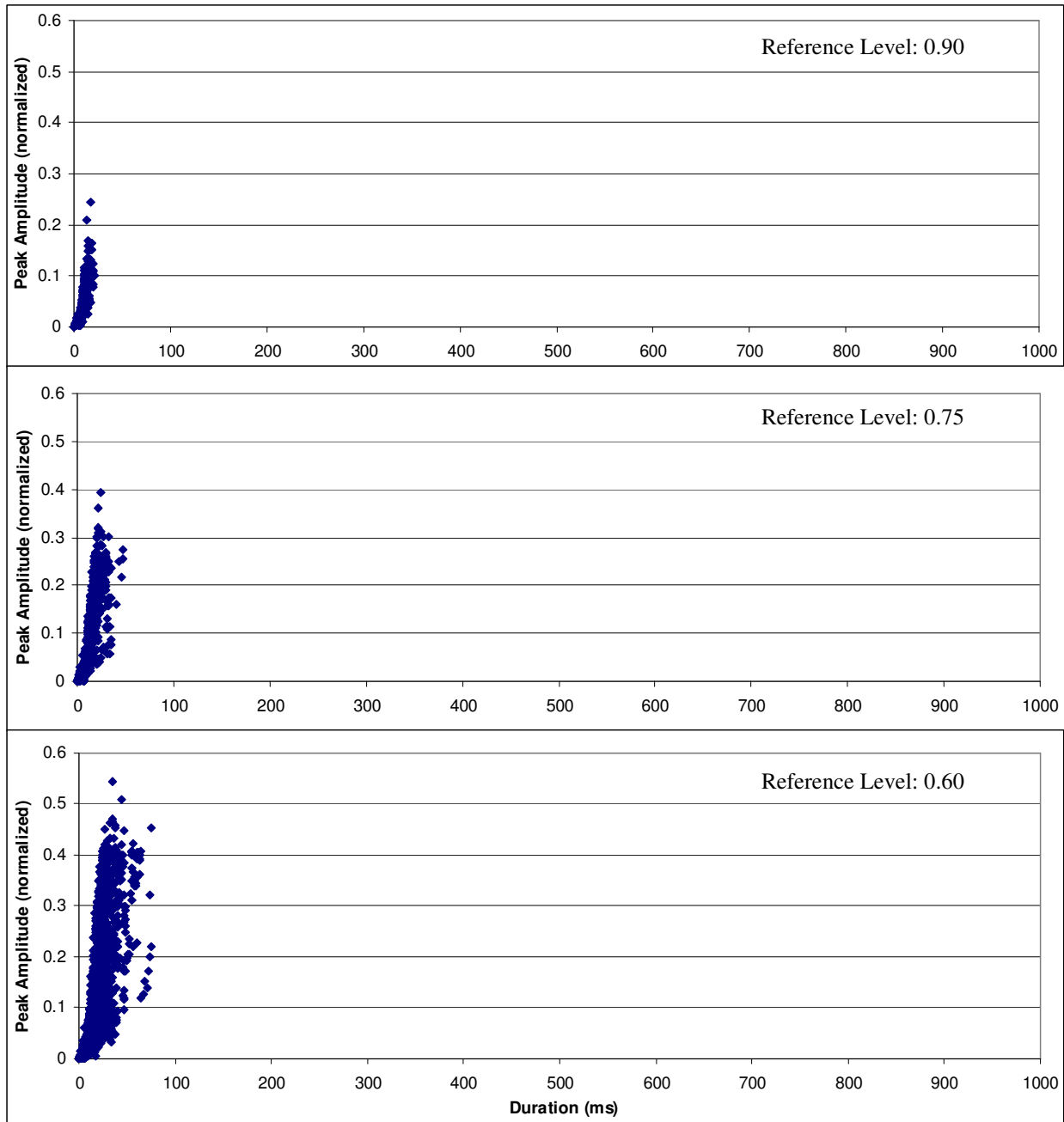
Figure 23: Scatter plots of overstroke peak amplitude versus duration at 908.52 MHz

5.2.2. Statistics of Overstroke Features for the Range of Test Frequencies

We next examine separately the overstroke features of peak multiplied by duration, peak divided by duration, peak, and duration. In the following, the peak amplitude is normalized and the duration is measured in units of milliseconds.

5.2.2.1. *Peak amplitude multiplied by duration*

The metric of peak multiplied by duration (aka "peak times duration") is related to the area of an overstroke. Figures 24 to 26 show the mean, standard deviation and root-mean-squared (RMS) values of the peak-times-duration overstroke metric for the full range of frequencies and overstroke reference levels (denoted Et) of 0.90, 0.75, and 0.60. Notice that the frequency axis is on an ordinal scale, not a linear or logarithmic scale. Also, note that the RMS is a compound statistical average that combines the mean and standard deviation. To see this, let X_{rms}, X_{mean}, and X_{sd} denote the RMS, mean and standard deviation of a value set, respectively. Then these statistical averages are related as follows: $X_{rms}^2 = X_{mean}^2 + X_{sd}^2$.

The overall trend in Figure 24 is that the mean area of the overstrokes decreases as the frequency increases. However, rather than decreasing monotonically, at every reference level the curves follow an undulating pattern by which the area can increase locally from one frequency to the next. We have no insight into the cause of this pattern, which is probably due to the resonance characteristics of the reverberation chamber. Interestingly, the standard deviation and, of course, the RMS value follow a similar trend across the frequency range. Also, notice that at every frequency, the magnitude of the standard deviation is similar to the mean, which implies that the spread of the distribution is to some extent proportional to its mean.
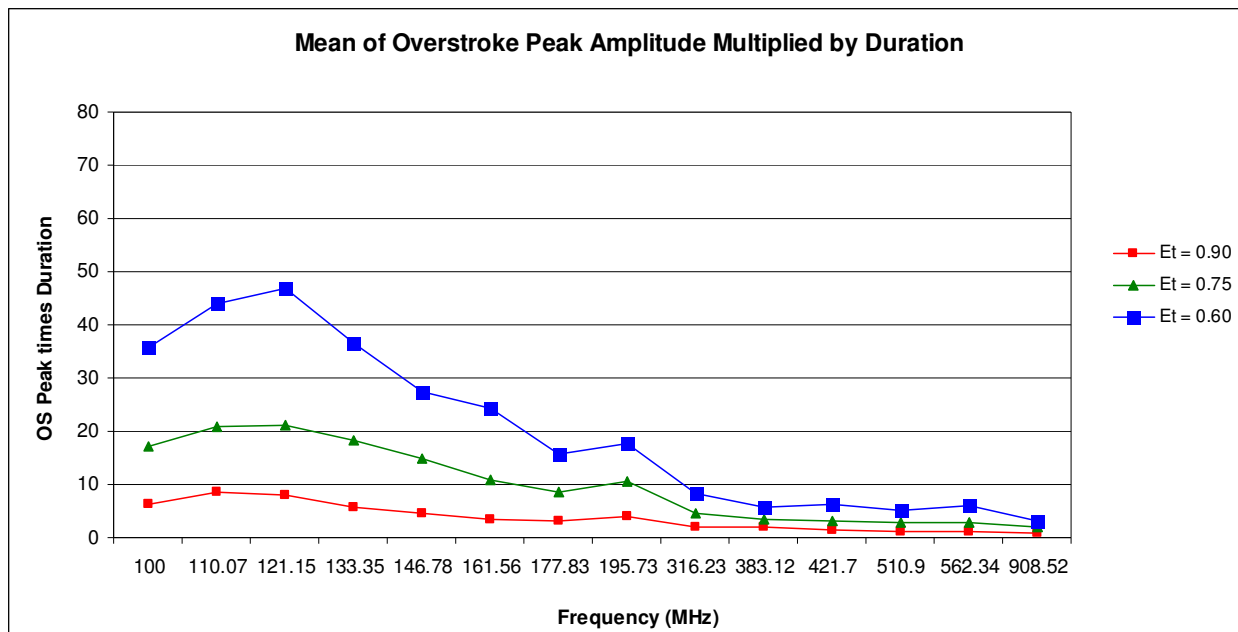
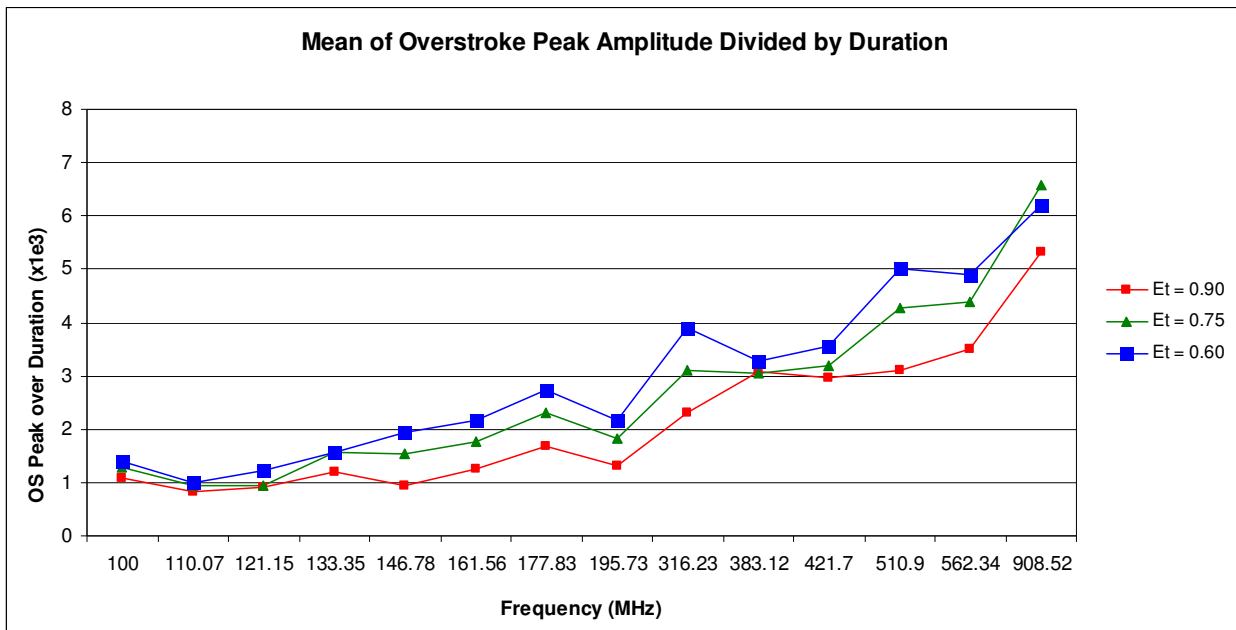Figure 24: Mean overstroke peak multiplied by duration for the range of test frequencies
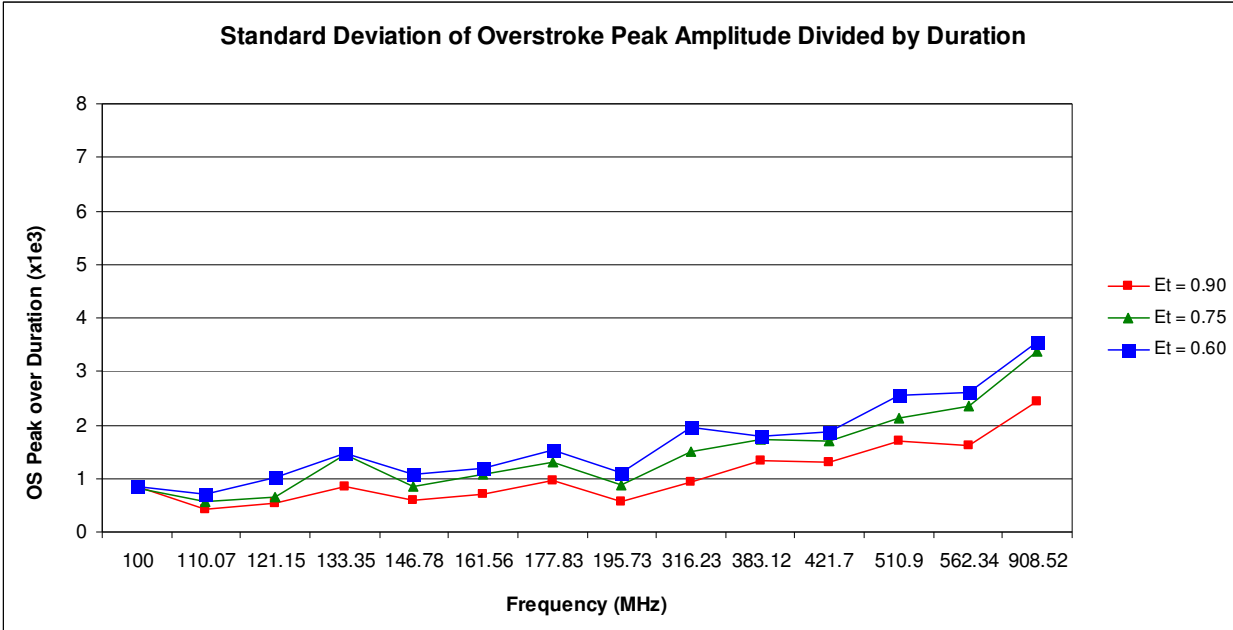
20
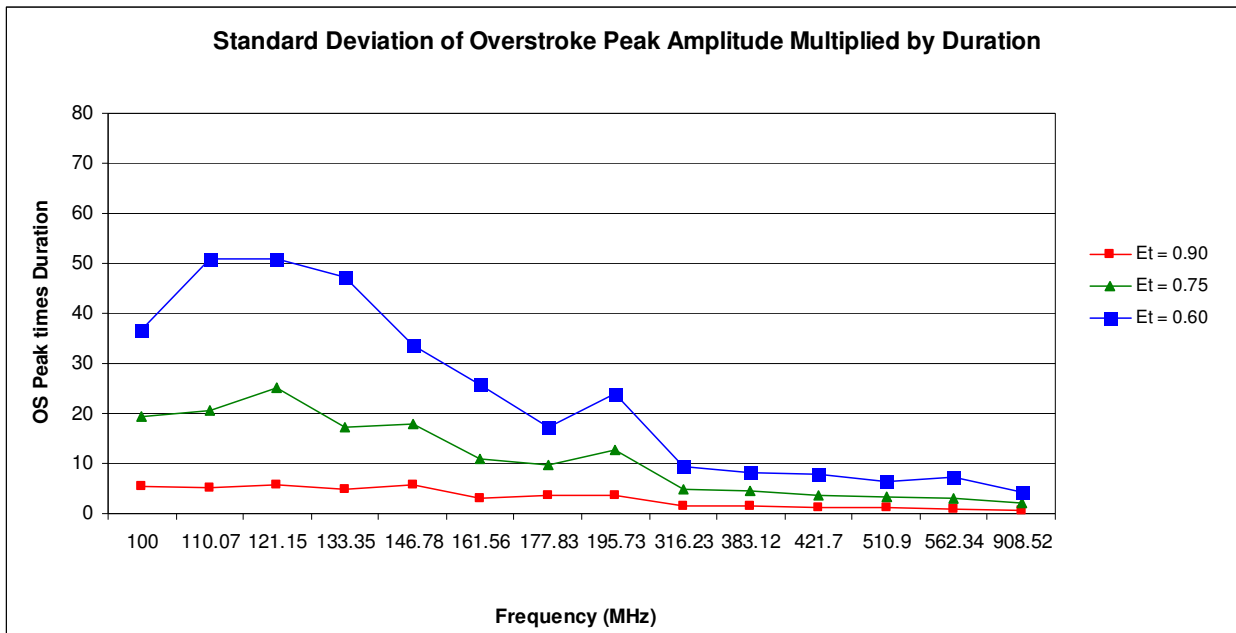
Figure 25: Standard deviation of overstroke peak multiplied by duration for the range of test frequencies
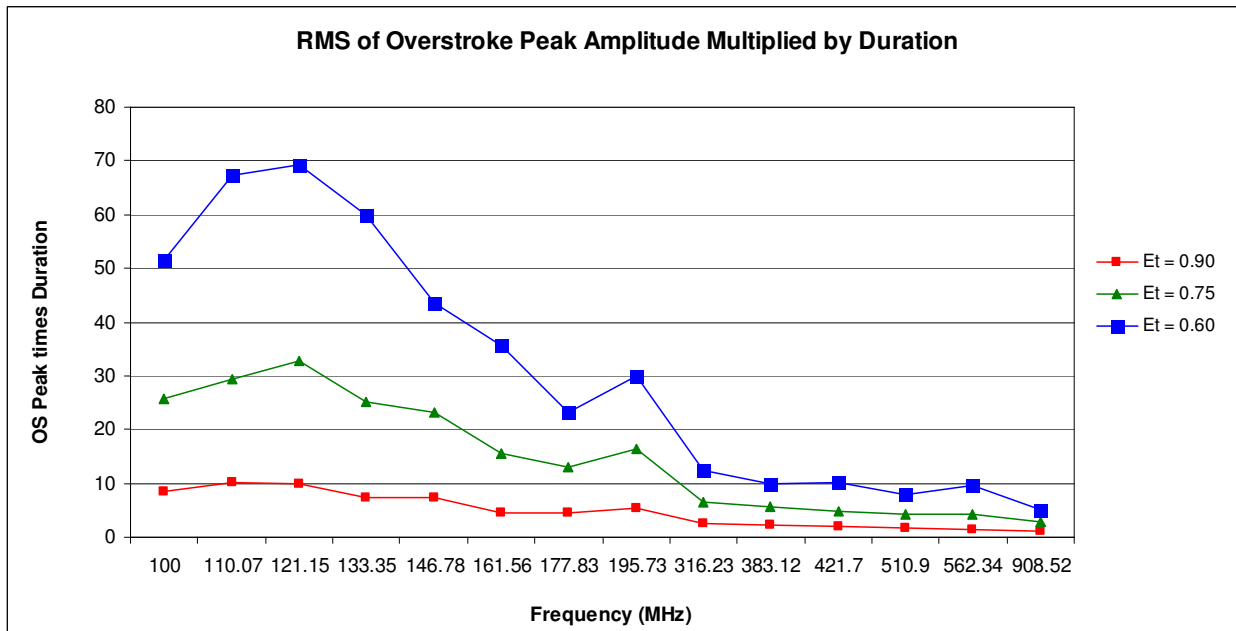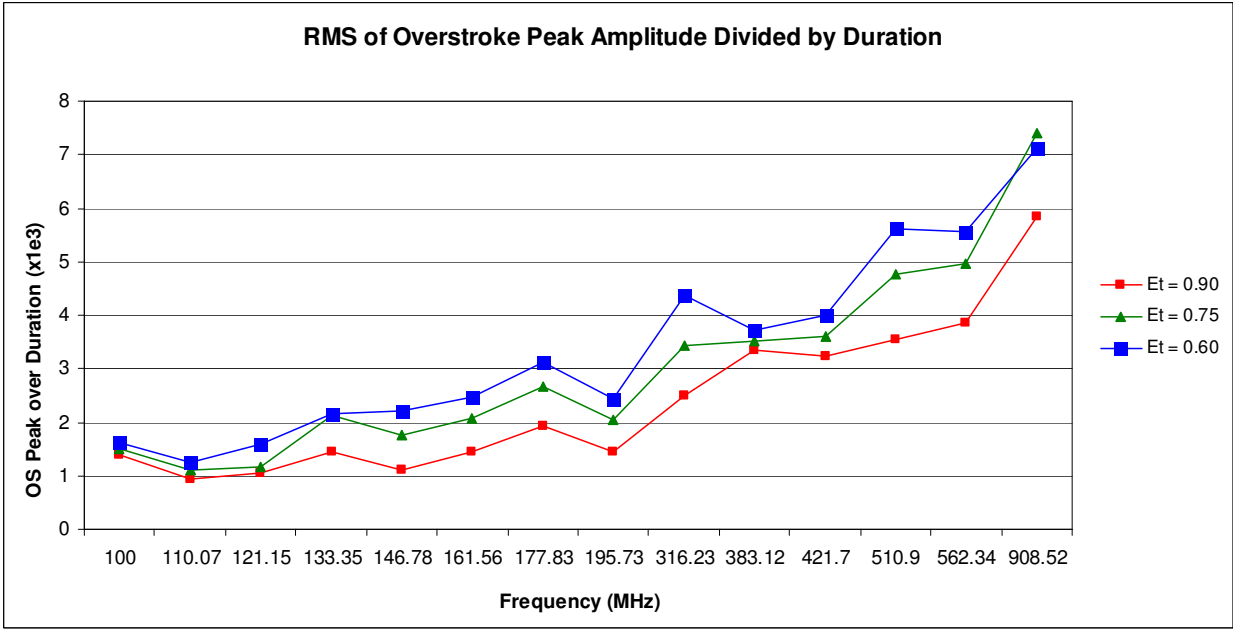

Figure 26: RMS overstroke peak multiplied by duration for the range of test frequencies

5.2.2.2. *Peak Amplitude Divided by Duration*

Figures 27 to 29 show the mean, standard deviation and RMS value of the overstroke peak amplitude divided by duration for the frequency range at selected reference levels. The peak-over-duration metric is related to the acuteness (i.e., pointiness) of the overstroke. Again, note that in these figures the values on the frequency axis are on an ordinal scale. Figure 27 shows that the acuteness of the overstrokes increases with the frequency, although locally from one frequency to the next the relation may be the opposite due to the resonance characteristics of the reverberation chamber. This global trend over the frequency range implies that the overstroke duration tends to decrease faster than the peak value. Also, notice in Figure 28 that the spread of the overstroke distribution with frequency is smaller than the mean value in Figure 29. This is interpreted to mean that the spread of the peak values grows larger with frequency than the spread of the durations. A comparison of Figures 27 and 28 shows that the spread of the peak-over-duration distribution is smaller than the mean by about one third, and in that sense, the spread is also smaller than for the peak-multiplied-by-duration distribution. The RMS curves in Figure 29 are determined mostly by the mean values, as the standard deviation values are smaller.

Figure 27: Mean overstroke peak divided by duration for the range of test frequencies

Figure 28: Standard deviation of overstroke peak divided by duration for the range of test frequencies

Figure 29: RMS overstroke peak divided by duration for the range of test frequencies

5.2.2.3. *Peak Amplitude*

The mean, standard deviation and RMS of the overstroke peak amplitude over the frequency range are shown in Figure 30 to 32. Overall, the averages of the overstroke peak do not change much across the frequency range for any reference level. The range of the mean value in Figure 30 varies from about 23% of the maximum at reference level 0.90 to about 34% at reference level 0.60. The general trends of the mean value are that it decreases with frequency and it grows faster at lower frequencies with decreasing reference level. As the nominal overstroke maximum peak value increases 4 times with the range of 0.1 to 0.4 over the reference level range of 0.9 to 0.6, the increase in the mean peak value is about 2.6 at 100 MHz and about 2.0 at 908.52 MHz. This shows that, in general, the mean peak value grows faster at lower frequencies and about half as fast as the nominal maximum peak value as the reference level decreases.

The standard deviation curves in Figure 31 show that the spread remains nearly constant over the frequency range, but it increases as the reference level decreases. The trends in the RMS curves in Figure 32 are determined mainly by the mean value of the distribution.
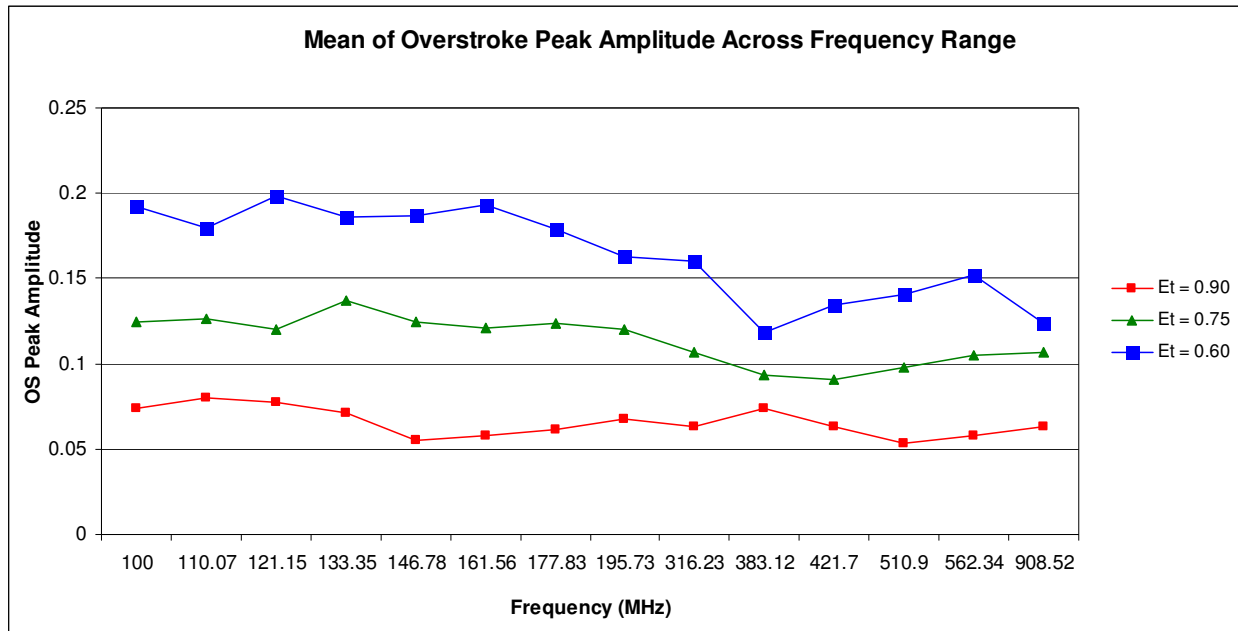
Figure 30: Mean overstroke peak across the test frequency range
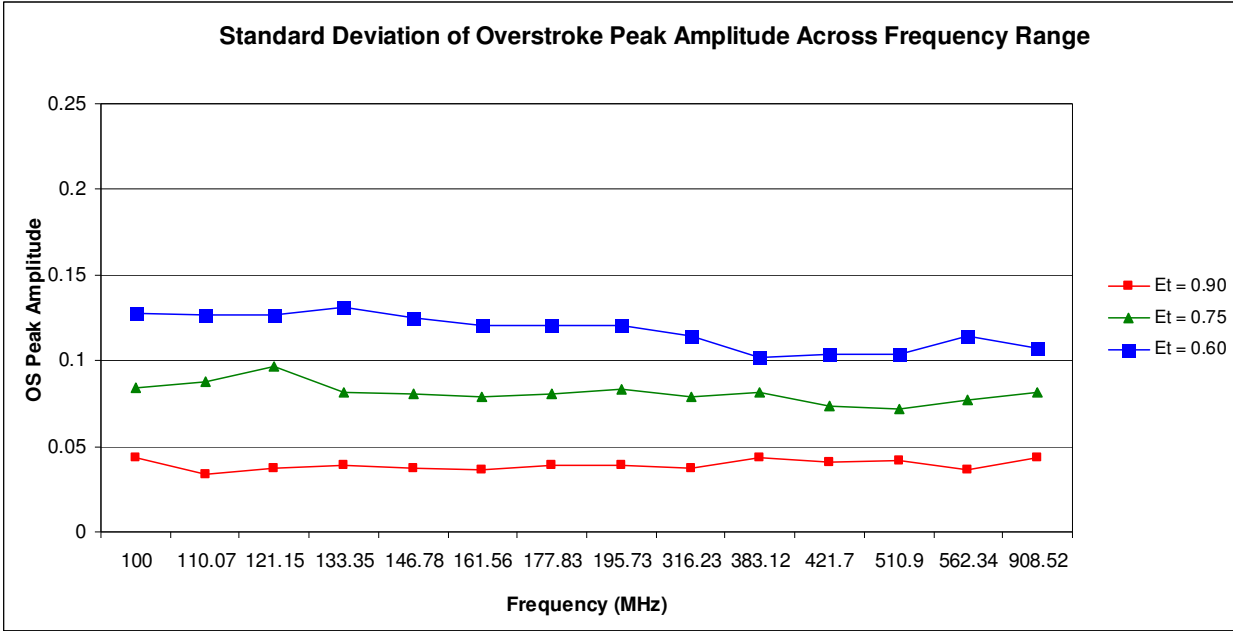
Figure 31: Standard deviation of overstroke peak across the test frequency range
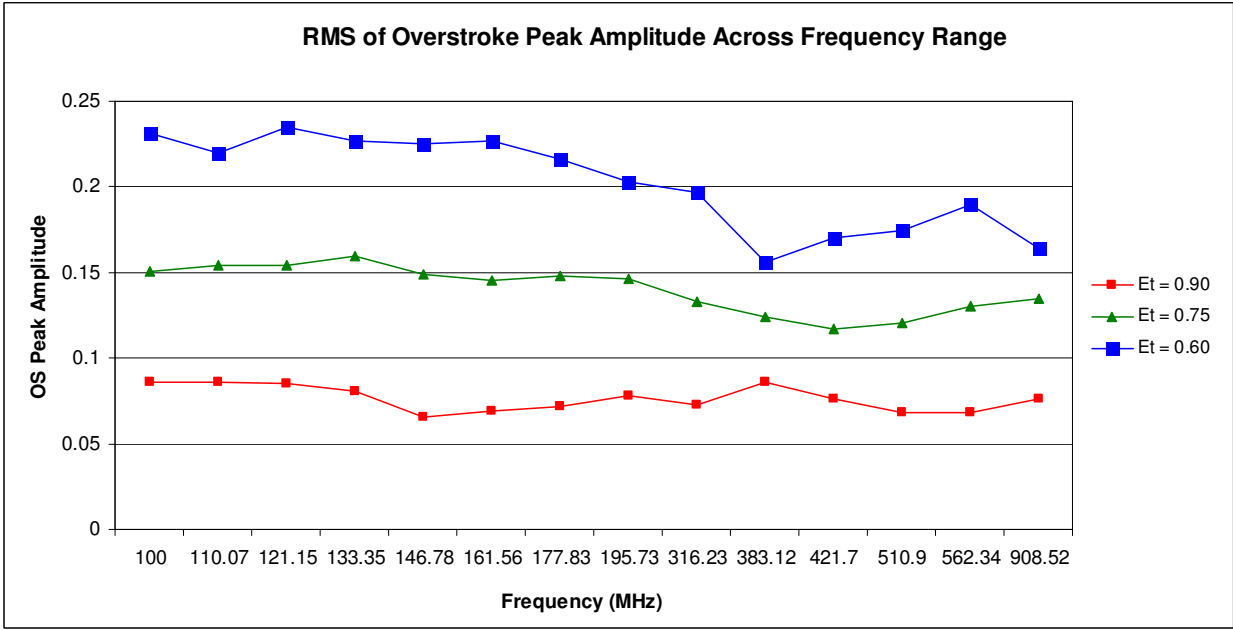
Figure 32: RMS overstroke peak across the frequency range

5.2.2.4. *Duration*

Figures 33 to 35 show the mean, standard deviation and RMS values of the overstroke duration over the test frequency range for decreasing values of the reference level. For these figures, the frequency is given on a linear scale. Overall, the overstroke duration seems to decrease exponentially over the frequency range. The features in these figures can be divided into two frequency intervals: below 200 MHz and above 300 MHz. Below 200 MHz, the mean overstroke duration varies widely and decreases quickly from about 121.15 MHz onward. Above 300 MHz, the mean overstroke duration decreases much more slowly and appears to approach a minimum value asymptotically. Notice that the standard deviation decreases as the mean value decreases and it too seems to approach a minimum value at higher frequencies. We believe that this overstroke duration profile is directly related to the number of resonance modes generated in the reverberation chamber, with more modes being generated at higher frequencies, which results in more dynamic SIM waveforms.
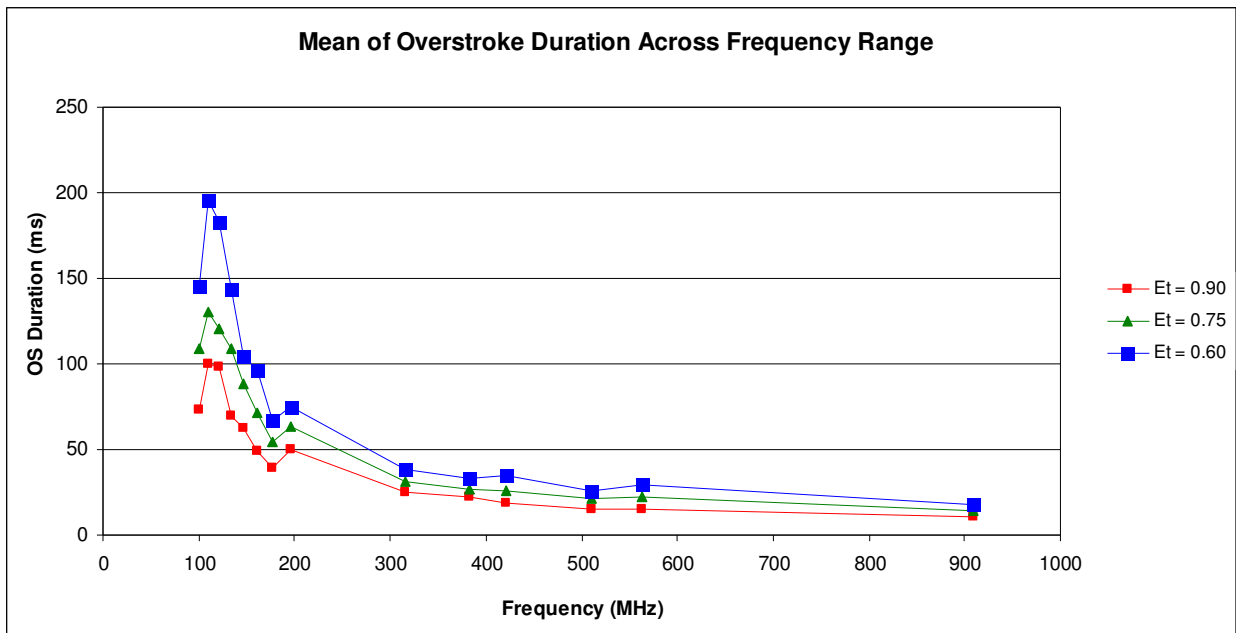
Figure 33: Mean overstroke duration over the frequency range on a linear scale
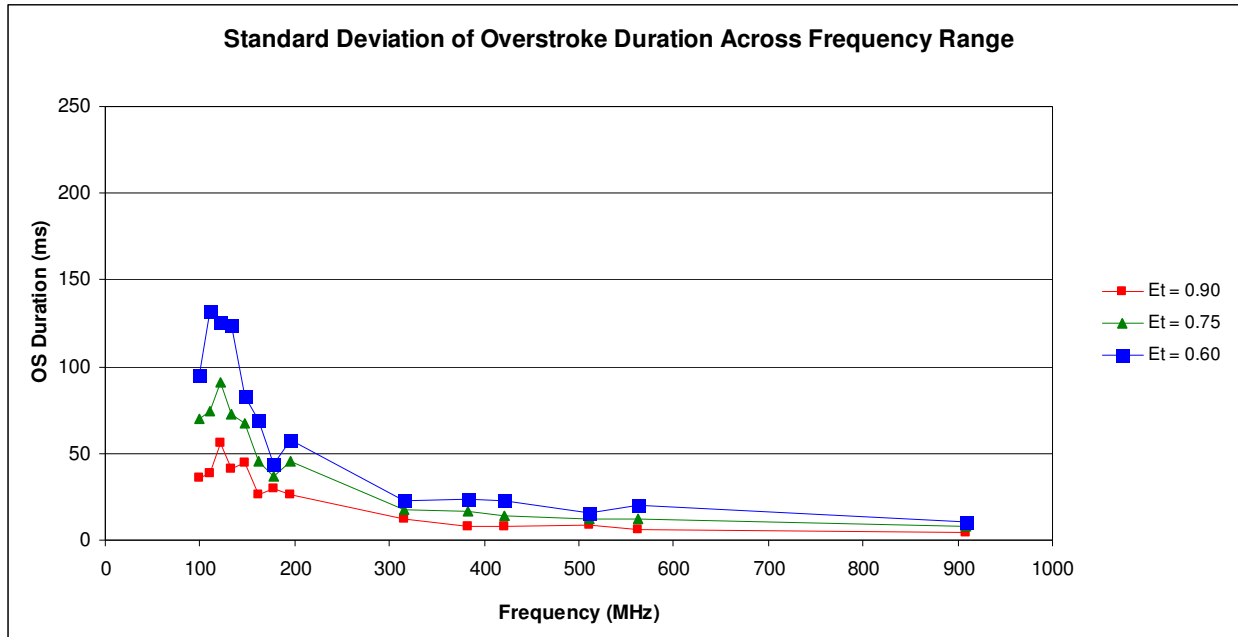
Figure 34: Standard deviation of overstroke duration over the frequency range on a linear scale
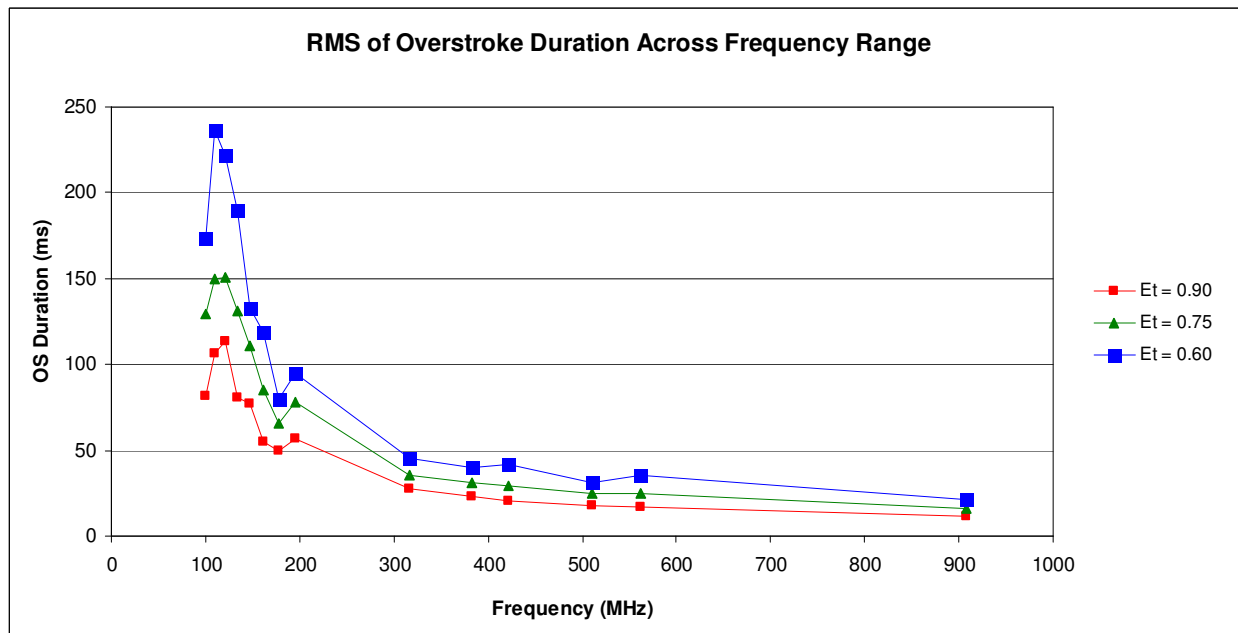
Figure 35: RMS overstroke duration over the frequency range on a linear scale

5.2.3. Statistics of Overstroke Features for the Range of Reference Levels

We next examine the statistical averages of the overstroke population for the features of peak amplitude and duration over a range of reference levels.

5.2.3.1. *Peak Amplitude*

Figures 36 to 38 show the mean, standard deviation and RMS values of the overstroke peak amplitude for reference levels in the range of 95% to 50% of the median maximum SIM amplitude. The curves are given only for three test frequencies, with 110.07 MHz representing the frequencies under 200 MHz, and 316.23 MHz and 908.52 MHz covering the much larger range above 300 MHz. We use E_t to denote a particular reference level, with $0 \leq E_t \leq 1$. The maximum overstroke peak amplitude is equal to $1 - E_t$, and the maximum peak amplitude grows at a rate (i.e., slope) of approximately 1.0 over the decreasing 1-to-0 range of E_t. In Figure 36, the mean peak amplitude grows at a rate of approximately 0.43 at 110.07 MHz and 0.23 at 908.52 MHz over the reference level range. At 95% reference level, the mean peak amplitude is about 86% of the maximum peak at 110.0 MHz and 908.52 MHz, but at 50% reference level, the mean is only about 48% of the maximum at 110.07 MHz and 29% at 908.52 MHz. This is consistent with the overstroke counts in Figure 20 in the sense that at higher frequencies and as the reference level decreases, many more overstrokes are generated with relatively small peak amplitudes, thus weighing down the overall mean value.

Figure 37 shows that the standard deviation of the peak amplitude increase essentially linearly with the reference level, which means that the population spread is proportional to the mean value. The RMS value in Figure 38 is determined mainly by the mean value.
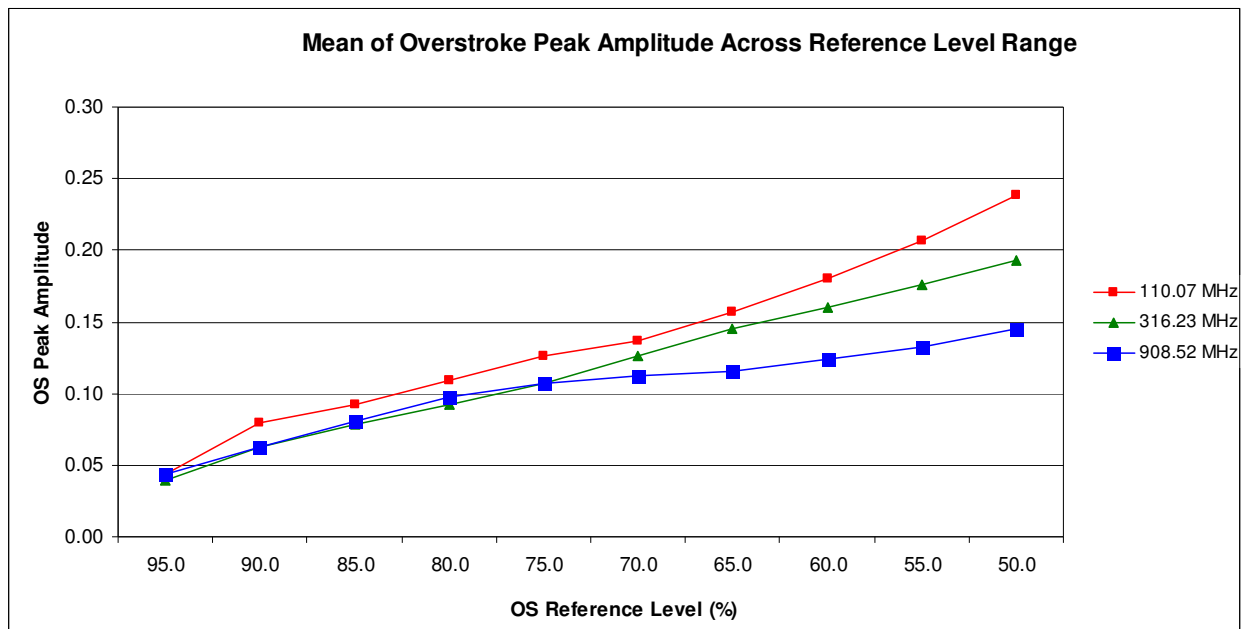
Figure 36: Mean overstroke peak amplitude for the range of reference levels
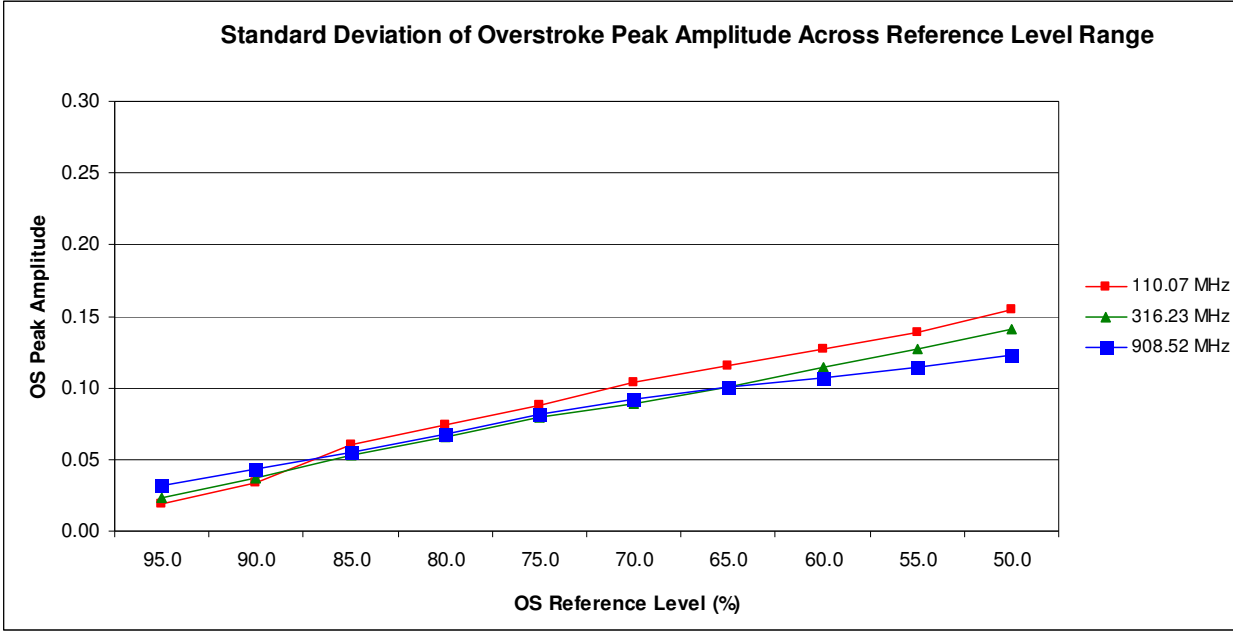
Figure 37: Standard deviation of overstroke peak amplitude for the range of reference levels
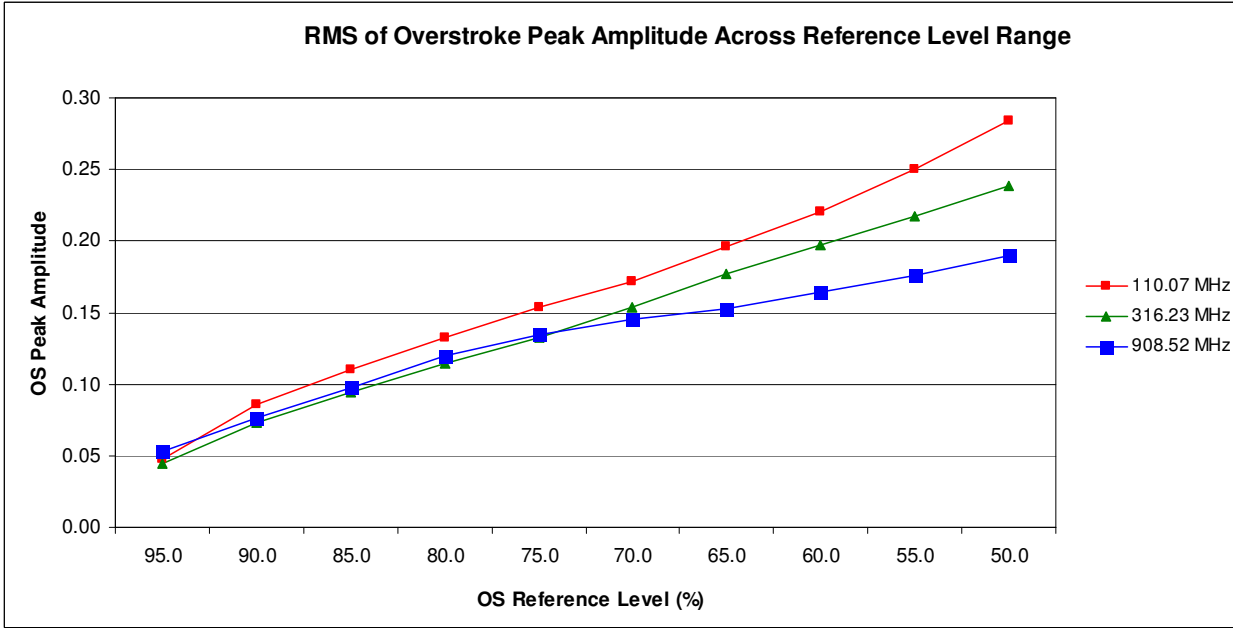
Figure 38: RMS overstroke peak amplitude for the range of reference levels

5.2.3.2. *Duration*

The mean, standard deviation and RMS overstroke duration for the range of reference levels are given in Figures 39 to 41. Figure 39 shows that the overstroke duration at low frequency is much more sensitive to the change in the reference level. The increases in the mean duration over the reference level range relative to the minimum durations at the 95% reference level are 2.58 times at 110.07 MHz, 1.17 at 316.23 MHz, and 1.46 at 908.52 MHz. These measures of overstroke duration are consistent with the SIM traces in Figure 19 in that, near the top of the SIM peaks, the field amplitude changes with a slower time rate at lower frequencies, which increases the overstroke duration; as we travel down the SIM peaks, the field amplitude changes much more slowly at lower frequencies, which causes the duration to increase faster; and as the frequency increases, the amplitude rate of change seems to asymptotically approach a bound, which causes the duration versus reference level profile to be very similar at different high frequencies.

As the reference level decreases, the standard deviations in Figure 40 increase not only in absolute value but also with respect to their corresponding mean values from 0.44 to 0.71 at 110.07 MHz, from 0.40 to 0.72 to 316.23 MHz, and from 0.44 to 0.67 at 908.52 MHz. This indicates that the spread of overstroke duration increases faster than the mean as the reference level decreases.

The RMS duration curves in Figure 41 follow the same trends as the curves for the mean and standard deviation values.
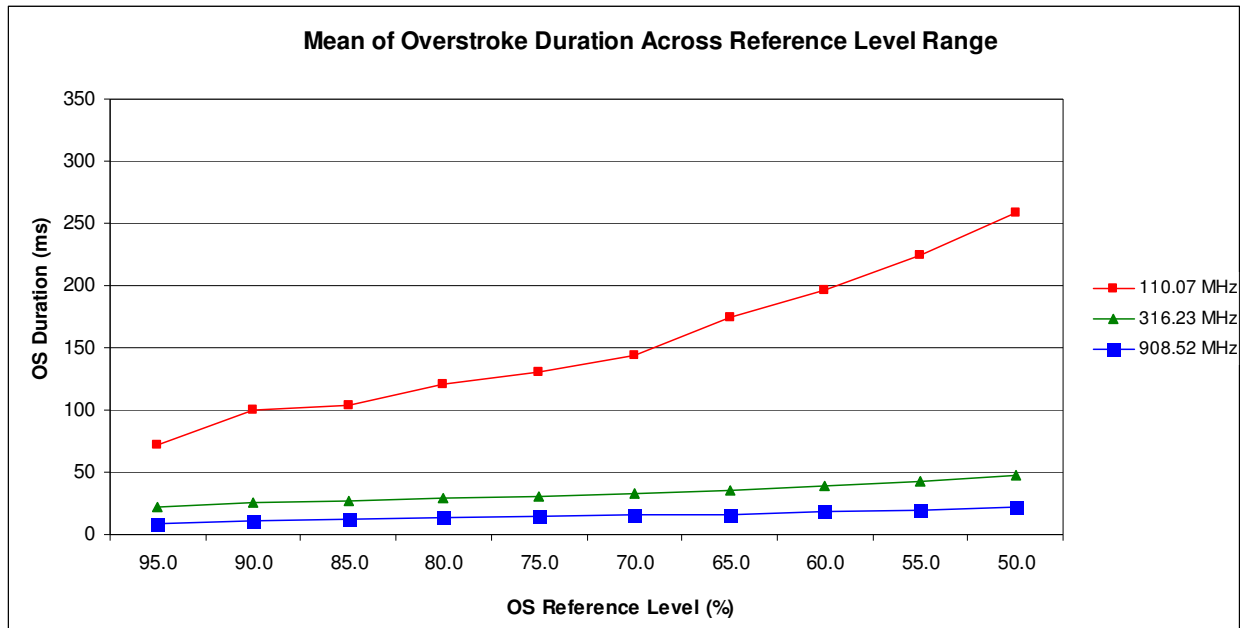
Figure 39: Mean overstroke duration for the range of reference levels
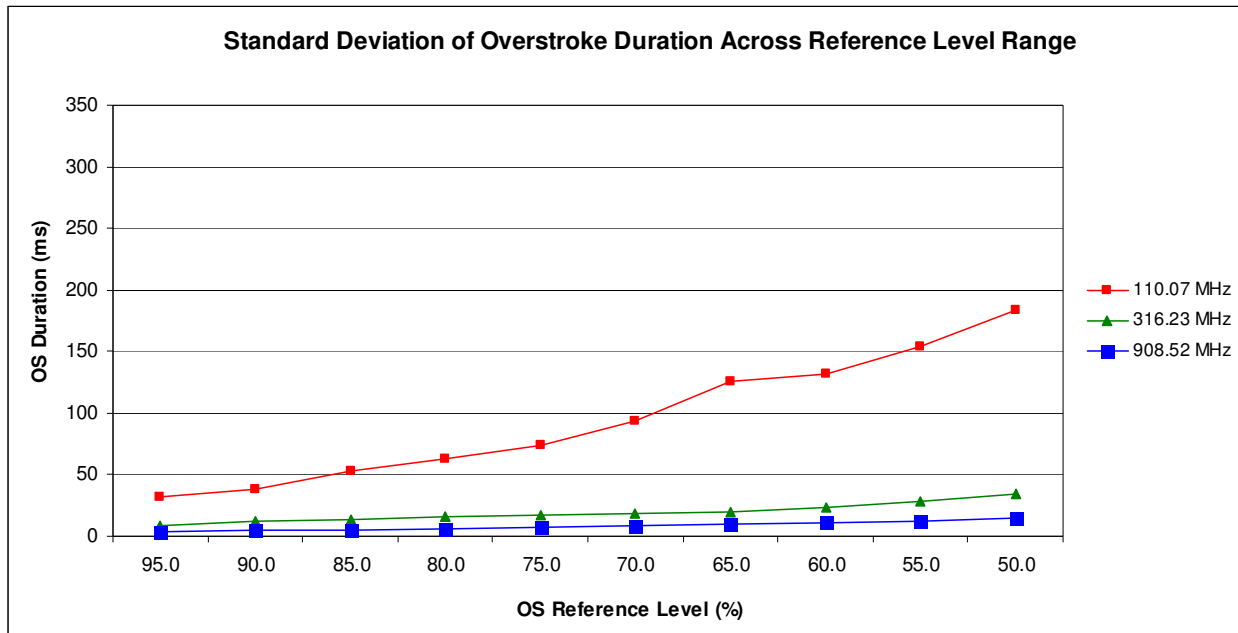
Figure 40: Standard deviation of overstroke duration for the range of reference levels
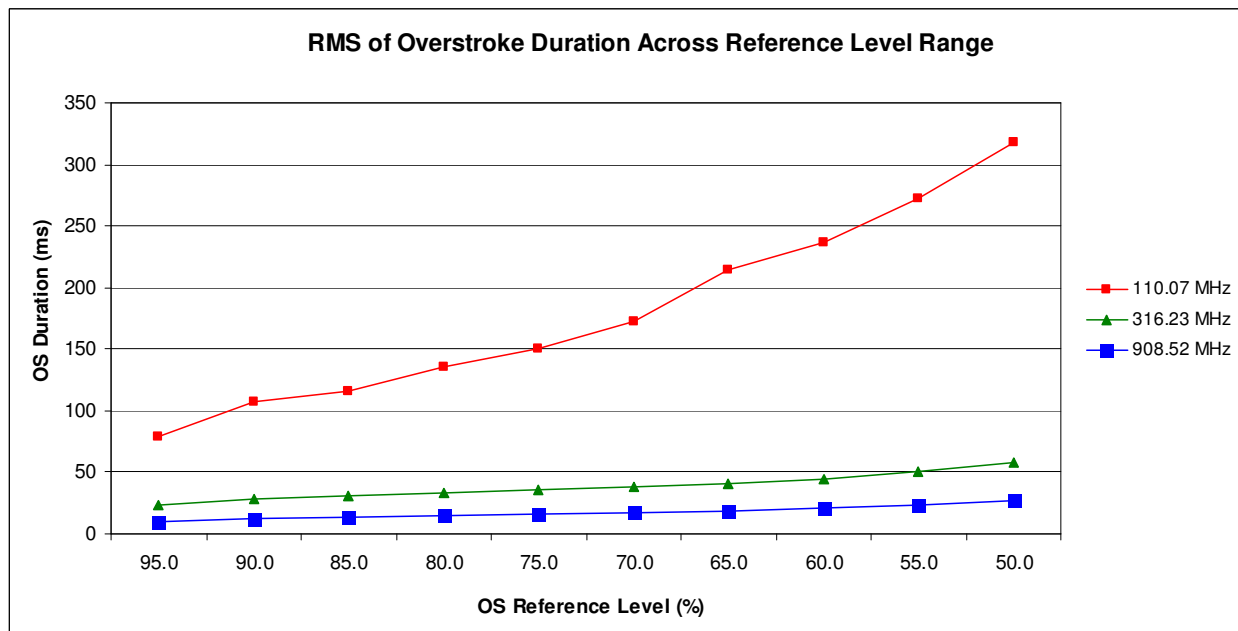
Figure 41: RMS overstroke duration for the range of reference levels

5.2.4. Variability of Statistics with Respect to Relative Stirrer Angular Offset

In the HEC experiment, the 5-second duration of the strikes was the same as the revolution period of the stirrers, and the strike period was 10 seconds (i.e., one 5-second strike was applied every 10 seconds). The timing of the strikes was independently controlled by a dedicated RF (Radio Frequency) signal generator, as illustrated in Figure 5. Due to the high timing accuracy of the signal generator and of the stirrer motor controller (which resulted in a near constant stirrer angular offset), the SIM waveforms were repeated identically for all the strikes in an HEC round. This means that for any two strikes in a round, the field strength traces were synchronized as shown in Figure 16, rather than unsynchronized as in Figure 15. Therefore, an SUT was exposed to approximately same set of overstrokes for each strike in a round.

As the stirrer angular offset was not a controlled variable in the HEC experiments (other than being constant in each round), it is likely that, for a given physical location in the chamber, different SUTs were exposed to different overstroke sets even when tested at the same frequency and nominal over-strength level. Given the direct relation between the overstrokes and the error bursts as shown in Section 3, it is of interest to determine how much can the overstroke feature statistics vary for overstroke sets generated with different stirrer angular offsets.

To evaluate this using the available SIM data, at each test frequency and stirrer angular offset, the SIM traces for the available stirrer revolutions were synchronized and the overstroke feature statistics were computed for the aggregate set of overstrokes at each reference level. We define the **variation** of a statistical average (i.e., mean, standard deviation or RMS value) of an overstroke feature as the difference between the maximum and minimum values across the range of stirrer angular offsets. For a given overstroke feature and statistical average, the variation is denoted by V and the maximum and minimum of the feature's statistical average are denoted by A_{max} and A_{min}, respectively. Then V is given by:

$$V = A_{max} - A_{min} \tag{1}$$

As shown in preceding sections, the statistics of the overstroke features are dependent on the frequency and reference level. To enable a meaningful comparison of variation across the ranges of frequency and reference levels, we define the **variability** of an overstroke feature's statistical average across the range of stirrer angular offsets at a particular frequency and reference level as the ratio of the variation divided by the feature's same statistical average for the overstroke set formed by aggregation over the range of stirrer angular offsets and revolutions with unsynchronized SIM traces. The overstroke aggregation conditions for this reference statistical average are the same used in the analysis in the preceding sections. With V_n denoting variability and A_{all} denoting the total aggregate value, then:

$$V_n = (A_{max} - A_{min})/A_{all} \tag{2}$$

The following sections examine the variability of overstroke peak amplitude and duration across the ranges of frequency and reference level.

5.2.4.1. Variability Across the Frequency Range

Figures 42 to 44 show the variability of the mean, standard deviation and RMS peak amplitude for the range of test frequencies. Neither the mean nor the RMS statistical average has a clearly discernible trend with respect to either frequency or reference level. The variability curves for these averages follow seemingly random patterns bounded between 0.2 and 1.2 for the mean and between 0.18 and 0.8 for the RMS. The variability curves for the standard deviation also seem essentially random, but there is an

apparent trend by which the variability value and the bound interval of the variability decrease as the reference level decreases across the frequency range. We have no insight into this pattern of the standard deviation variability.
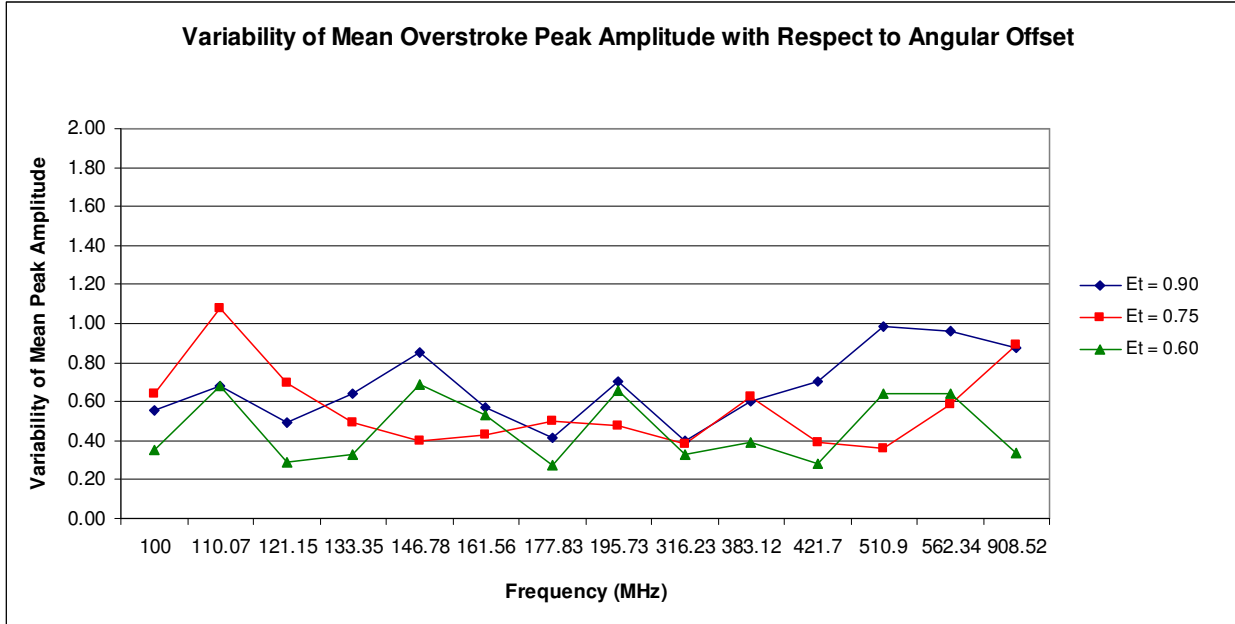

Figure 42: Variability of mean overstroke peak amplitude for the range of test frequencies
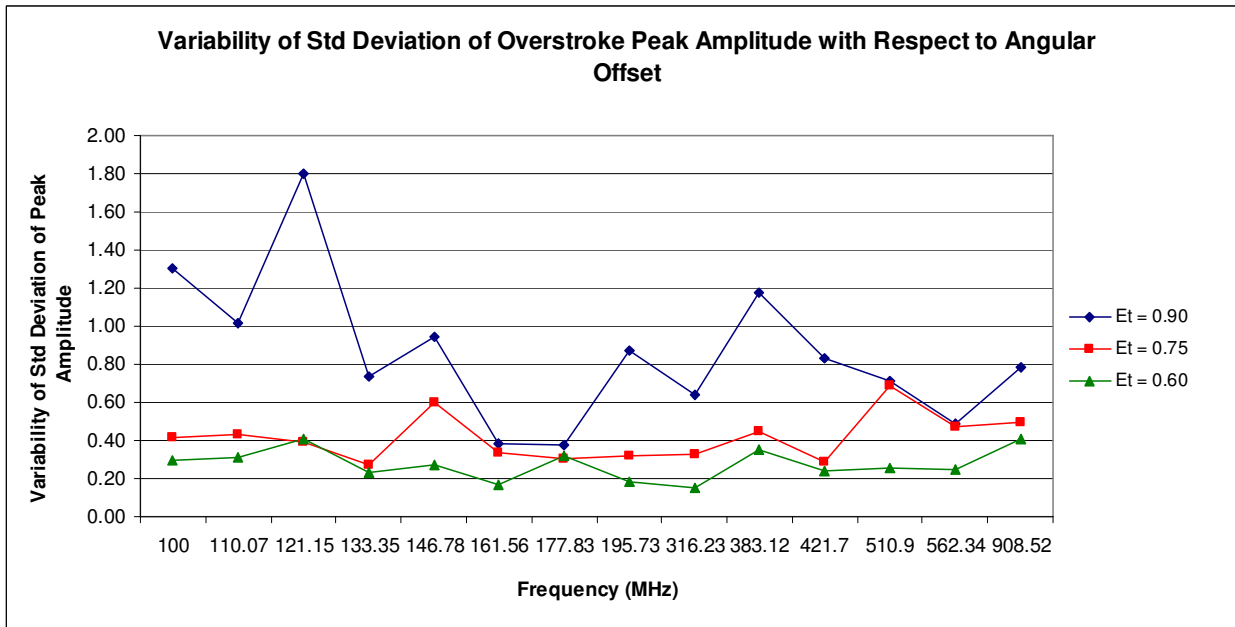

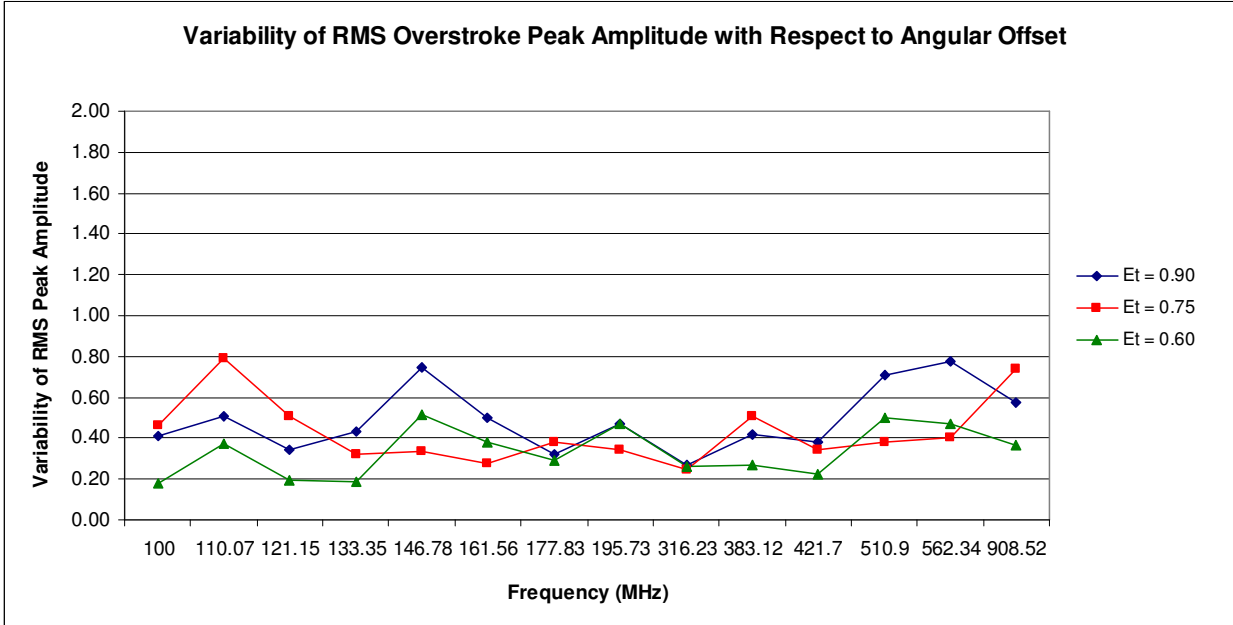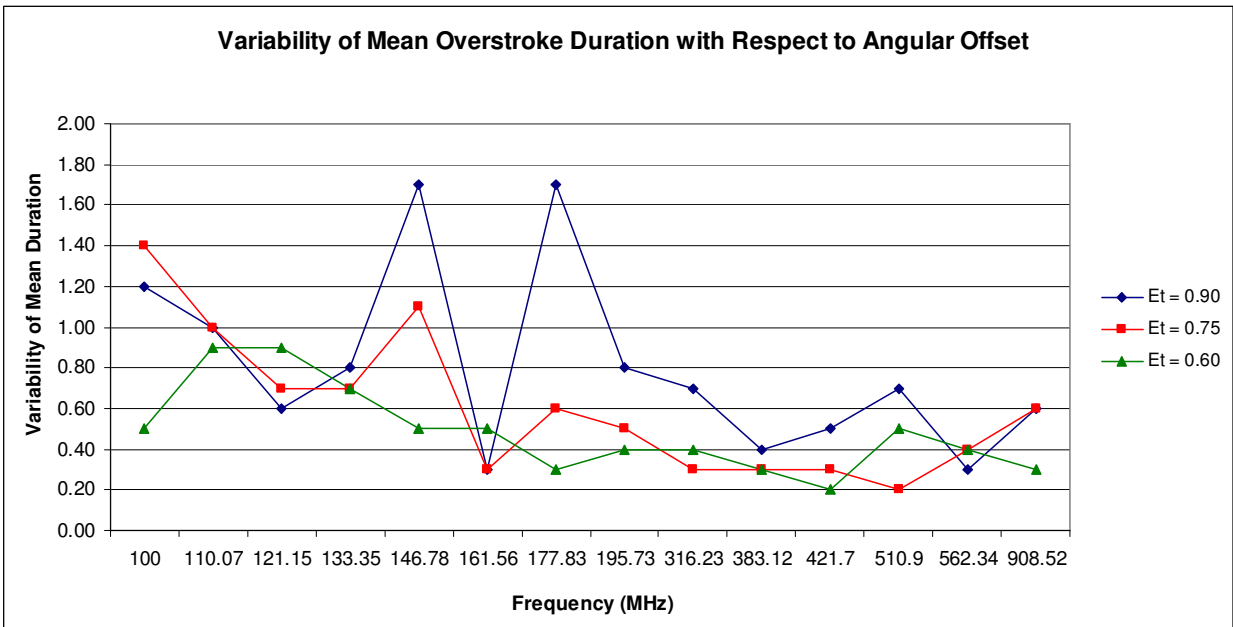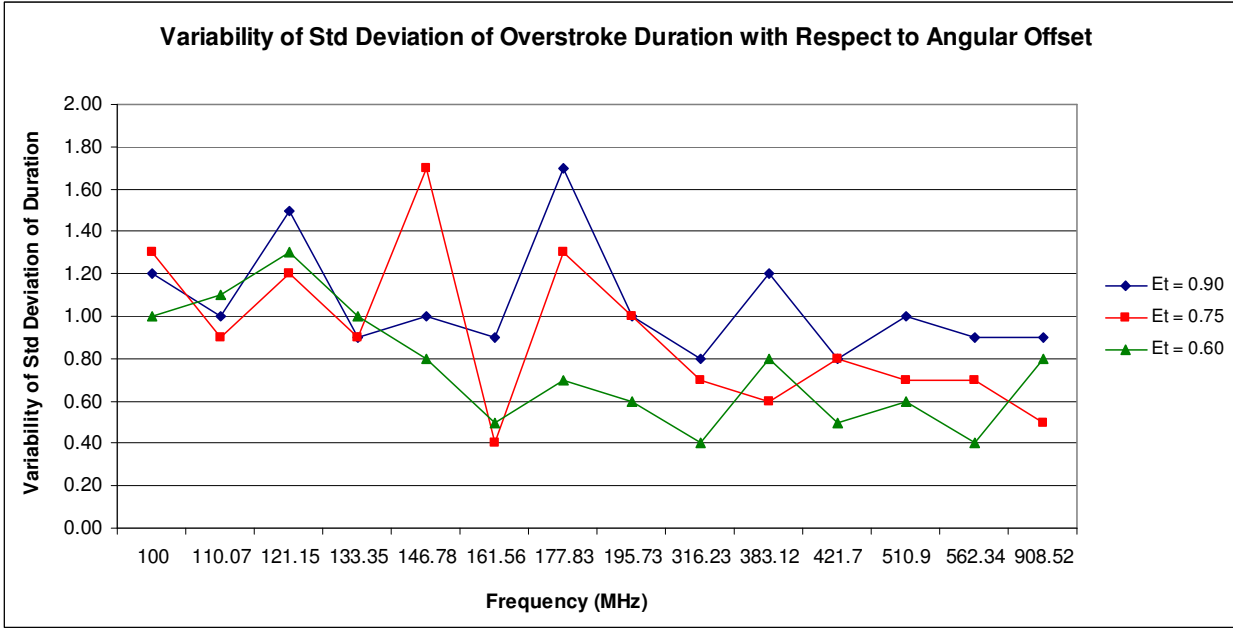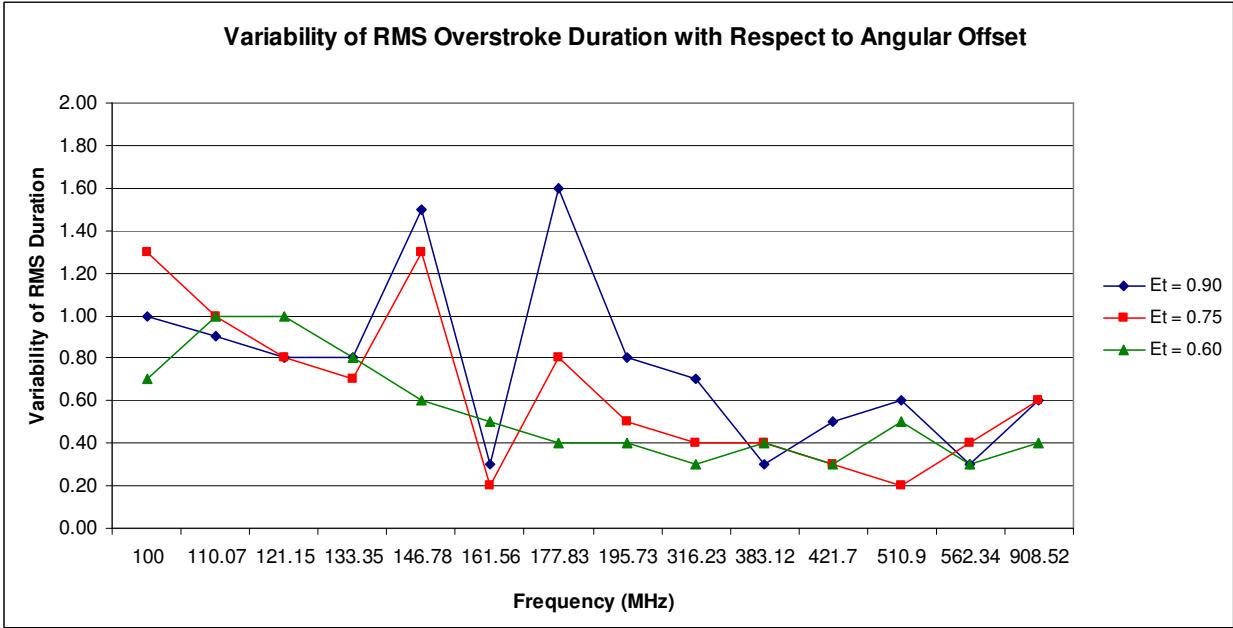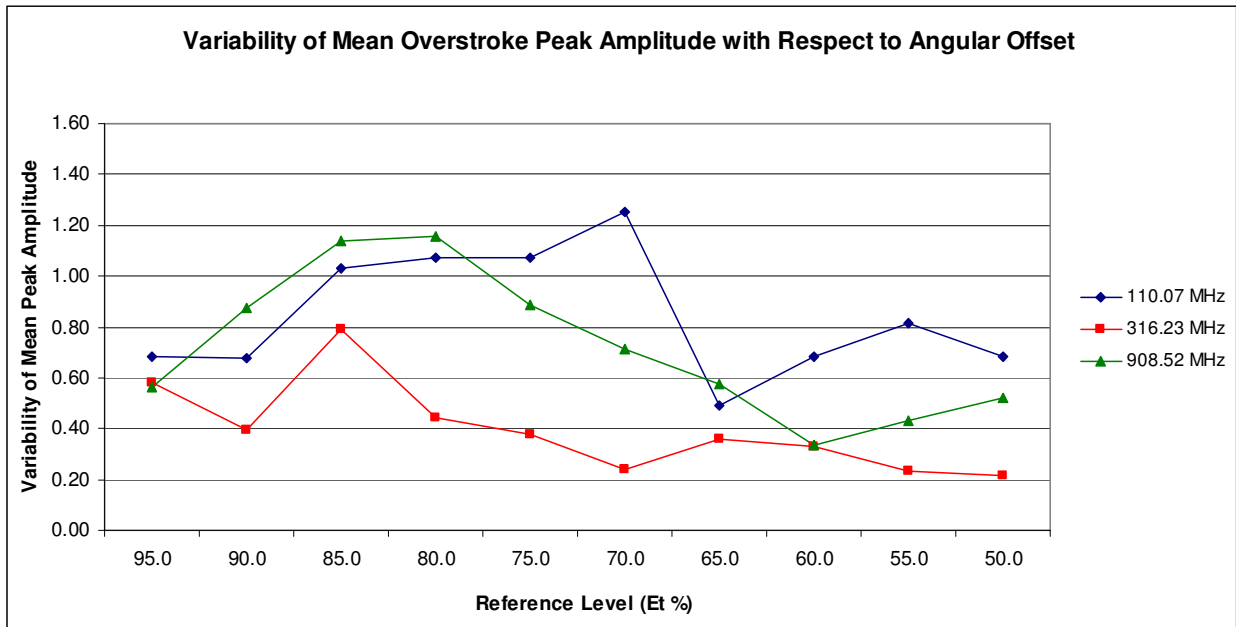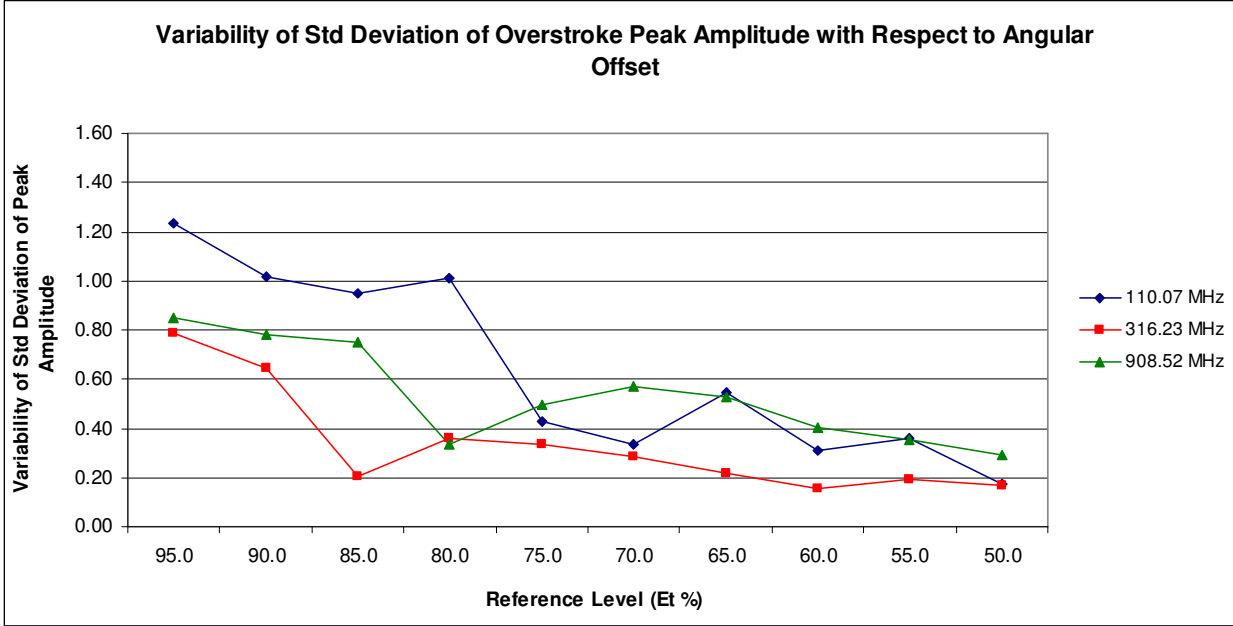Figure 43: Variability of the standard deviation of overstroke peak amplitude for the range of test frequencies

Figure 44: Variability of the RMS peak amplitude for the range of test frequencies

The variability of the mean, standard deviation and RMS overstroke duration for the range of test frequencies are shown in Figures 45 to 47. None of the figures shows a clear trend of the variability with respect to the reference level. However, although there is a lot of variation across the frequency range, there seems to be a pattern of decreasing variability as the frequency increases for all the statistical averages. This patterns expands the trends observed previously, which show the duration to vary over an increasingly small range as the frequency increases.
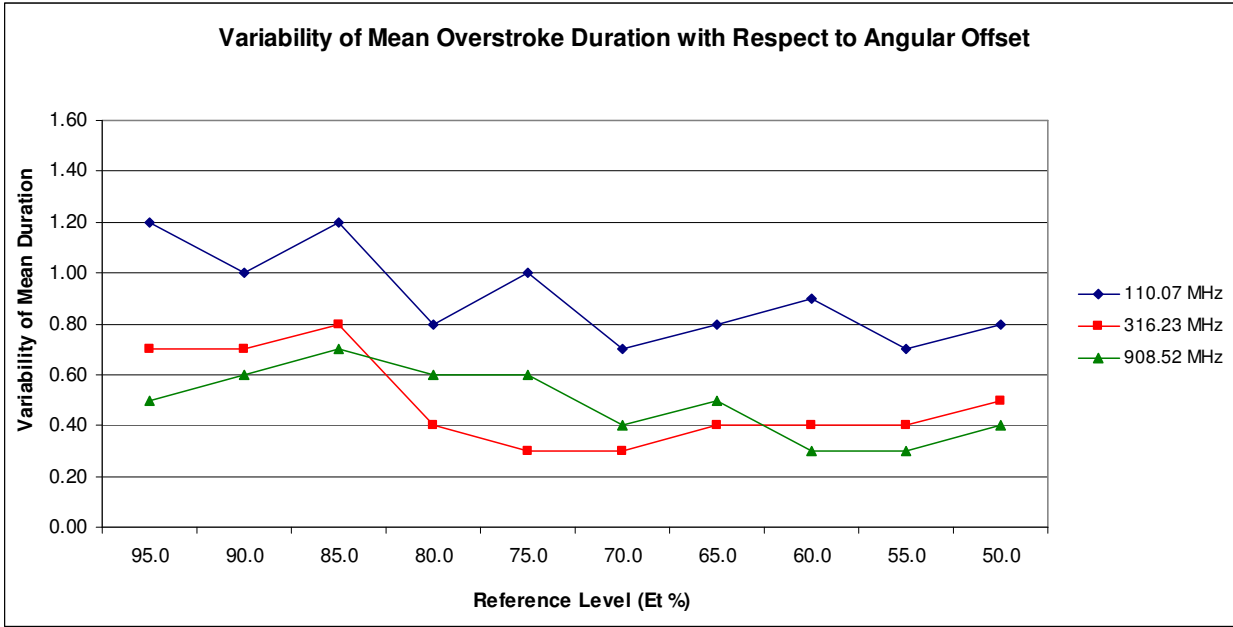

Figure 45: Variability of mean overstroke duration across the range of test frequencies
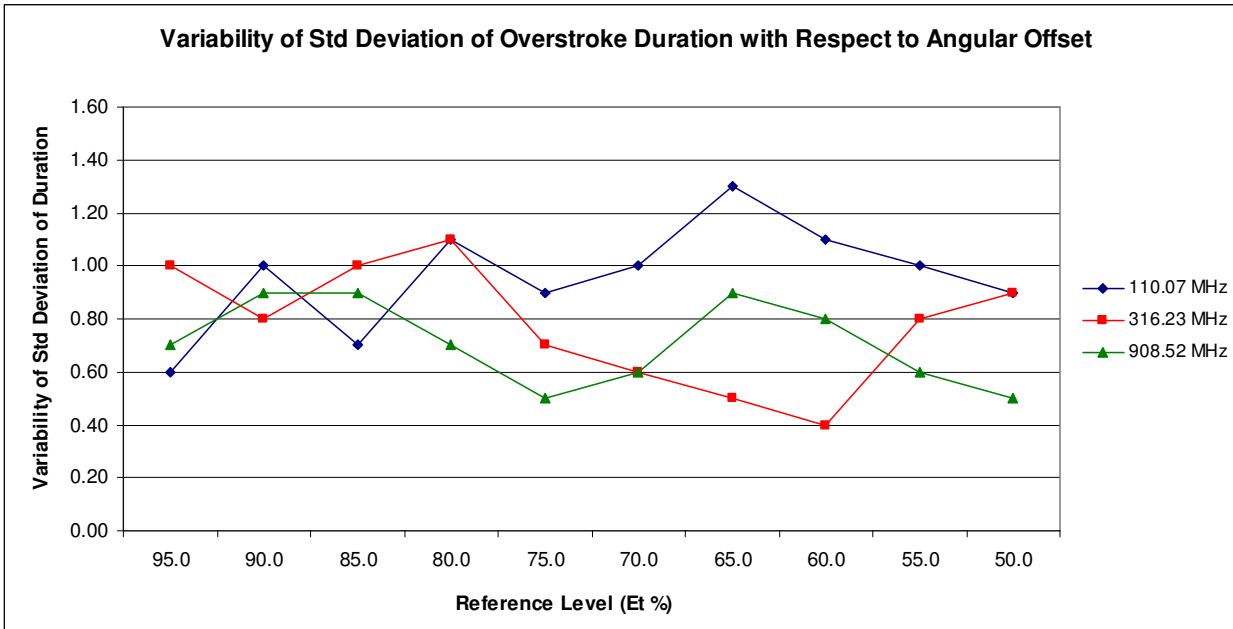
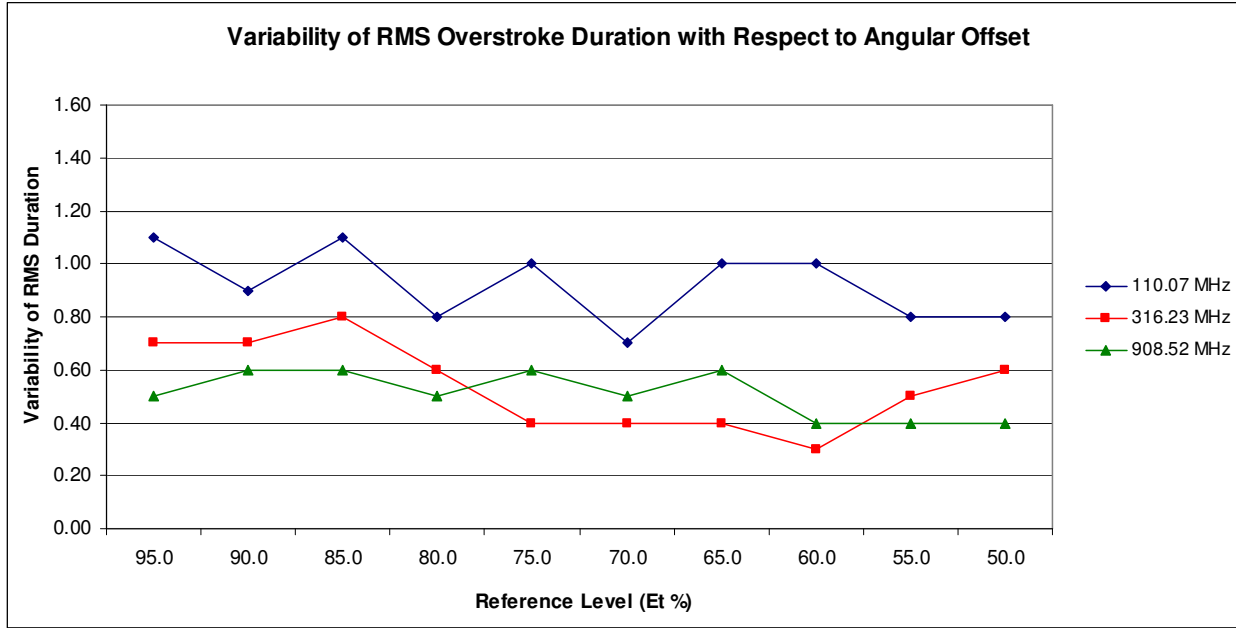Figure 46: Variability of the standard deviation of overstroke duration across the range of test frequencies

Figure 47: Variability of RMS overstroke duration across the range of test frequencies

5.2.4.2. Variability Across the Reference-Level Range

Figures 48 to 50 show the variability of the mean, standard deviation and RMS overstroke peak amplitude across the range of reference levels. The variability of the mean is contained between 0.2 and 1.3 for all the frequencies. There appears to be a common convex interval in the variability of the mean between the reference levels of 95.0% and around 65.0%, but this could be a coincidence and we have no insight into what this curve feature represents. Additionally, notice that the variability of the standard deviation decreases as the reference level decreases, which induces a slightly similar decreasing pattern on the variability of the RMS average.

Figures 51 to 53 show the variability of the averages for the overstroke duration across the range of reference levels. The variability of the mean shows the previously observed general (but not always consistent) trend of decreasing variability as the frequency increases. The most significant information from these figures are the bounds on the variability of between 0.2 and 1.2 for the mean, between 0.4 and 1.4 for the standard deviation, and between 0.3 and 1.1 for the RMS.

Figure 48: Variability of mean overstroke peak amplitude across the range of reference levels

Figure 49: Variability of the standard deviation of overstroke peak amplitude across the range reference levels
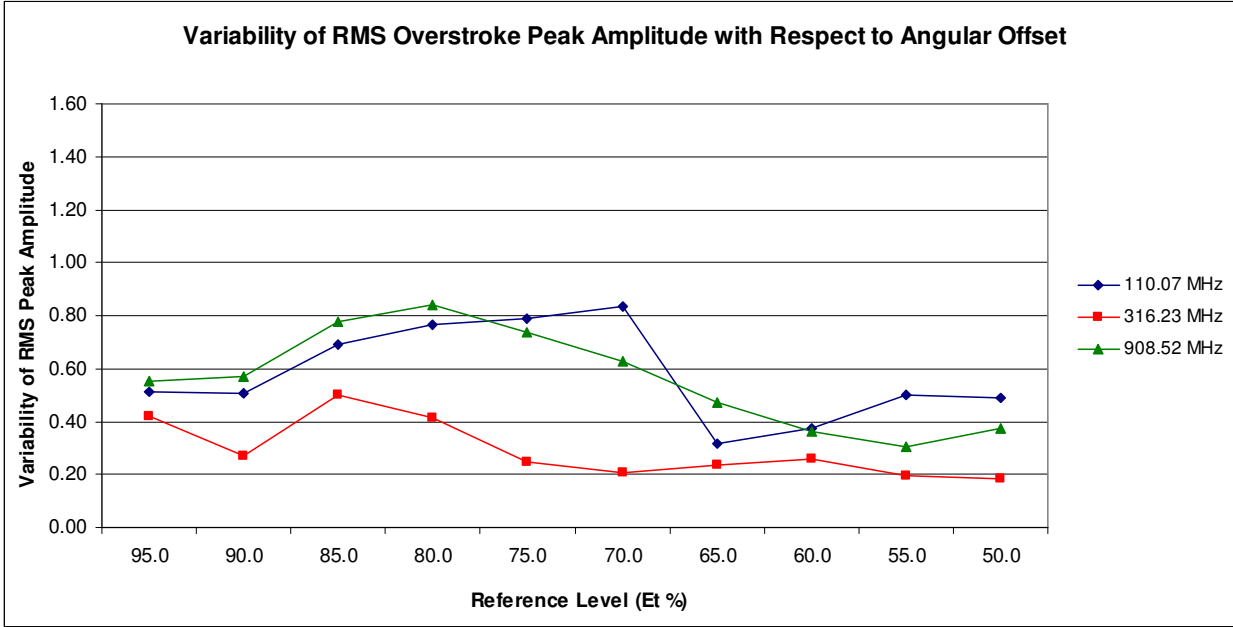
Figure 50: Variability of RMS overstroke peak amplitude across the range reference levels

Figure 51: Variability of mean overstroke duration across the range reference levels

Figure 52: Variability of the standard deviation of overstroke duration across the range reference levels

Figure 53: Variability of RMS overstroke duration across the range reference levels

5.3.   Agregated Overstrokes for Mean HSTC Node Susceptibility Threshold Profile

As described in a previous section, in the HEC experiment, the SUTs were exposed to radiation bursts at nominal field over-strengths of 0, 10 and 20 V/m at each test frequency. If we aggregate overstrokes over the frequency range, the HEC experiment can be modeled as a stimulus-response experiment in which the field over-strength is the primary controlled variable of the stimulus and variables like test frequency, stirrer angular offset and revolution are secondary variables. In this section, we consider the SIM overstroke populations aggregated over the frequency range using the HSTC susceptibility thresholds to specify the overstroke reference-level profile.

Figure 54 shows the measured susceptibility threshold results in the HSTC experiment for the eight physical nodes tested [3]. The figure shows the test frequencies at which none of the nodes experienced detectable susceptibility at or below nominal field strength of 300 V/m. In the following analysis, we determine the overstroke reference level by using the mean susceptibility threshold at the frequencies with demonstrated susceptibility. This HSTC mean-susceptibility-threshold profile is given in Figure 55, where the frequencies at which no susceptibility was observed have been removed from the set. The remaining frequencies shown in Figure 55 are also the ones listed in Table 1. Let E_t denote the susceptibility threshold at a particular frequency and E_{OS} denote the nominal overstroke over-strength. The normalized overstroke reference level, denoted S_T, is then computed as follows:

$$S_T = E_t/(E_t + E_{OS}) \tag{3}$$

Figure 56 shows the overstroke reference-level profiles for the nominal over-strengths. These reference levels were applied to the SIM waveforms across the frequency range to generate aggregate overstroke sets for each over-strength level. We analyze these overstroke sets by first considering their spread over the space of peak amplitude and duration. We then examine the set statistics for the overstroke features of peak time duration, peak over duration, peak and duration.
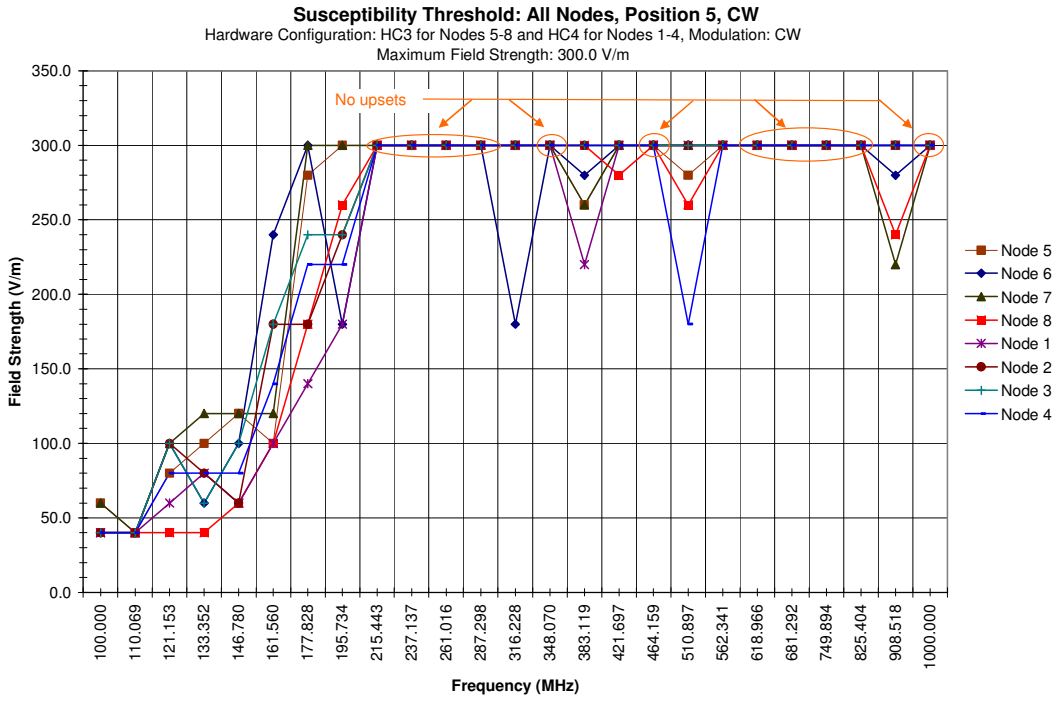
Figure 54: Measured susceptibility thresholds in the HSTC experiment for the full set of physical nodes
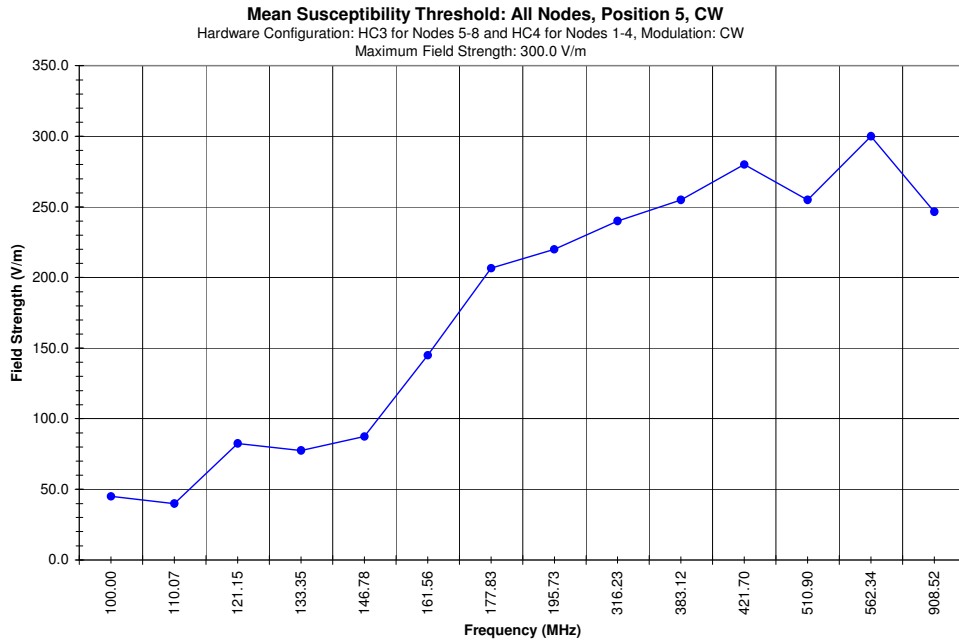

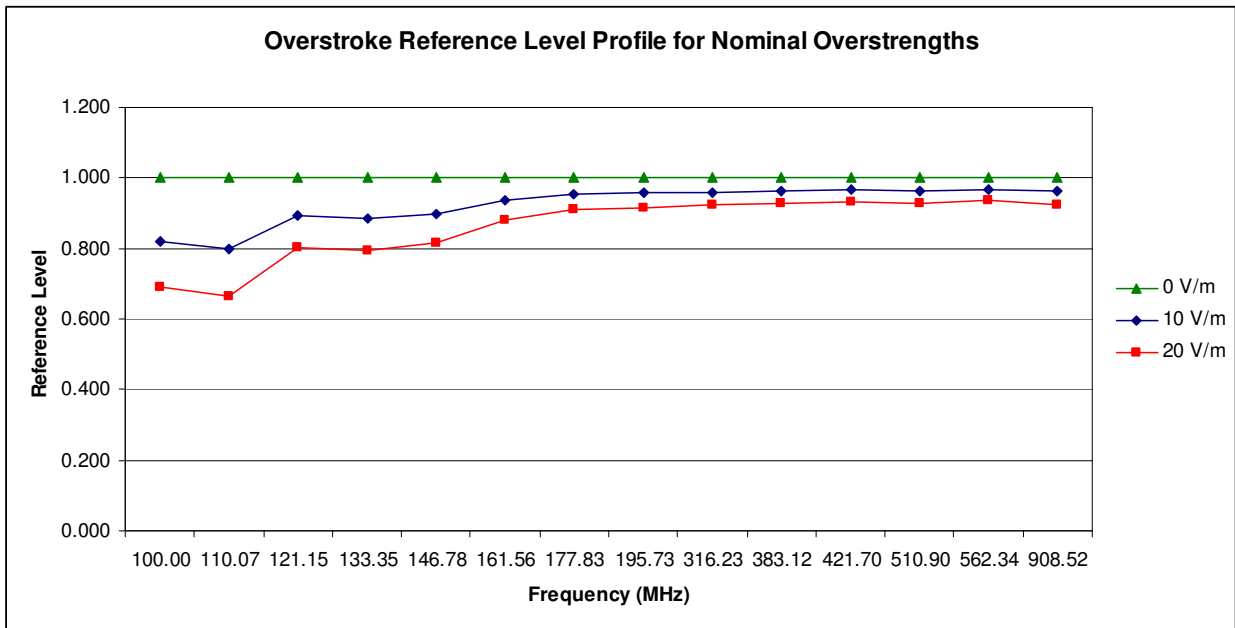Figure 55: Mean HSTC node susceptibility thresholds for the set of test frequencies

Figure 56: Reference levels across the frequency range for the nominal overstroke over-strengths

5.3.1. Population Spread

The number of overstrokes at each over-strength level is shown in Figure 57. Interestingly, the overstroke count increases linearly in this over-strength range, with about 1740 additional overstrokes for every 10 V/m step in nominal over-strength. This is not completely surprising when we consider that, based on Figure 20, at most frequencies the relation between overstroke count and reference level is approximately linear, and that the counts in Figure 57 are the result of a sum of overstrokes across the frequency range with the contribution at each frequency determined by the reference level profiles in Figure 56.
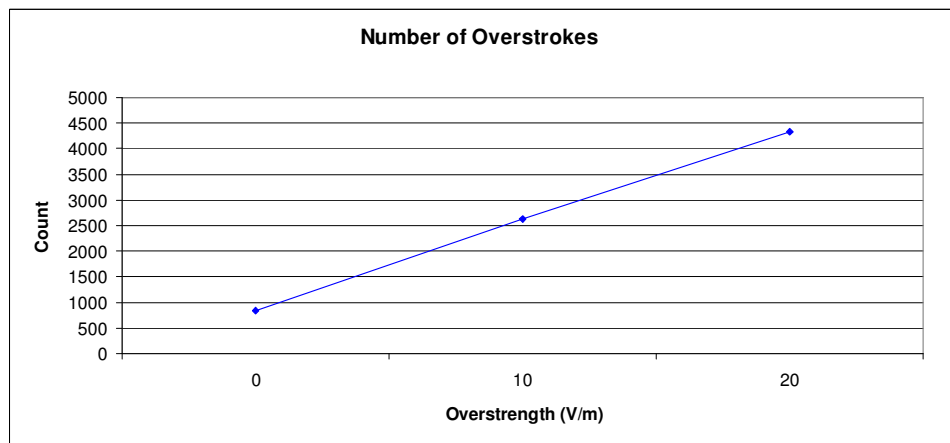
Figure 57: Number of overstrokes for the range of over-strength values

Figure 58 shows the scatter plots of overstroke peak amplitude and duration. Compared to the plots in Figures 21 to 23, the overstrokes in Figure 58 have a larger and more uniform range of coverage, especially within the area for overstrokes of less than 0.20 peak amplitude and 150 ms duration. Notice in Figure 58 that as the over-strength decreases, the overstroke set for a lower over-strength seems to be a subset of the overstroke set at the next higher over-strength. Increasing the over-strength simply increases the overstroke spread to a larger area that includes the area covered by overstrokes at lower over-strength.
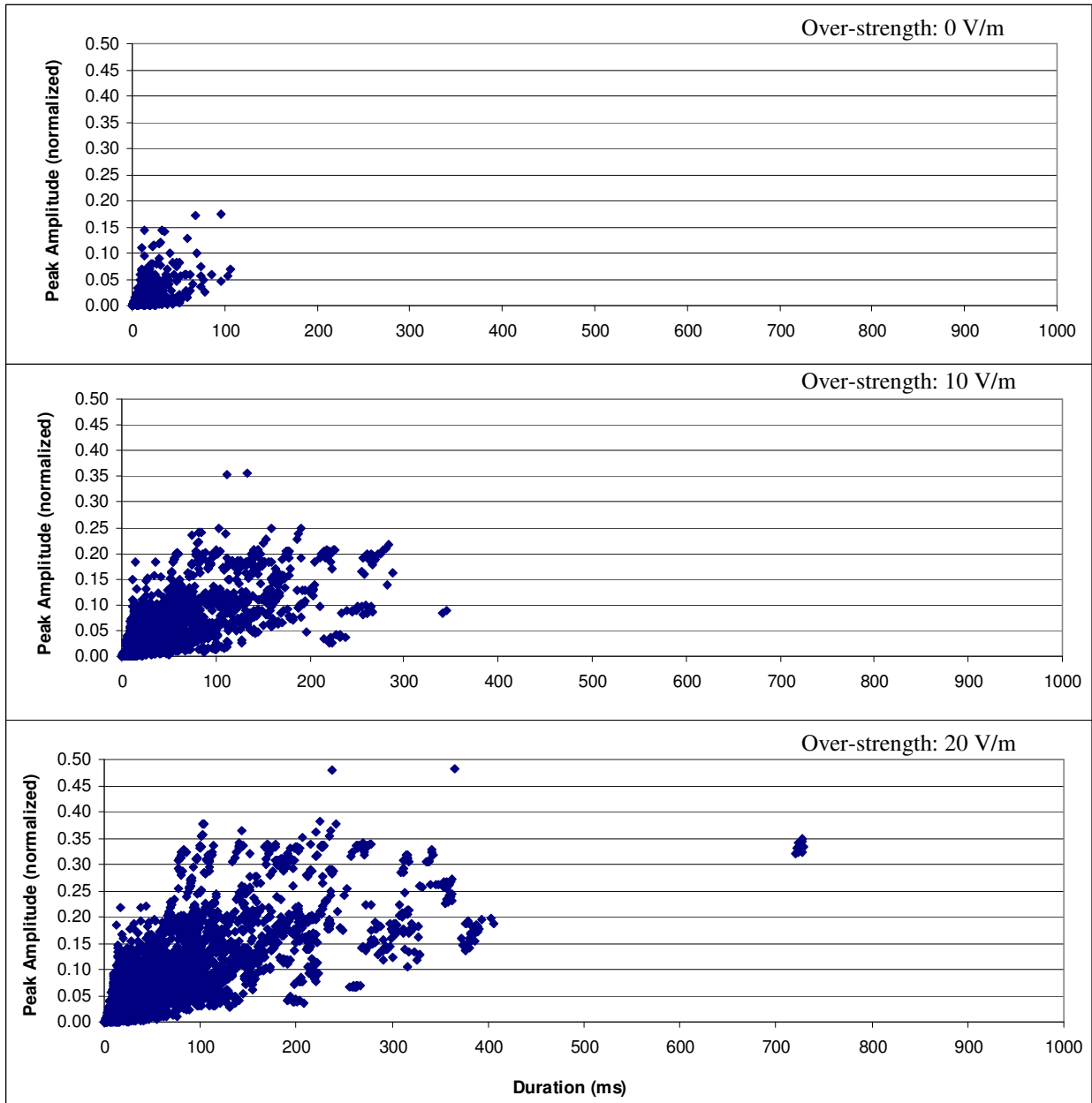
Figure 58: Scatter plots of overstroke peak amplitude versus duration for the set of over-strength values

5.3.2. Statistics of Overstroke Features for the Range of HEC Nominal Overstrengths

We now consider the set averages, including mean, standard deviation and RMS, for the overstroke features of peak amplitude multiplied by duration, peak amplitude divided by duration, peak amplitude and duration.

5.3.2.1. *Peak Amplitude Multiplied by Duration*

The set averages of the overstroke normalized peak amplitude multiplied by duration (in ms) for the range of nominal over-strength levels are shown in Figure 59. The RMS value is clearly driven by the standard deviation, which is about twice as large as the mean across the over-strength range. The standard deviation grows faster than linear relative to the over-strength because of the simultaneous increase in the spread of the basic overstroke dimensions of peak amplitude and duration for larger over-strength, as can be seen in the scatter plots in Figure 58. The relatively small value of the mean is related to the high density clustering of overstrokes at the low end of the peak amplitude and duration where, as seen in Figure 58, the area coverage is also very high compared to other areas of the plots.
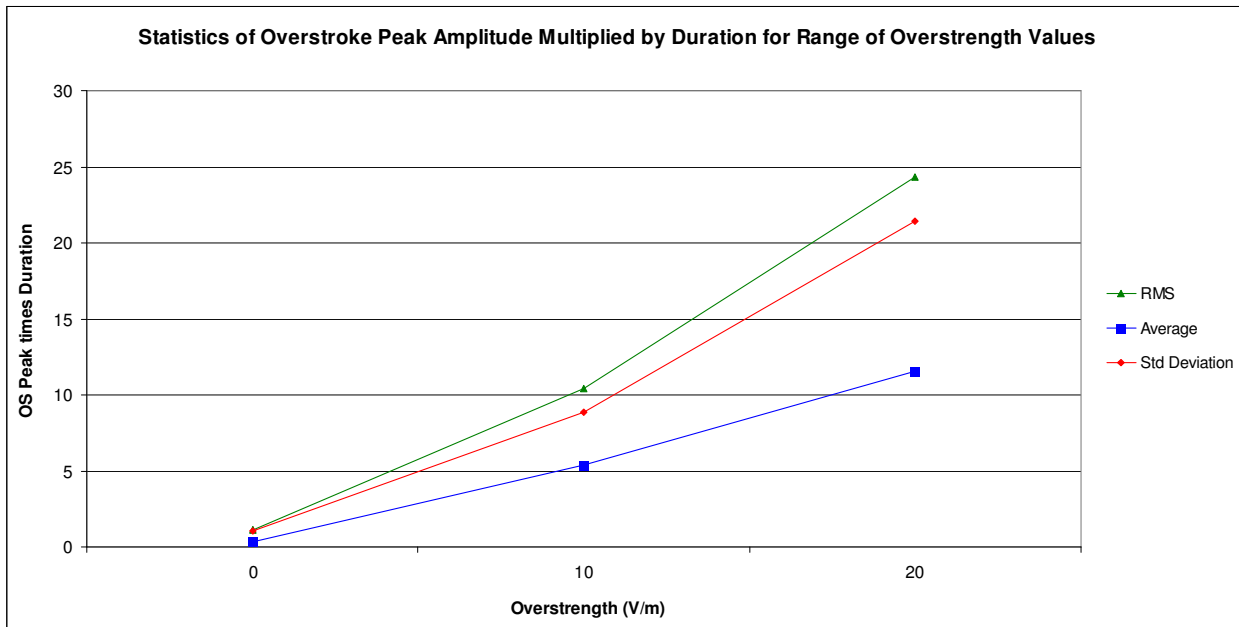
Figure 59: Averages of the overstroke peak amplitude multiplied by the duration for the range of over-strength values

5.3.2.2. *Peak Amplitude Divided by Duration*

Figure 60 shows the statistical averages for the overstroke peak amplitude divided by the duration for the range of over-strengths. The sub-linear increase in the mean is an indication that the overstroke duration increases faster than the peak amplitude as the over-strength increases. The standard deviation increases by a small amount from one end to the other of the over-strength range, but it actually decreases slightly in going from 0 to 10 V/m. From comparing the curves in Figures 37 and 40, we suspect that this trend in the standard deviation is the result of the interplay between the standard deviations of the peak amplitude and the duration as the reference level decreases (i.e., as the over-strength increases). Another possibility is that the values at 0 V/m (i.e., 100% reference level) are not representative of overstrokes

generated by the full set of available SIM waveforms because those with absolute peak amplitude smaller than the normalizing median peak amplitude do not contribute overstrokes to the 0 V/m set. Further analysis would be required to explain the pattern in Figure 60. Finally, the RMS profile is mainly determined by the mean value.
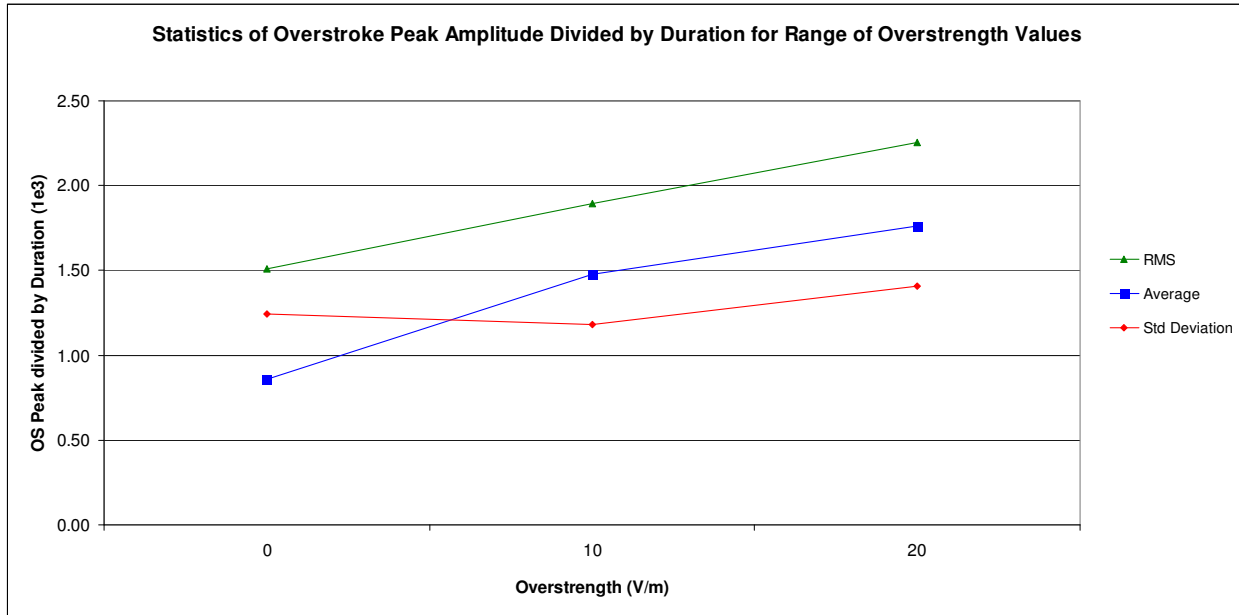
Figure 60: Averages of the overstroke peak amplitude divided by the duration for the range of over-strength levels

5.3.2.3. *Peak Amplitude*

The statistical averages of the overstroke peak amplitude across the over-strength levels are shown in Figure 61. The pattern of these curves is consistent with the plots of peak amplitude averages versus reference level in Figures 36 to 38. An interesting feature of the statistical mean in Figure 61 is the reduction in the rate of increase as the over-strength increases. This trend may be related to the slower rate of increase of the peak amplitude as the reference level decreases for high frequencies, as shown in Figure 36. However, more in-depth analysis is needed to gain insight into the cause of this trend.

5.3.2.4. *Duration*

Figure 62 shows the statistical averages for the overstroke duration over the range of over-strengths. The trends for the duration are similar to those for the peak amplitude in Figure 61, though there is a larger reduction in the rate of increase of the mean. Based on the results in Figure 39 to 41, we were expecting the duration averages in Figure 61 to maintain the rate of increase as the over-strength increases. The reduction actually shown in Figure 61 may be related to the reference level profile in Figure 56. Here again, more detailed analysis is needed to understand the cause of this trend.
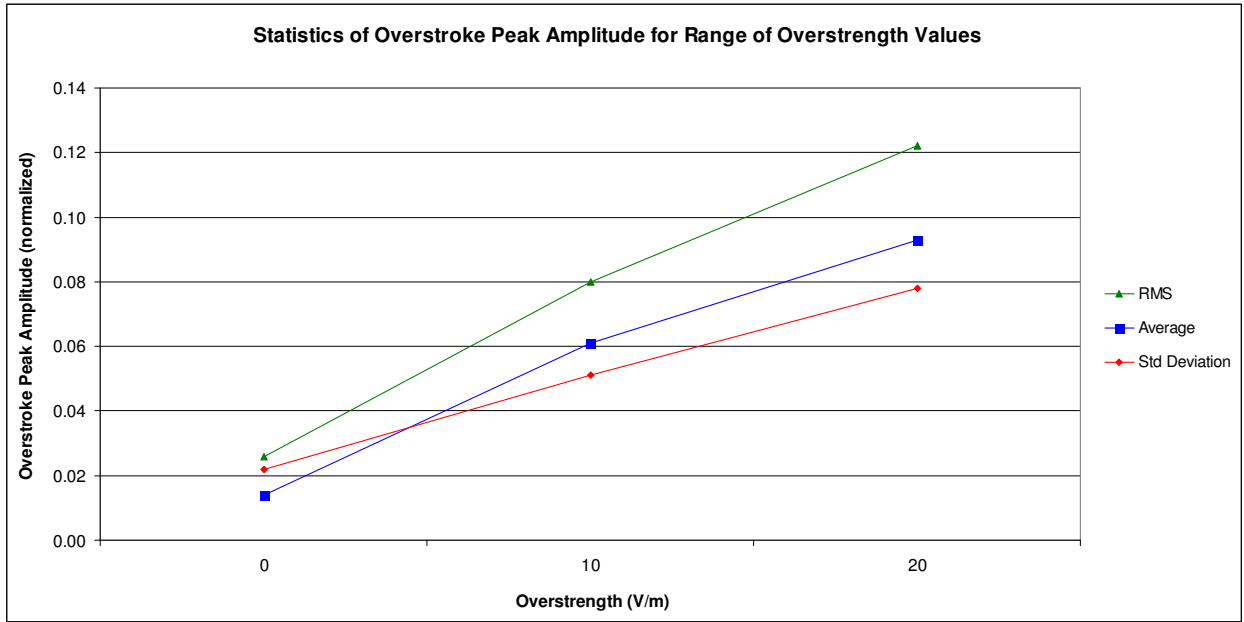
Figure 61: Averages of the overstroke peak amplitude for the range of over-strength levels
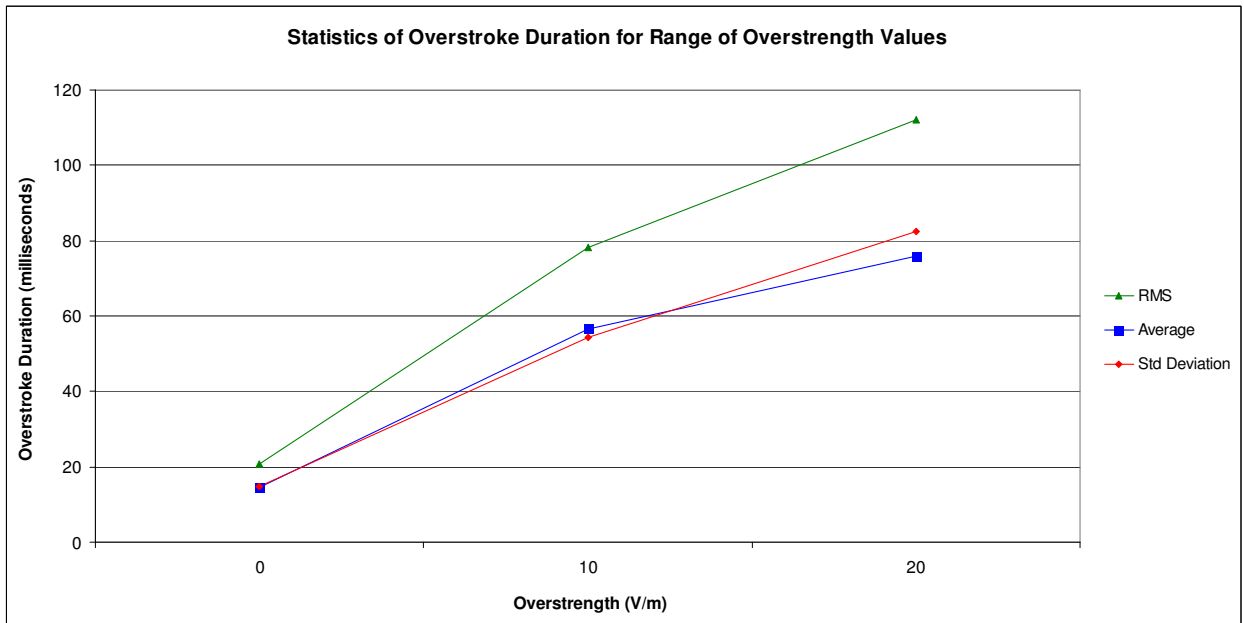
Figure 62: Averages of the overstroke duration for the range of over-strength levels

6. Final Remarks

In this report, we have analyzed the radiated field strength in an electromagnetic reverberation chamber as an upset-inducing stimulus for digital systems. It has been shown that, for a given input power and test frequency, the field strength at a point in the chamber varies as a function of the stirrer angular position and relative angular offset between the stirrers, and that it is cyclic with period equal to the time for the stirrers to complete a revolution. We have given strong evidence that the magnitude of the field strength beyond the susceptibility threshold of the SUT has a causal relation with the characteristics of the error bursts observed at the outputs of the SUT. The statistics of the field overstroke features of peak amplitude and duration have been analyzed, and it was shown how the features are dependent on the test frequency and overstroke reference level, which is equal to the ratio of the SUT's susceptibility threshold divided by the peak field strength. We have determined bounds for the differences in the statistical averages of the overstroke features between tests with different stirrer angular offsets. Finally, for a representative susceptibility profile across the test frequency range, it was shown how the statistics of the overstroke features vary as a function of the nominal field over-strength.

The analysis presented here is for field strength measurements taken at the fixed position of the receive antenna in the reverberation chamber, as shown in Figures 1 to 3. At this time, we have no direct evidence that these measurements are applicable to other areas of the chamber. However, the fact that the measured susceptibility thresholds in the HSTC experiment followed a similar profile when the SUTs were located at different positions in the chamber, and the previously measured field strength uniformity given in report [7], both serve as indirect evidence that the results given here apply throughout the test volume of the chamber. We believe that the effect of a change in position is similar to the effect of a change in stirrer angular offset. This may be investigated in future tests.

Appendix A.   Stirrer-Induced Modulation Waveforms

This appendix contains some of the field strength traces gathered during the Stirrer Induced Modulation Test. The traces are given for every test frequency at 0-degree stirrer angular offset and include all the revolution samples taken at intervals of 30 seconds. The traces are amplitude normalized and synchronized.
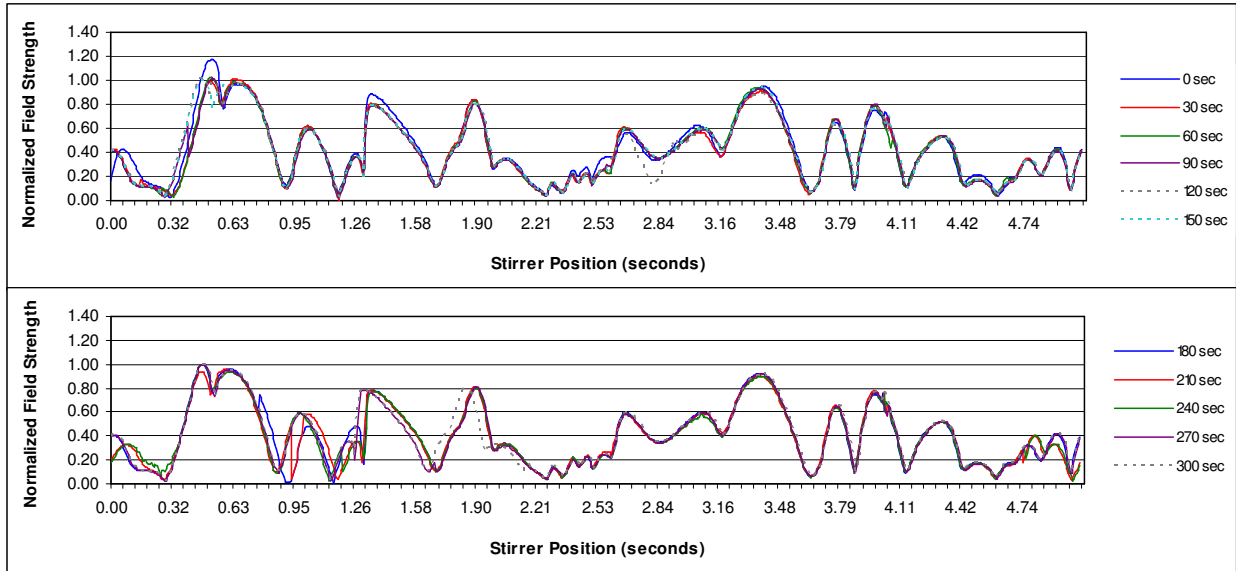
Figure A.1: Stirrer induced modulation at 100.00 MHz
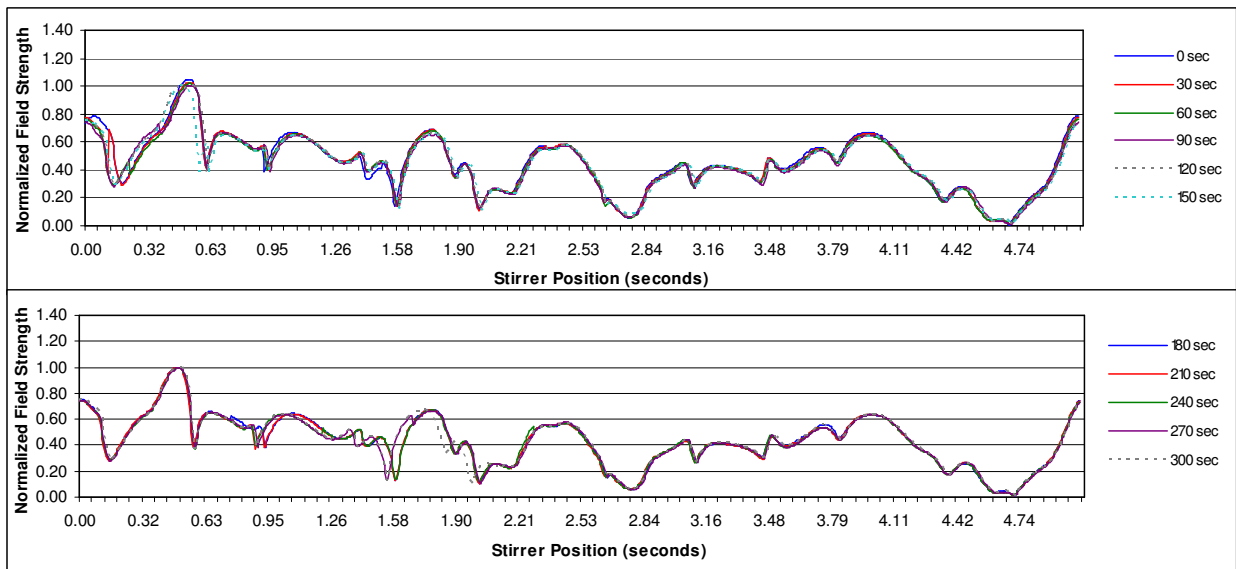
Figure A.2: Stirrer induced modulation at 110.07 MHz
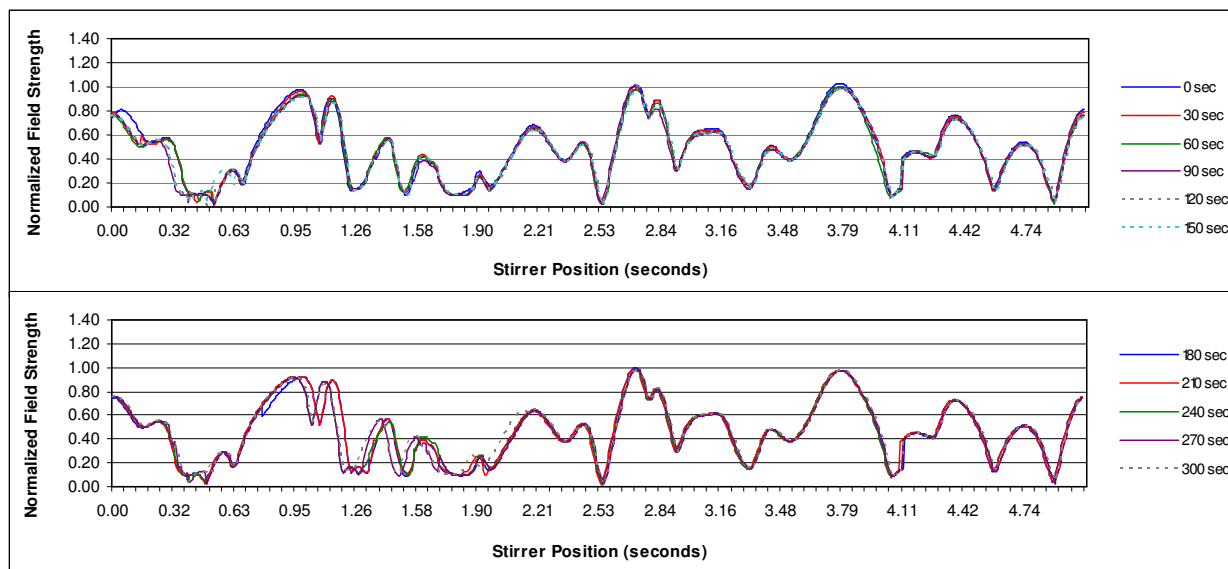
Figure A.3: Stirrer induced modulation at 121.15 MHz
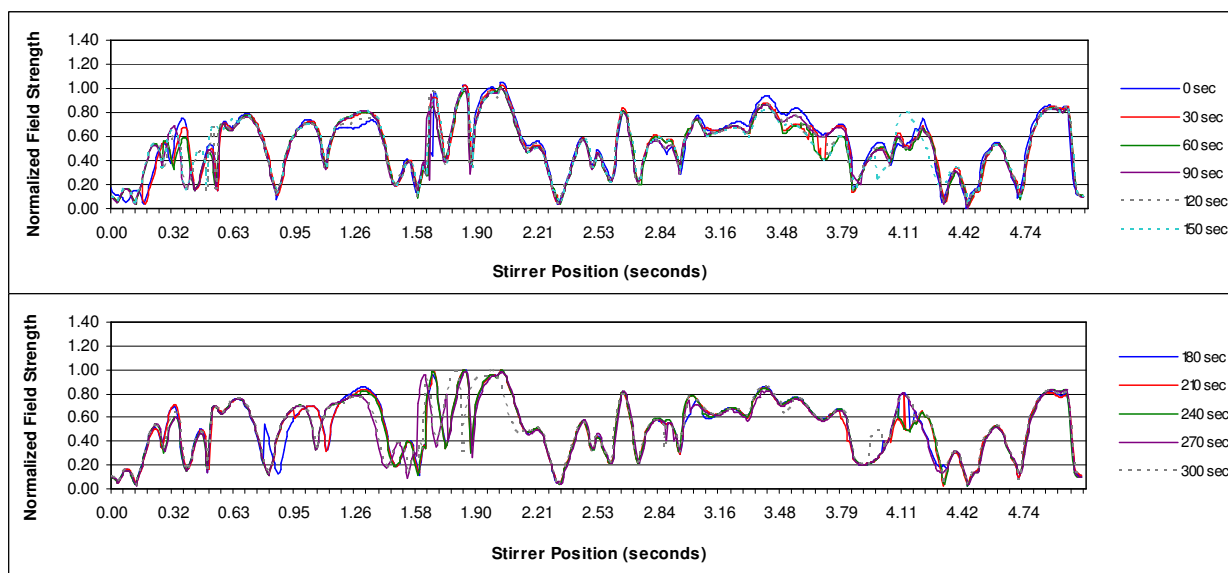
Figure A.4: Stirrer induced modulation at 133.35 MHz
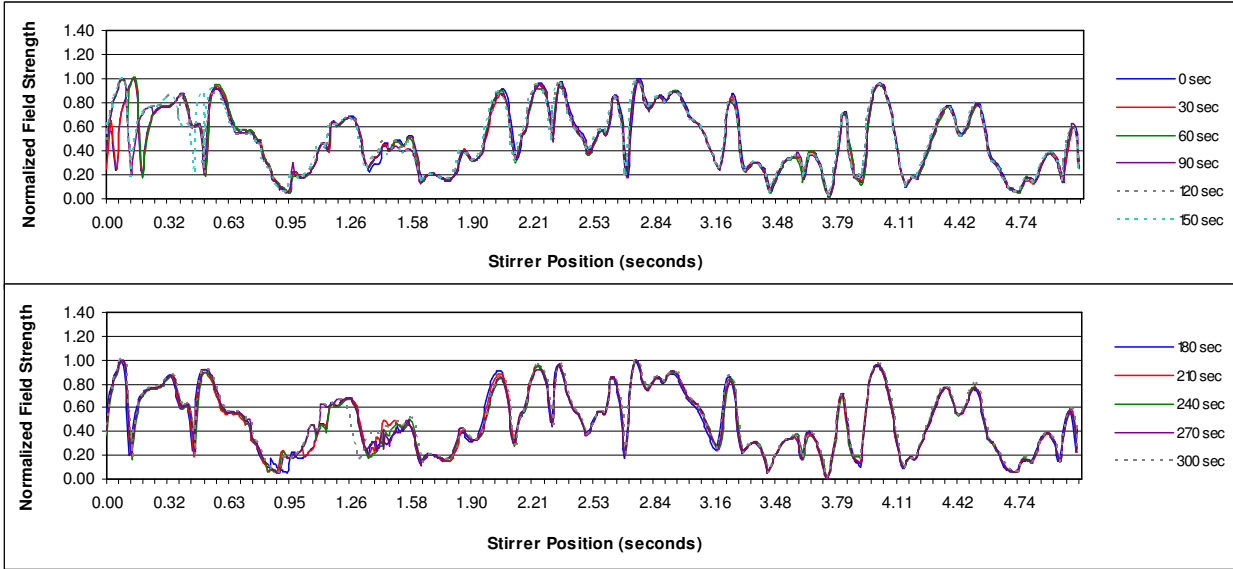
Figure A.5: Stirrer induced modulation at 146.78 MHz
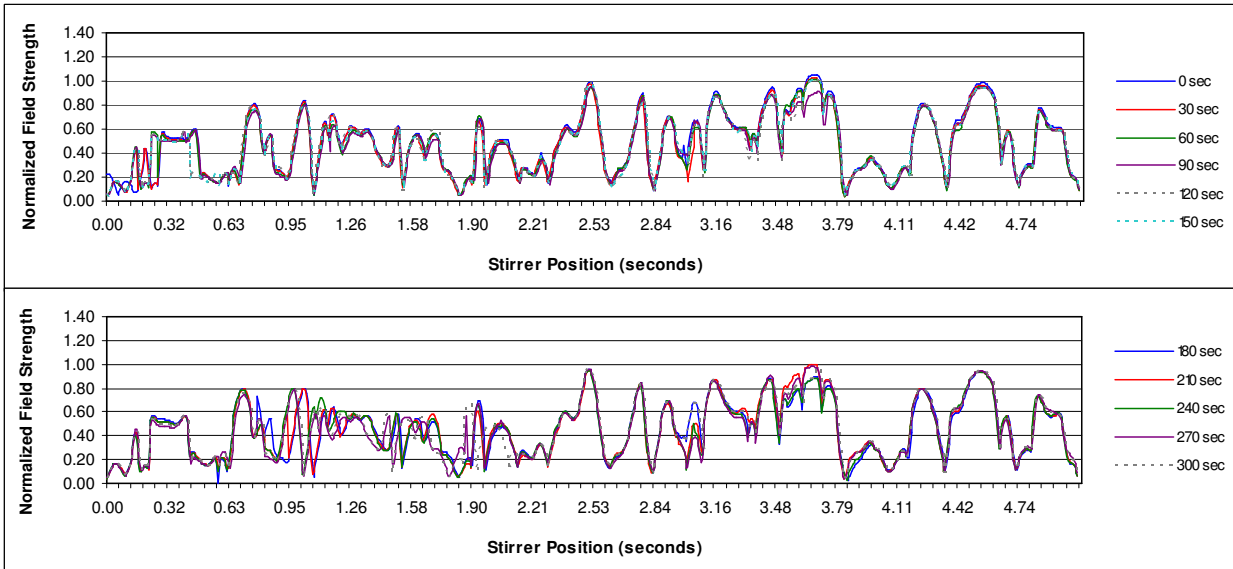
Figure A.6: Stirrer induced modulation at 161.56 MHz
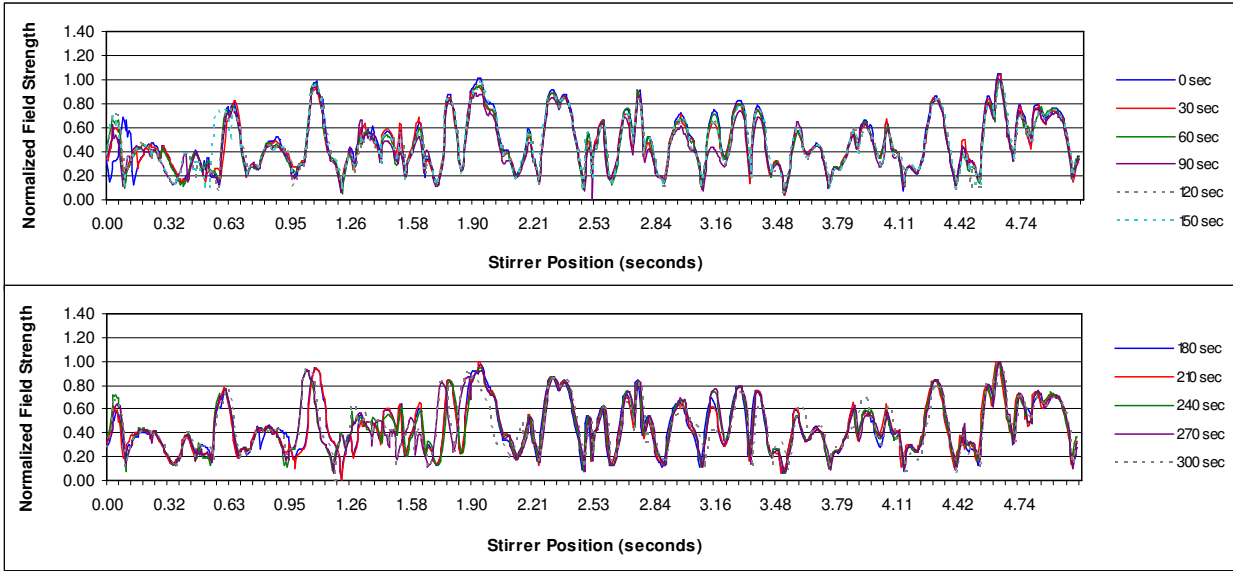
Figure A.7: Stirrer induced modulation at 177.83 MHz
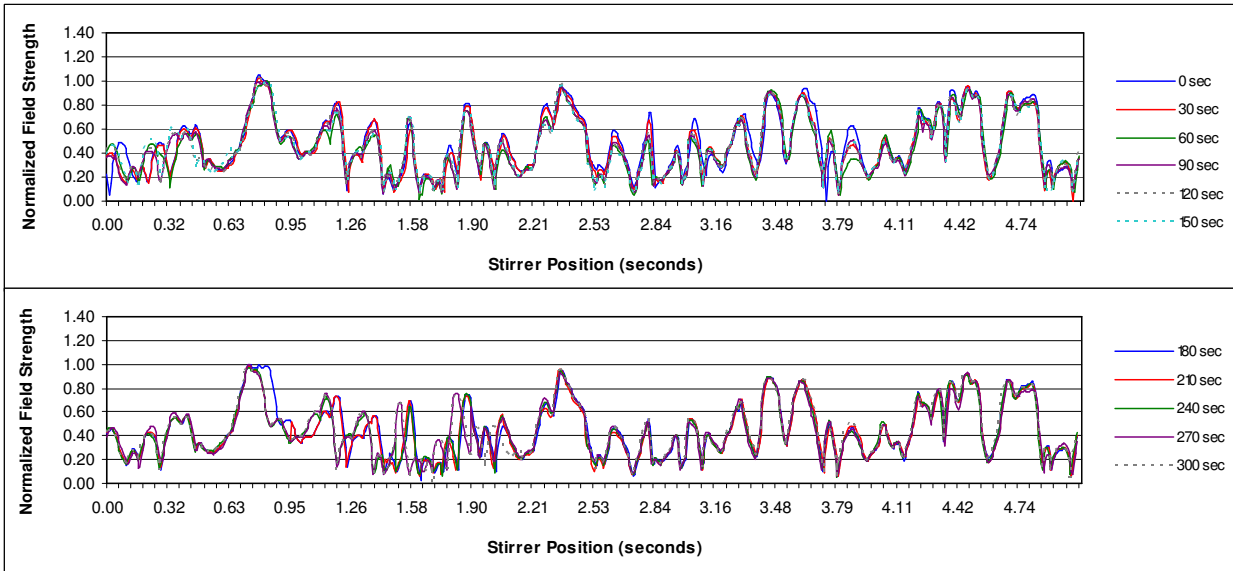
Figure A.8: Stirrer induced modulation at 195.73 MHz
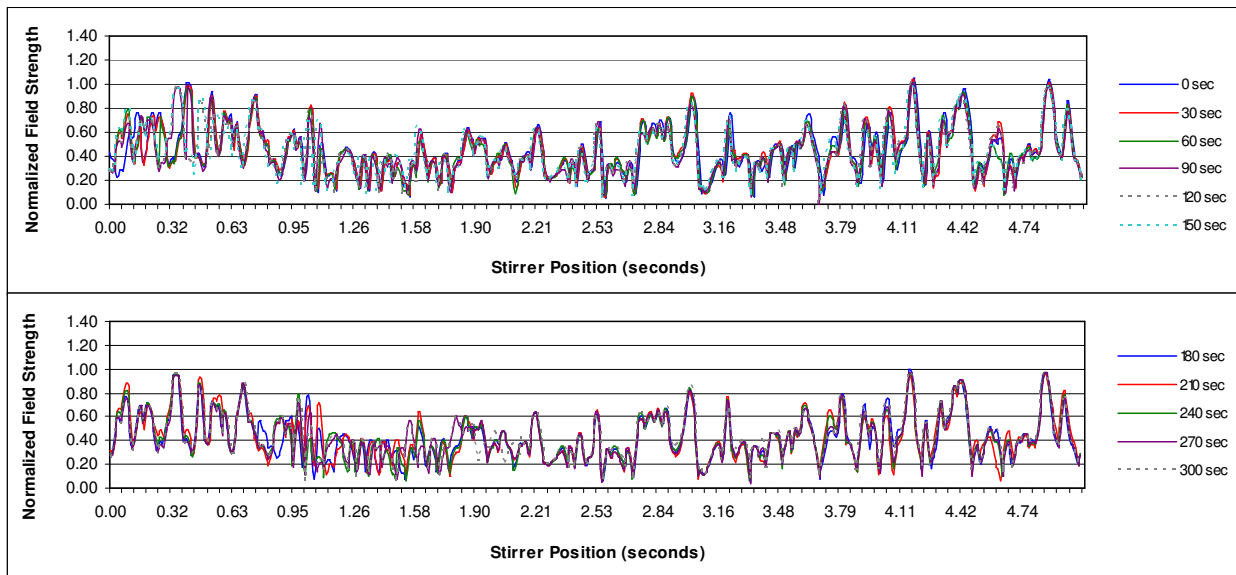
Figure A.9: Stirrer induced modulation at 316.23 MHz
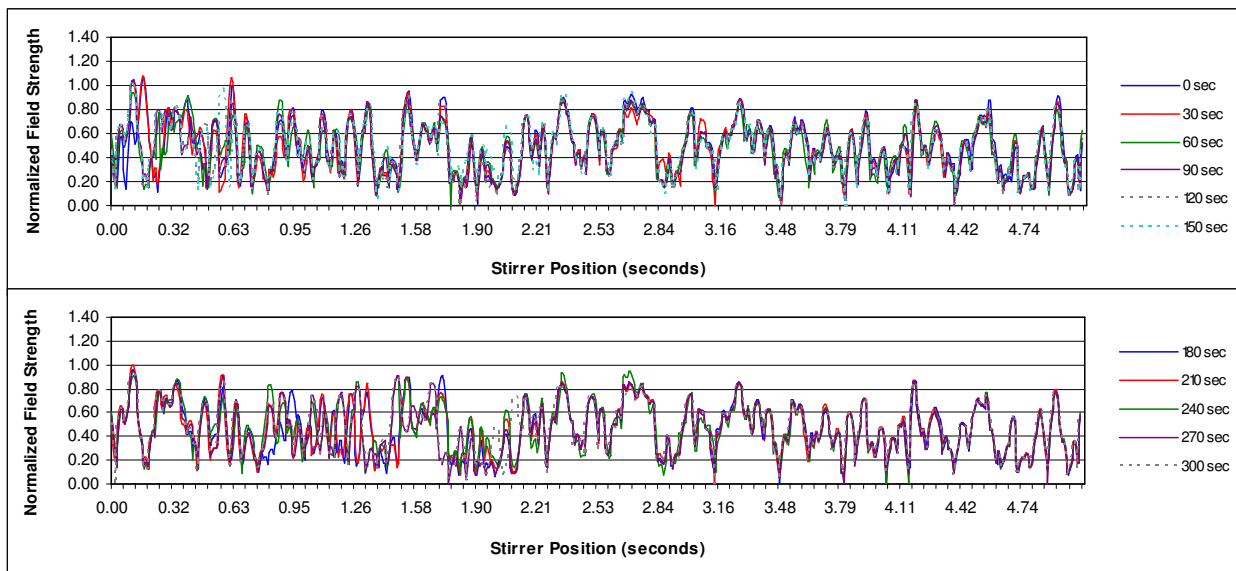
Figure A.10: Stirrer induced modulation at 383.12 MHz
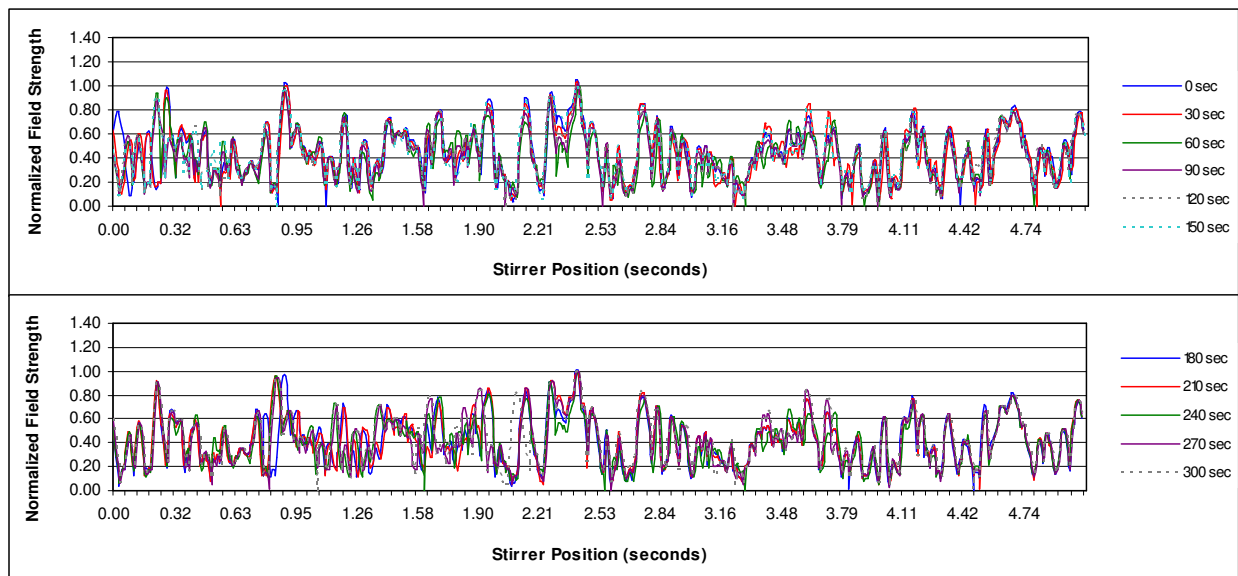
Figure A.11: Stirrer induced modulation at 421.70 MHz
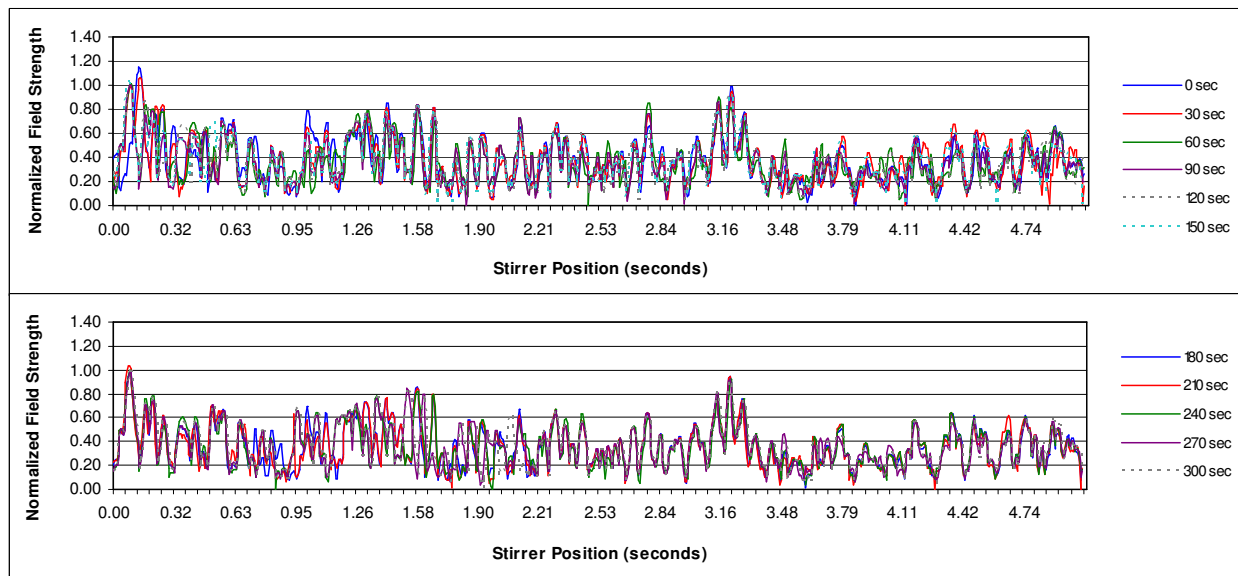
Figure A.12: Stirrer induced modulation at 510.90 MHz
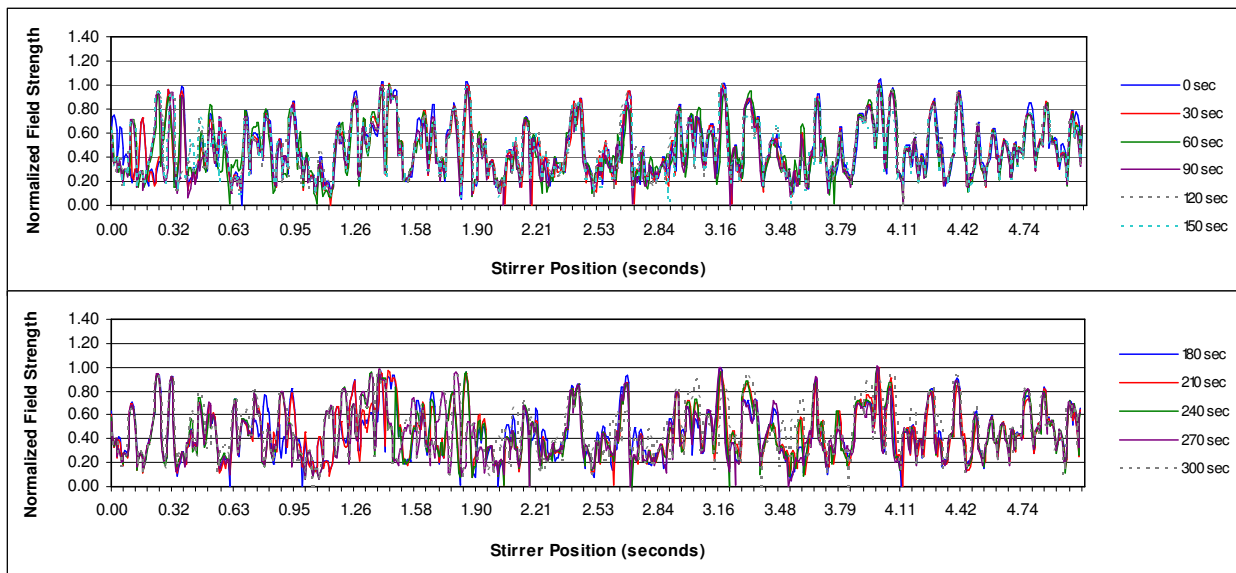
Figure A.13: Stirrer induced modulation at 562.34 MHz
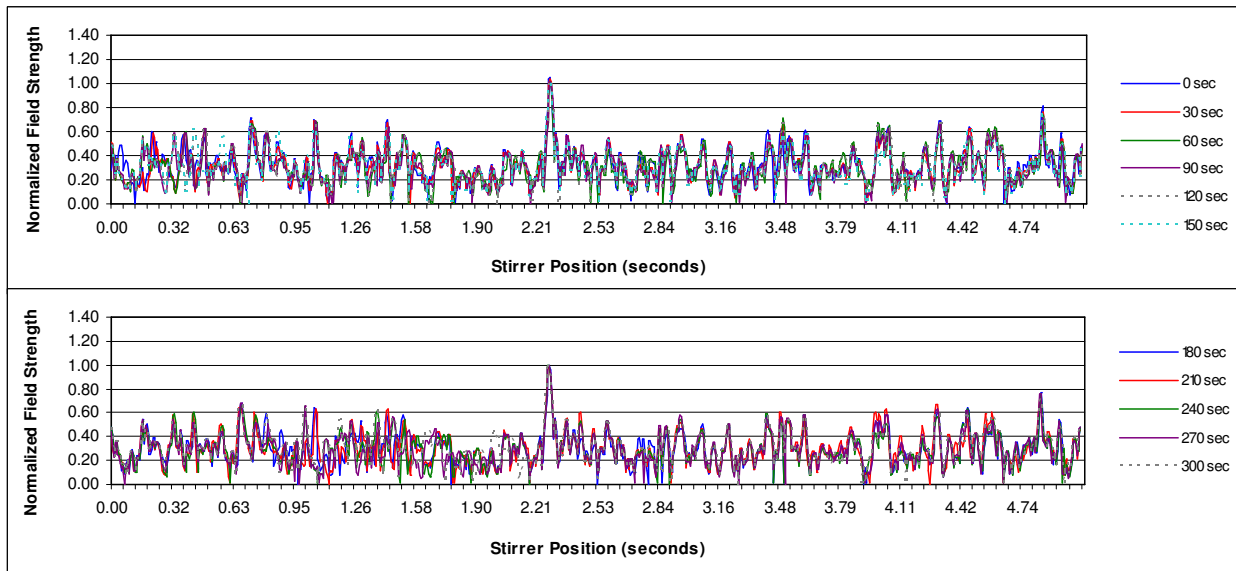
Figure A.14: Stirrer induced modulation at 908.52 MHz

Appendix B.   Overstroke Population at Test Frequencies

This appendix contains scatter plots of overstroke peak amplitude versus duration for the full set of the frequencies at reference levels of 0.90, 0.75, and 0.60. The overstroke sets were formed by aggregation over the range of stirrer angular offsets and revolutions. SIM traces with the same frequency and angular but for different revolutions were not synchronized prior to generation of the overstrokes.
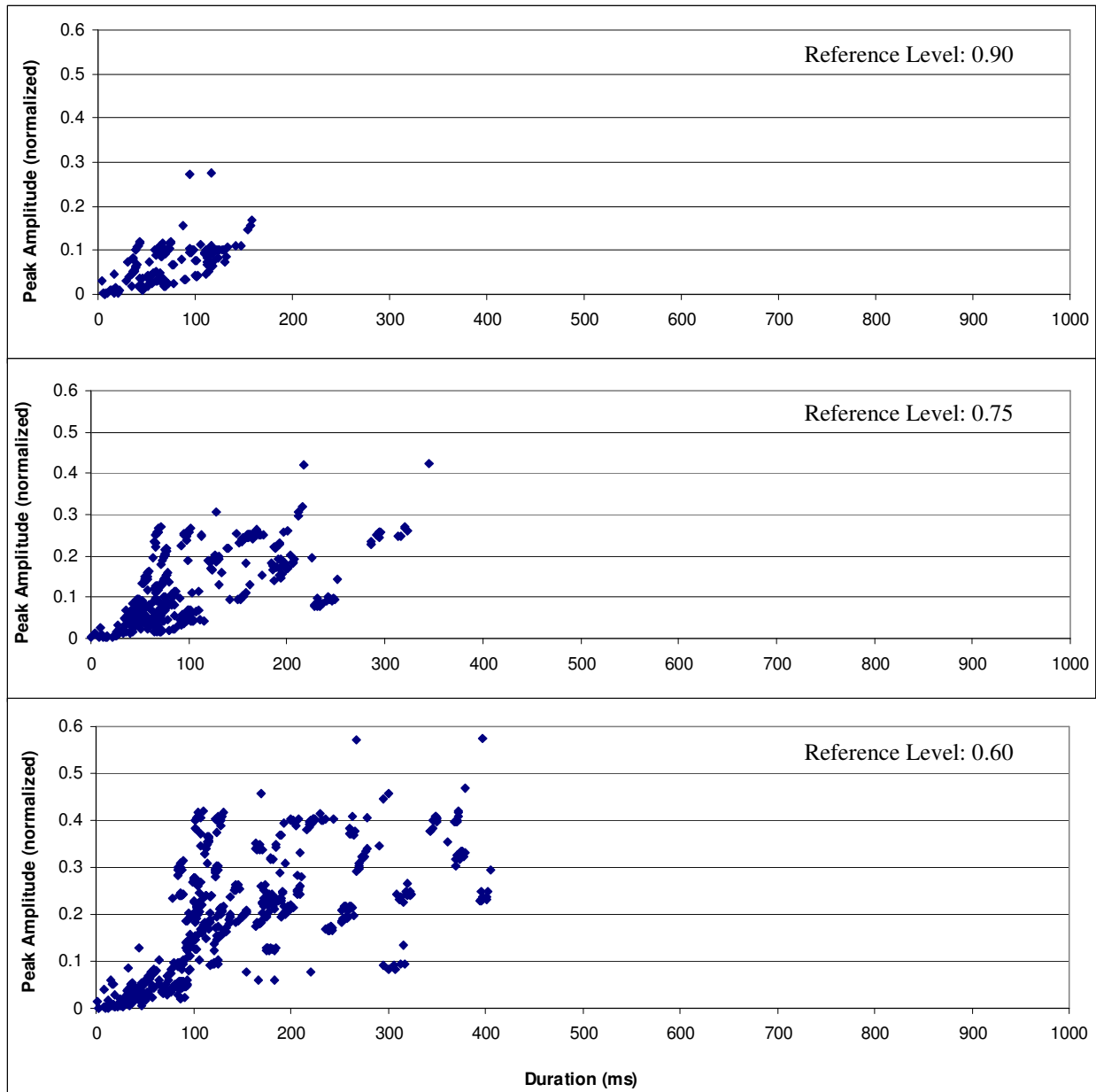
Figure B.1: Scatter plots for overstroke peak amplitude versus duration at 100.00 MHz
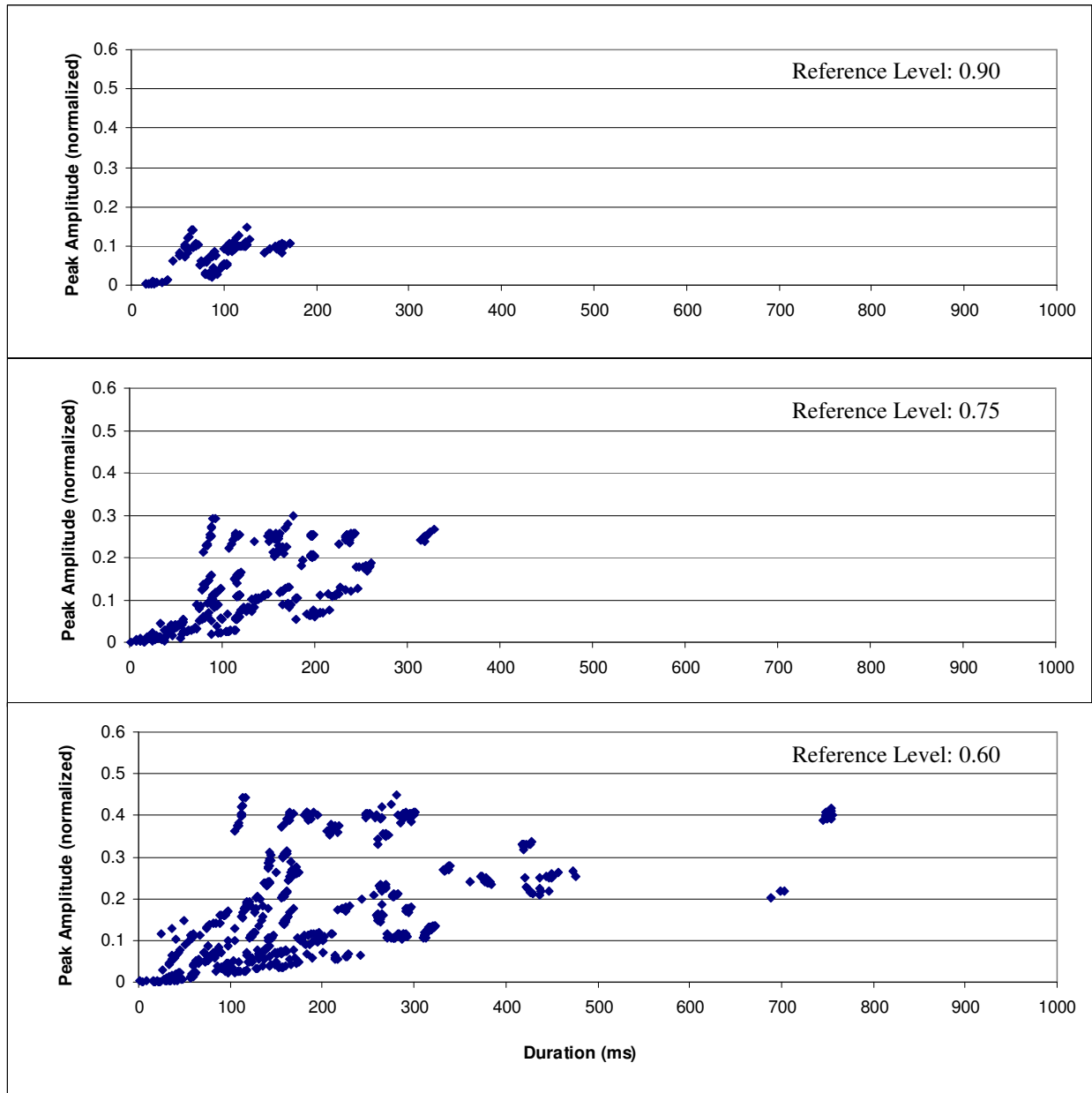
Figure B.2: Scatter plots for overstroke peak amplitude versus duration at 110.07 MHz
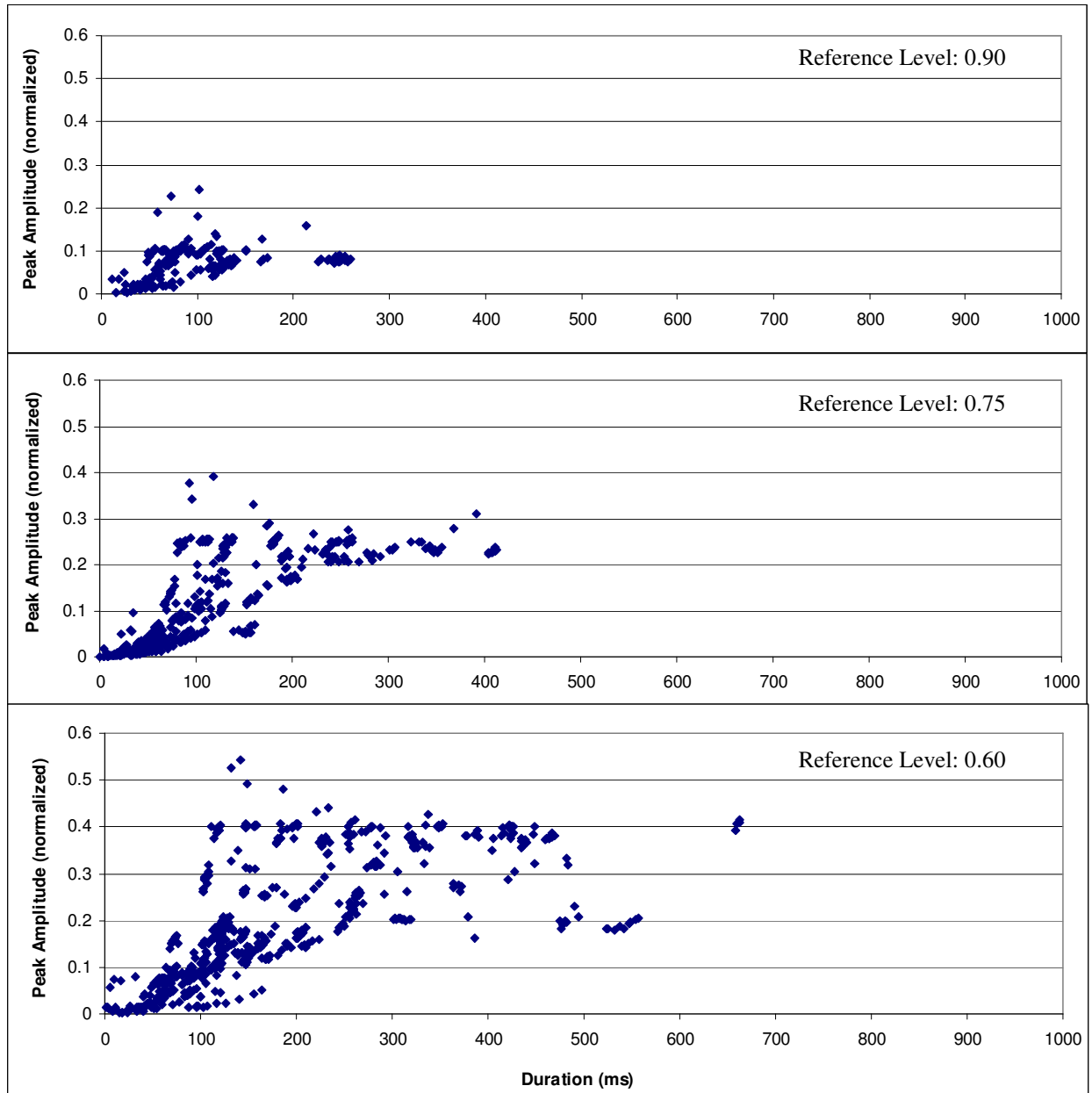
Figure B.3: Scatter plots for overstroke peak amplitude versus duration at 121.15 MHz
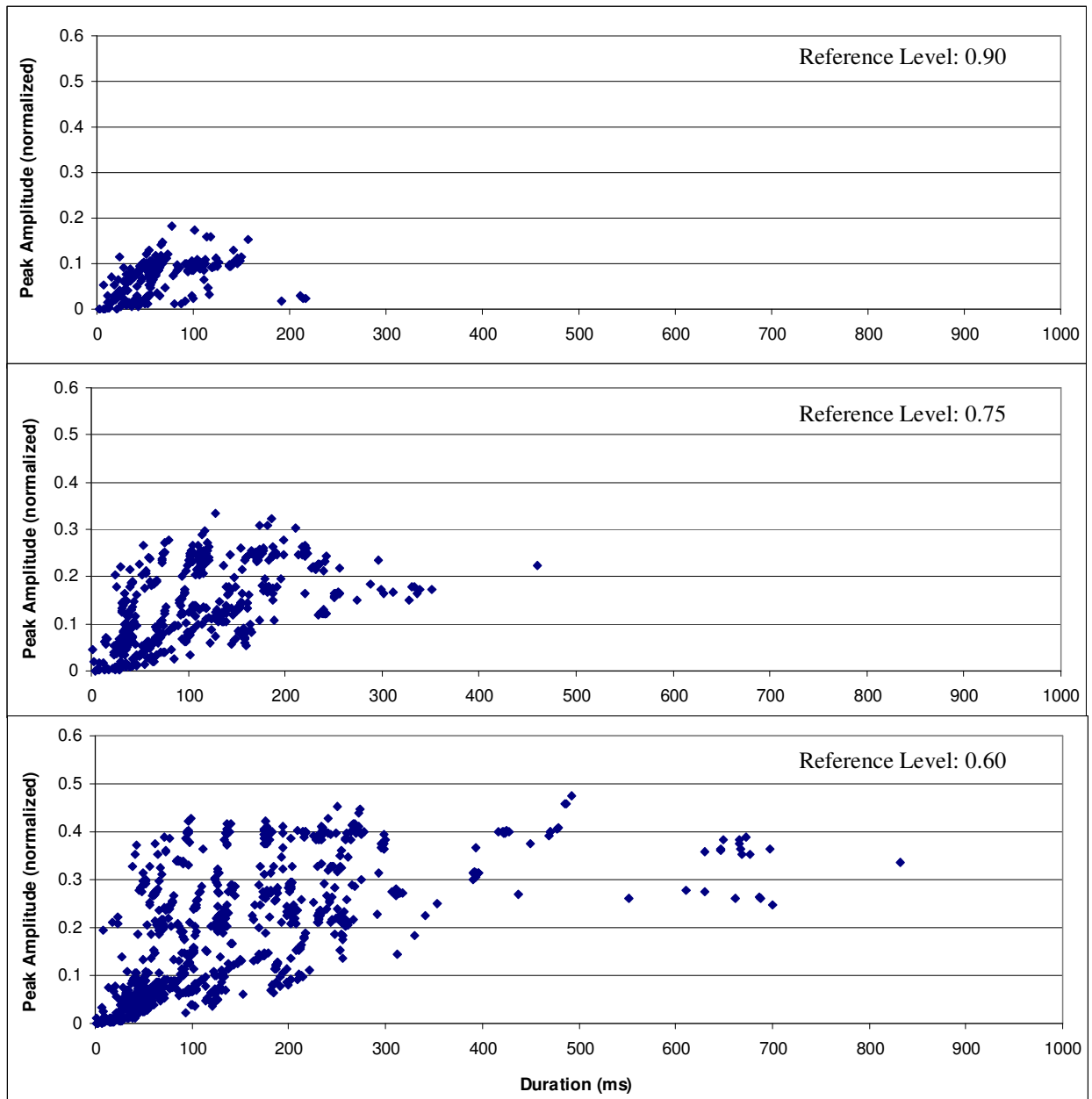
Figure B.4: Scatter plots for overstroke peak amplitude versus duration at 133.35 MHz
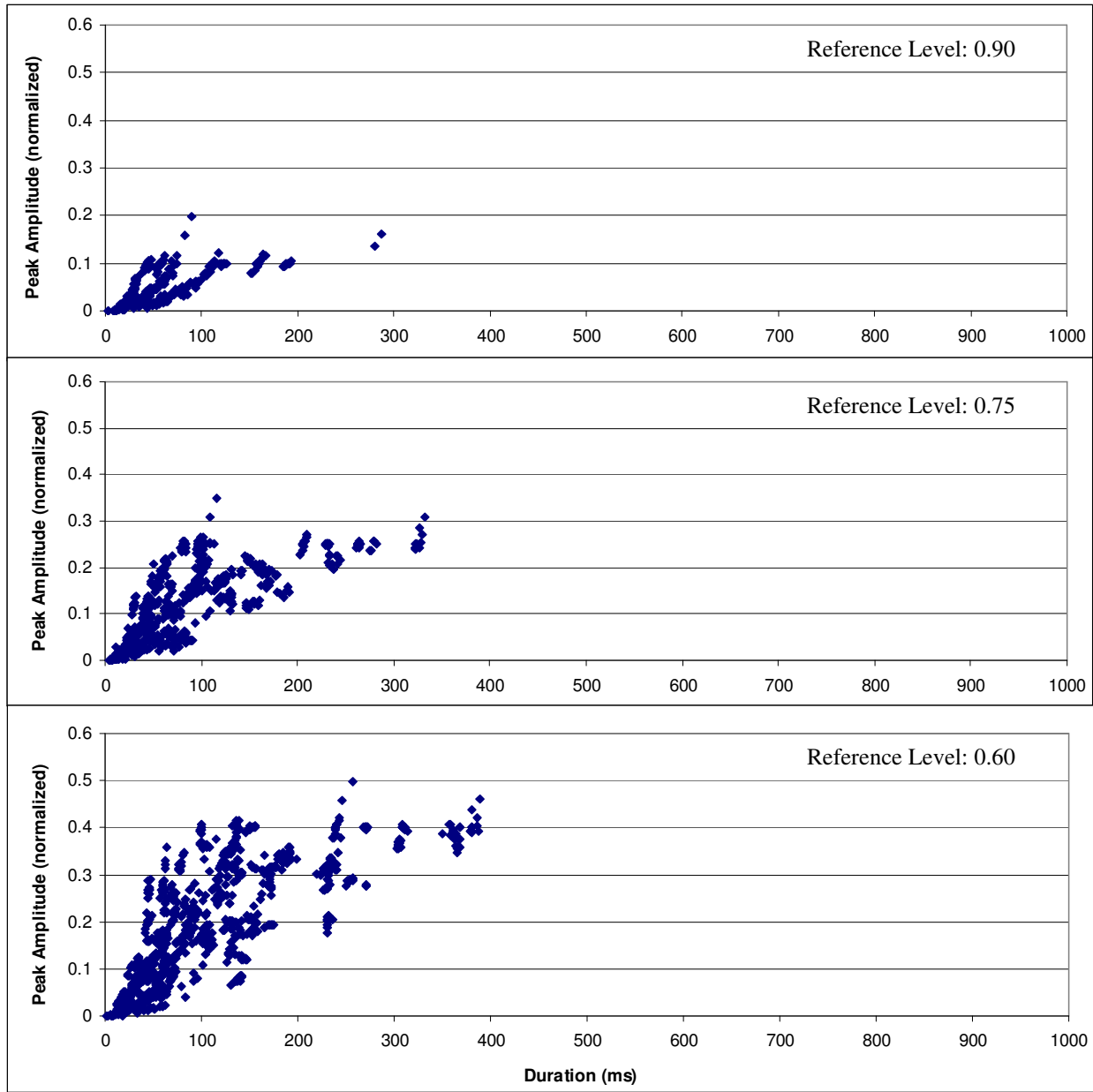
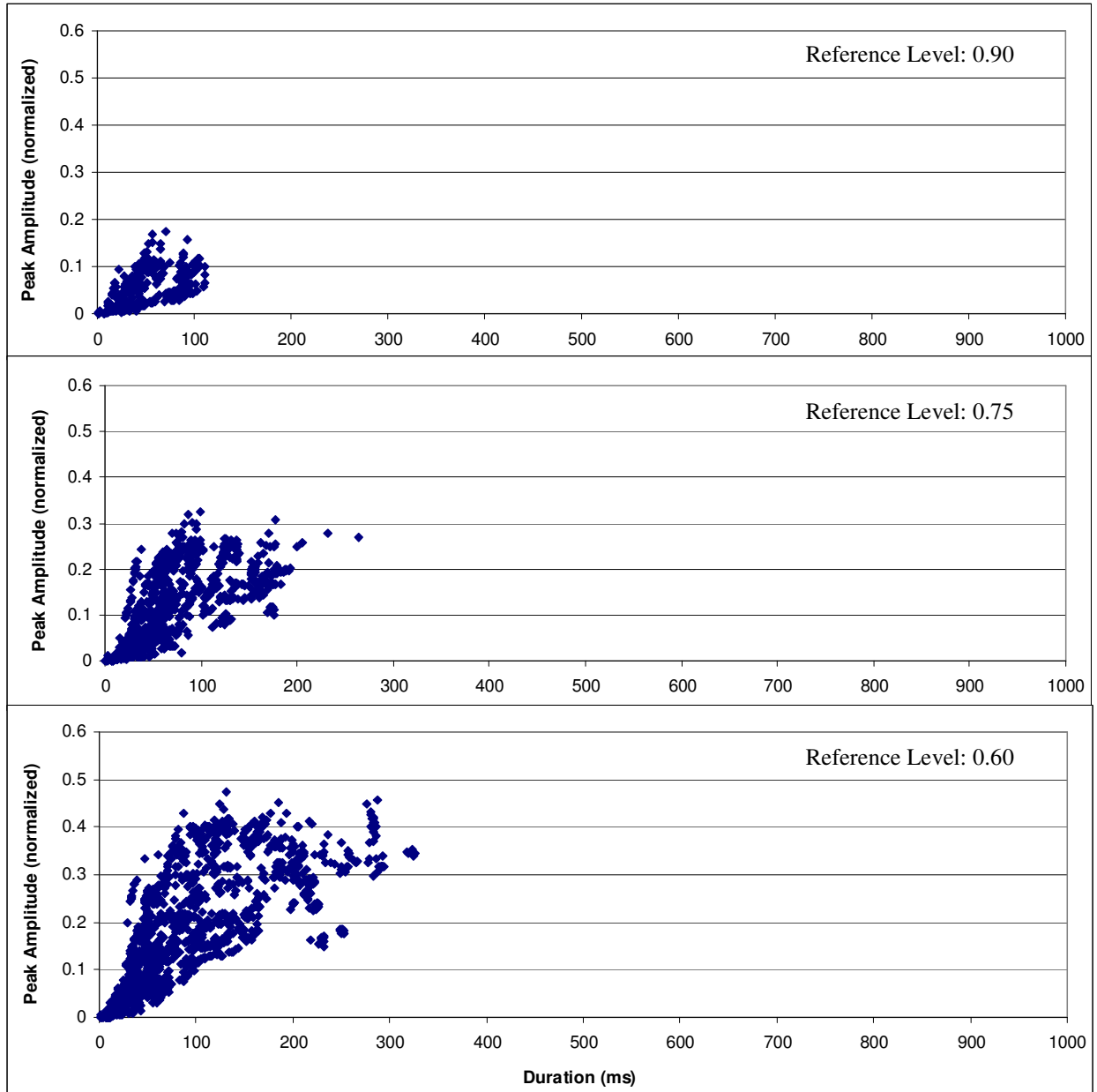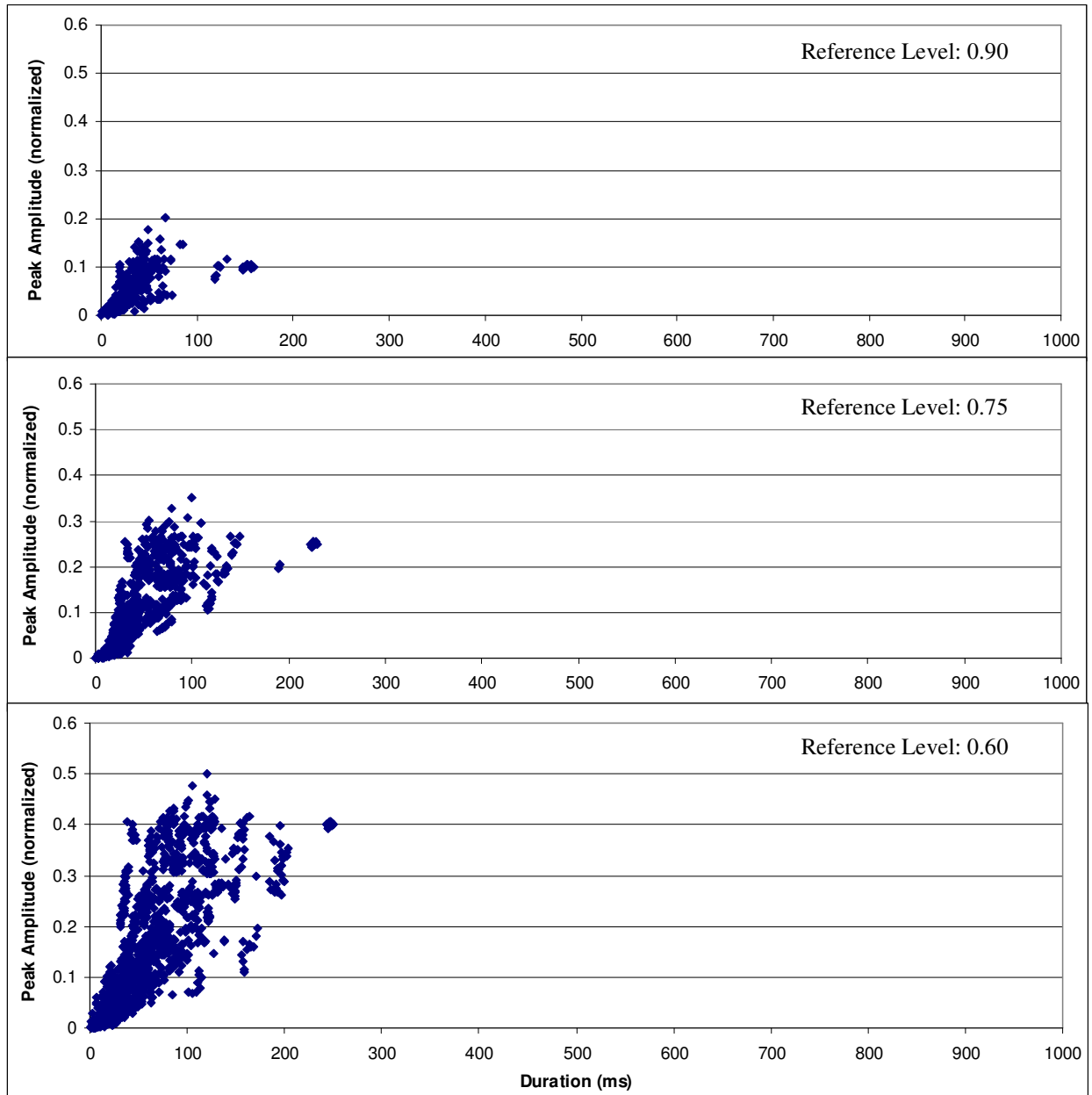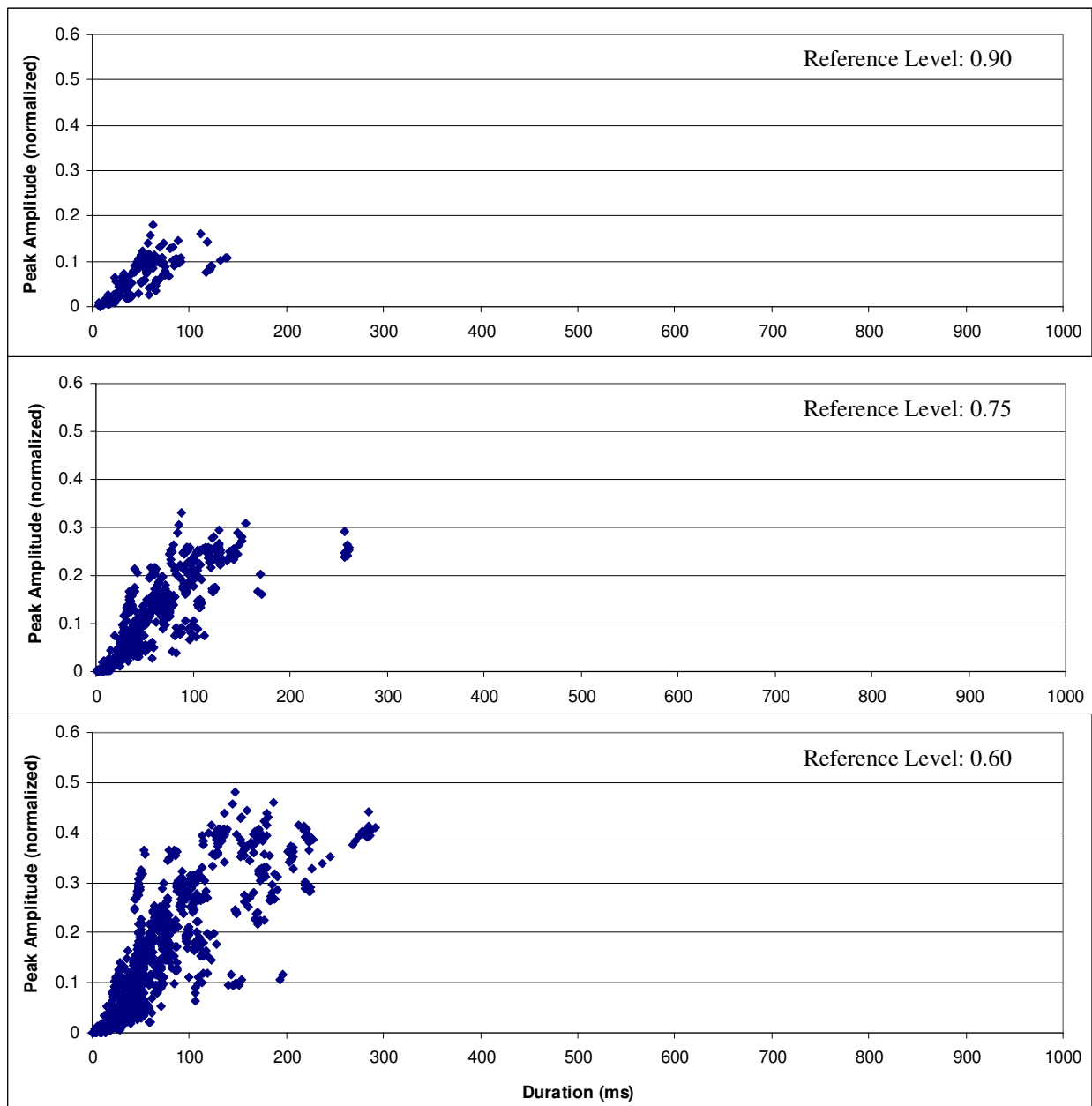Figure B.5: Scatter plots for overstroke peak amplitude versus duration at 146.78 MHz

Figure B.6: Scatter plots for overstroke peak amplitude versus duration at 161.56 MHz

Figure B.7: Scatter plots for overstroke peak amplitude versus duration at 177.83 MHz

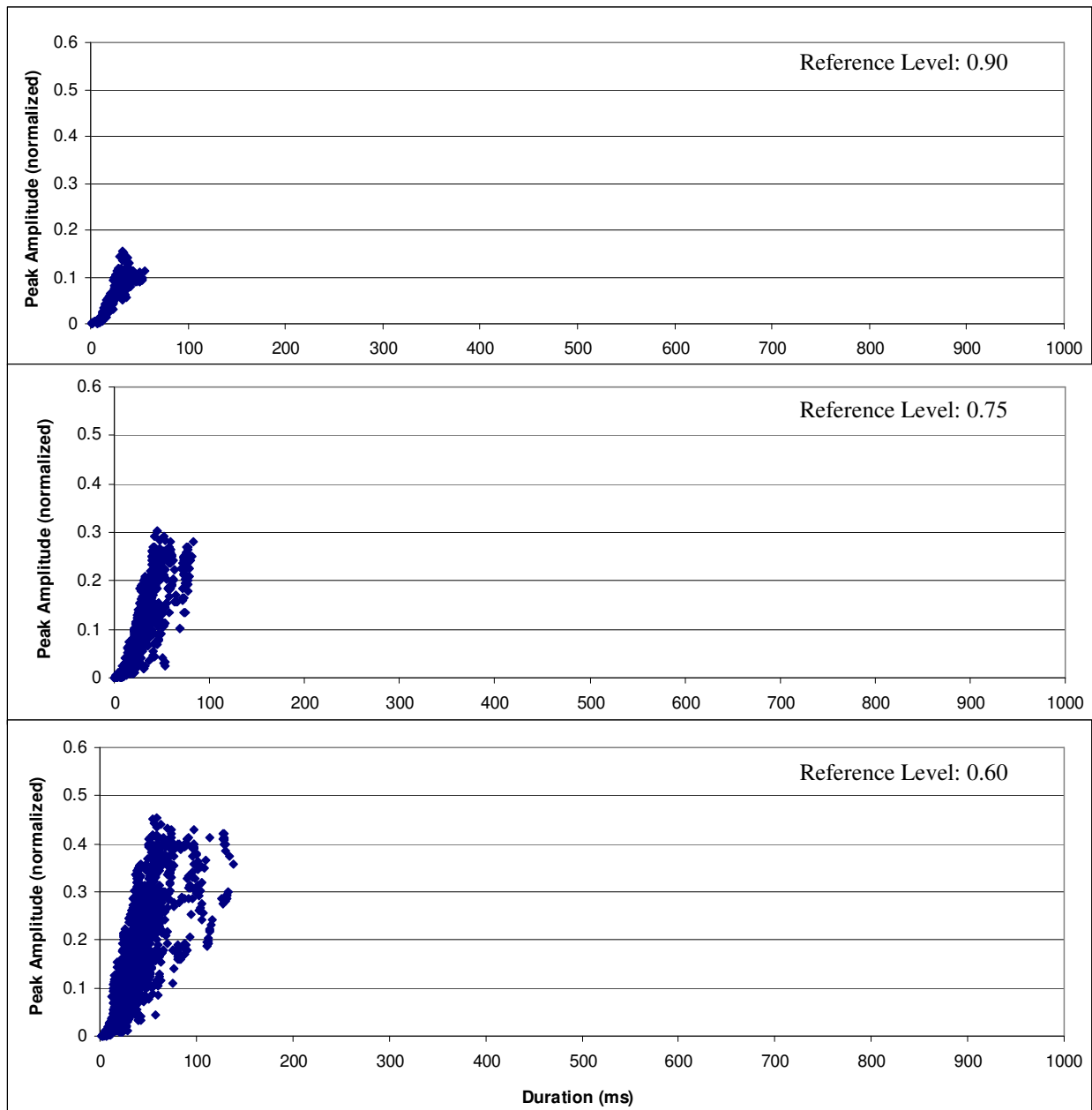Figure B.8: Scatter plots for overstroke peak amplitude versus duration at 195.73 MHz

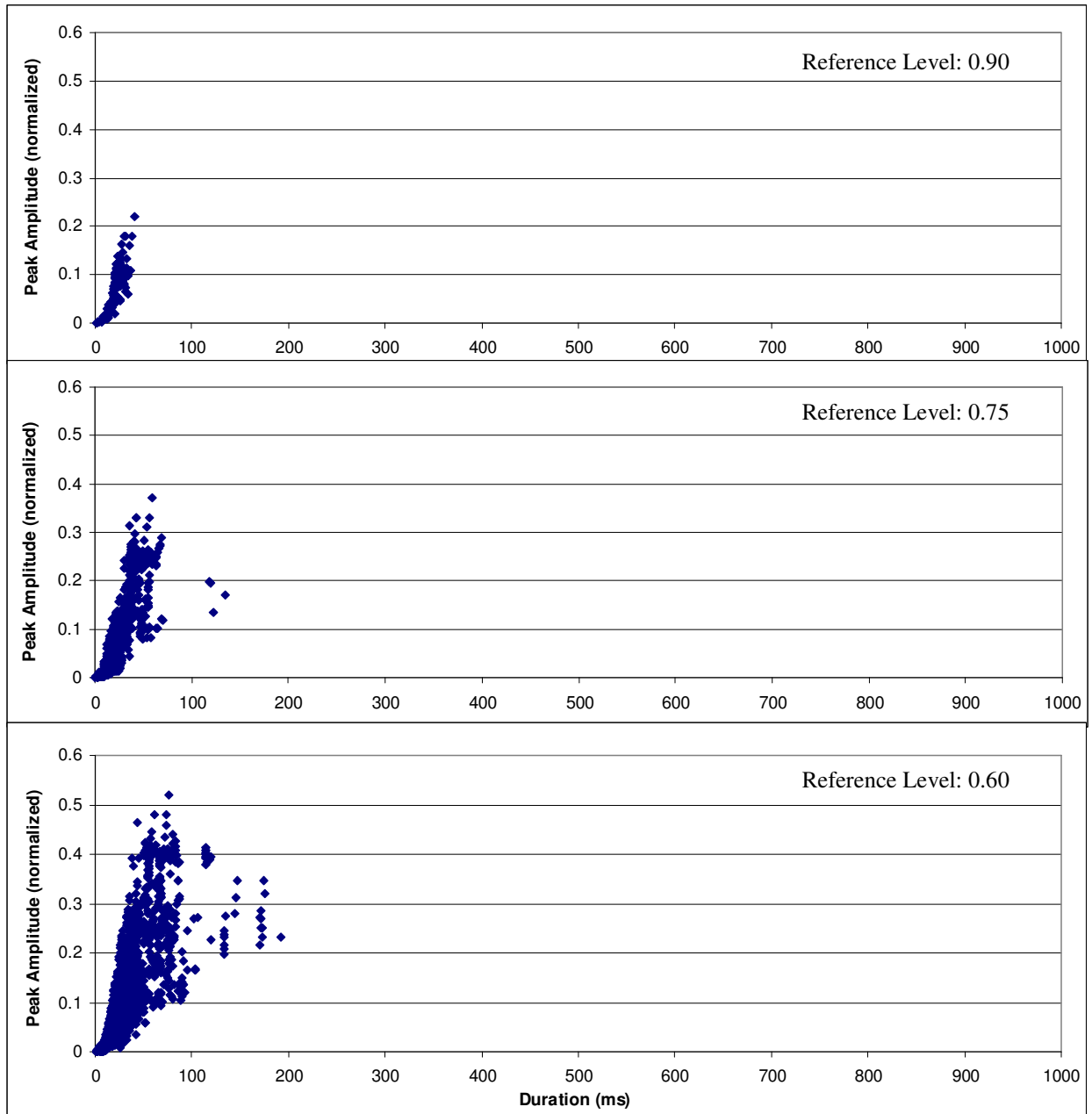Figure B.9: Scatter plots for overstroke peak amplitude versus duration at 316.23 MHz

Figure B.10: Scatter plots for overstroke peak amplitude versus duration at 383.12 MHz
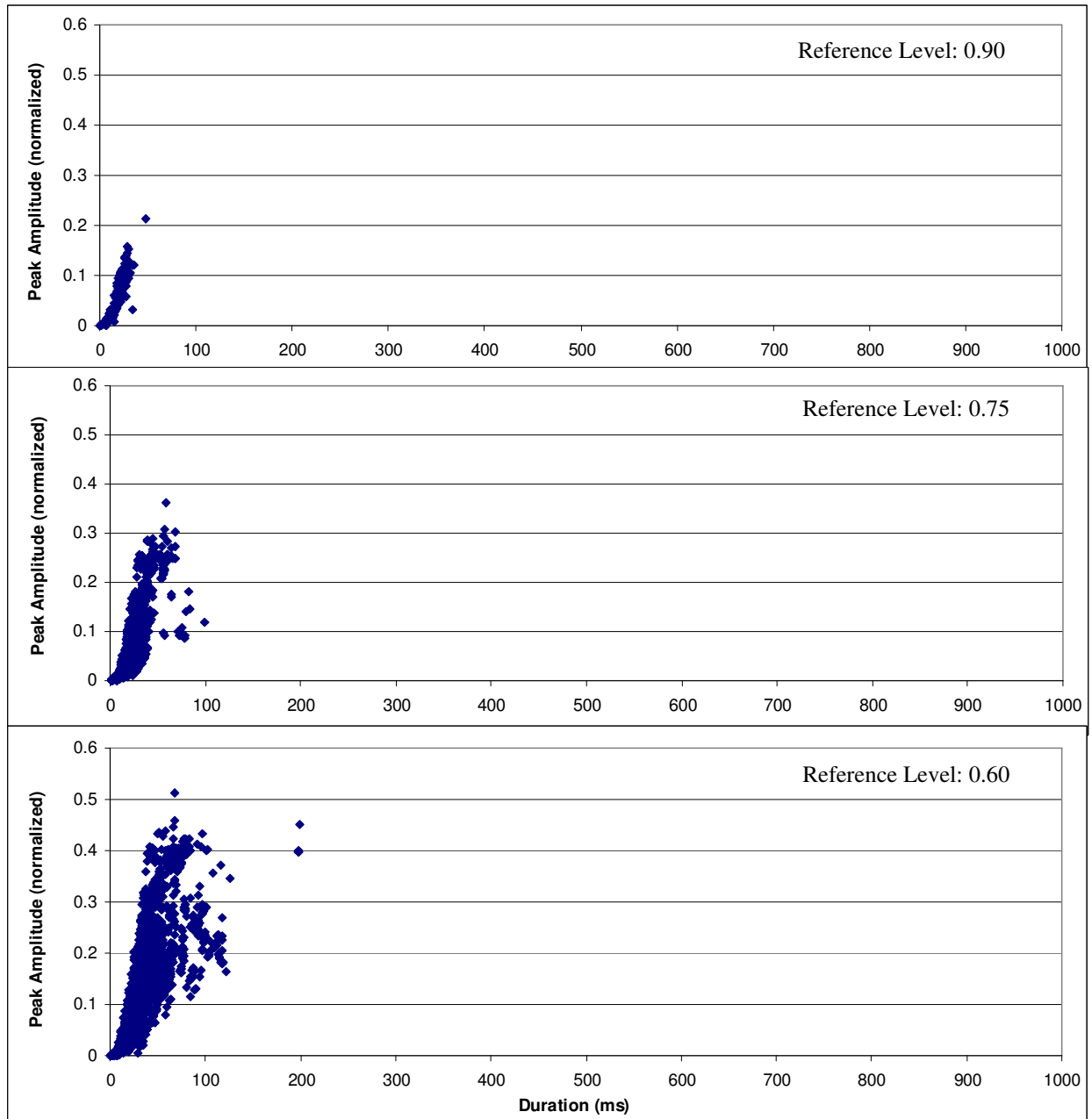
Figure B.11: Scatter plots for overstroke peak amplitude versus duration at 421.70 MHz
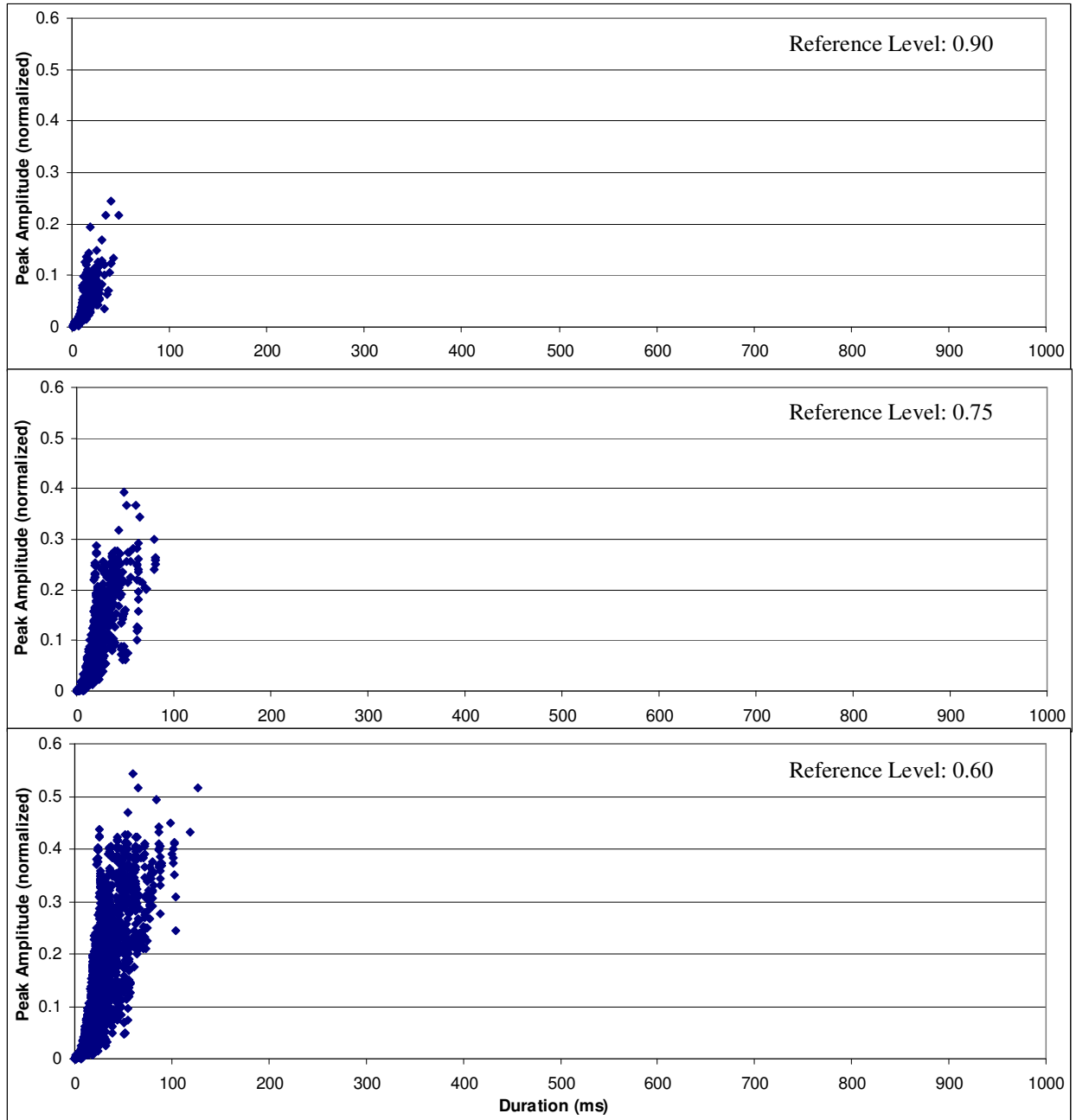
Figure B.12: Scatter plots for overstroke peak amplitude versus duration at 510.90 MHz
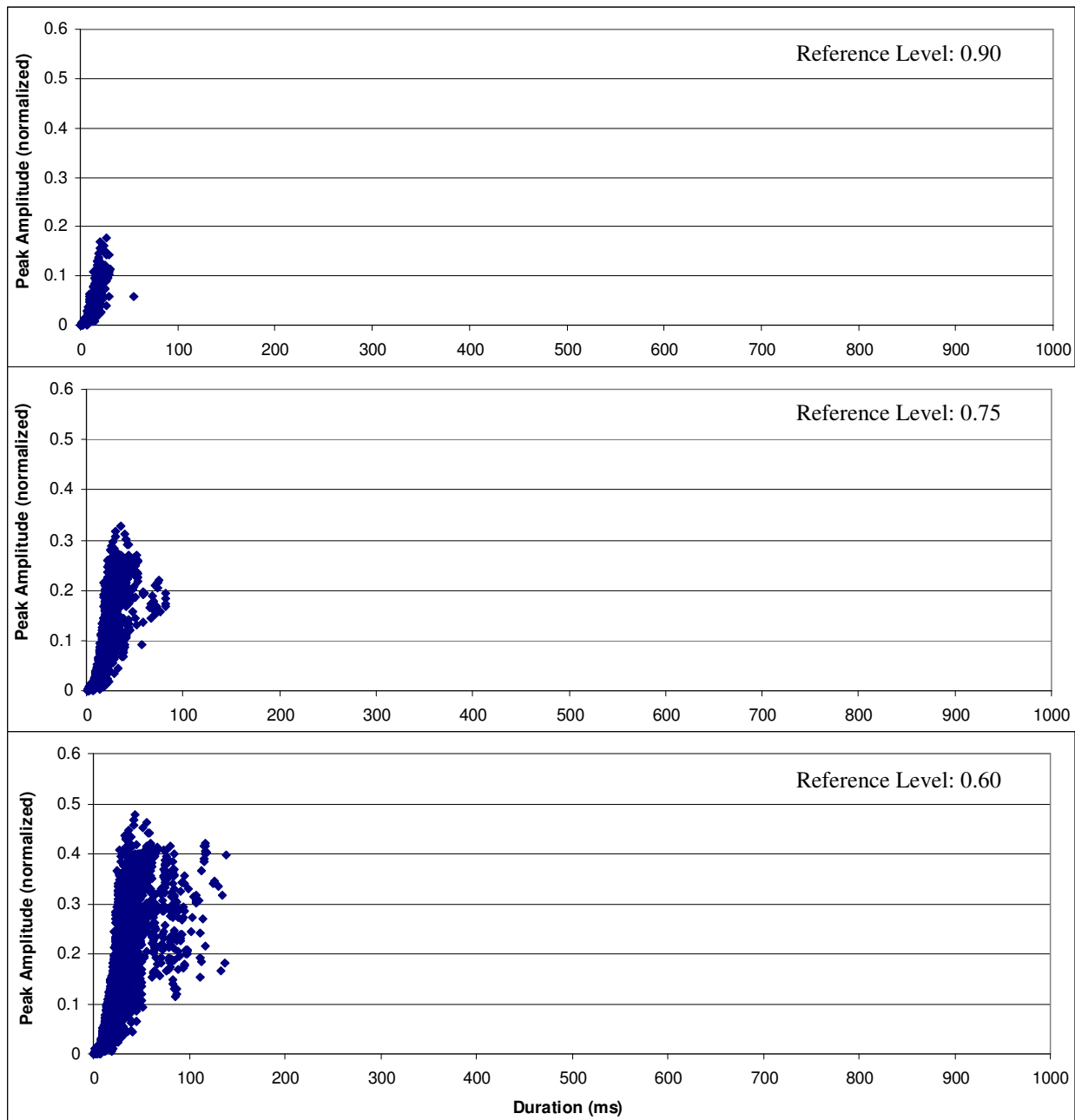
Figure B.13: Scatter plots for overstroke peak amplitude versus duration at 562.34 MHz
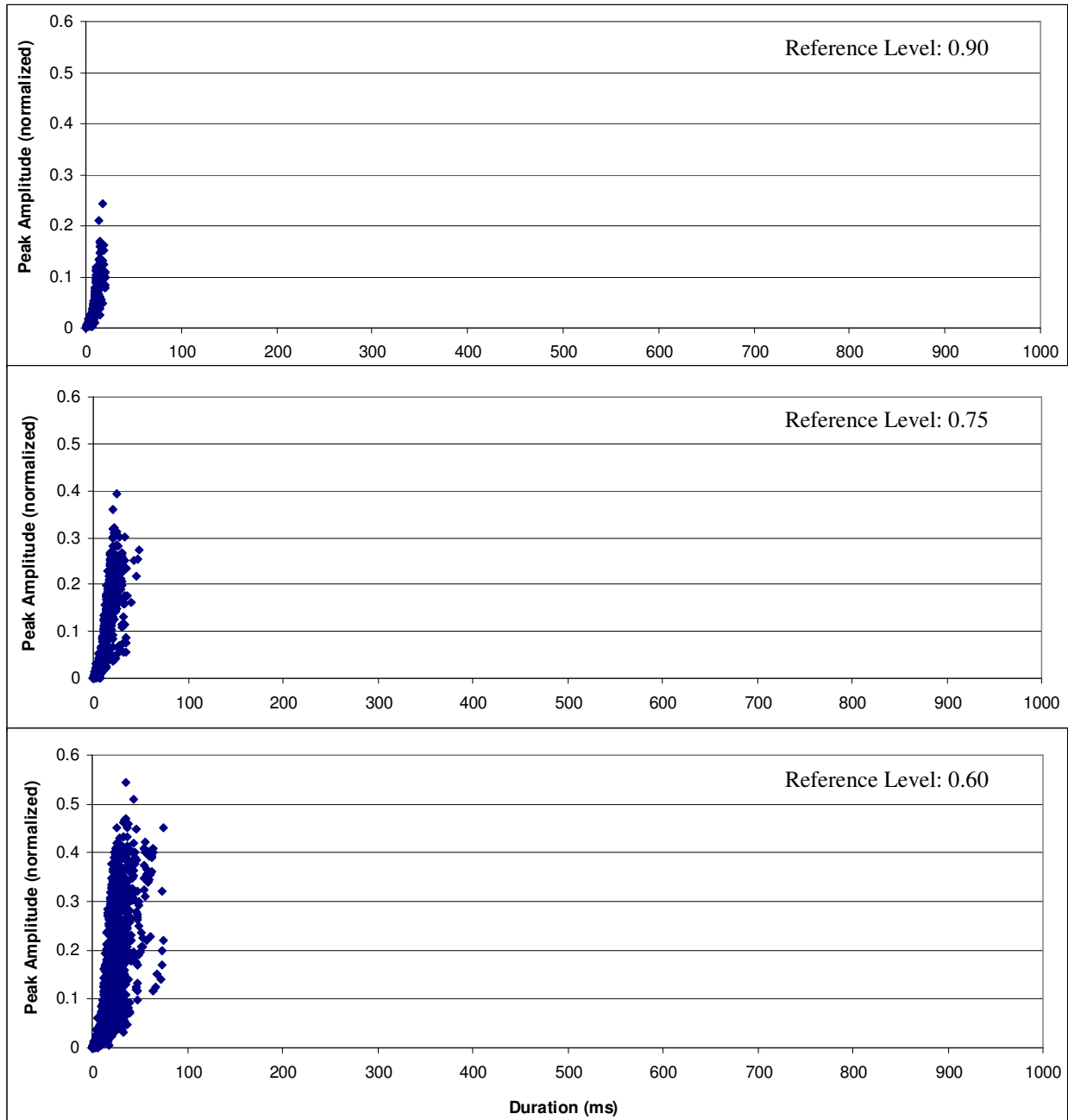
Figure B.14: Scatter plots for overstroke peak amplitude versus duration at 908.52 MHz

References

[1] Torres-Pomales, W.; et al: *Plan for the Characterization of HIRF Effects on a Fault-Tolerant Computer Communication System.* NASA-TM-2008-215306, May 2008.

[2] Torres-Pomales, W.; et al: *Design of Test Articles and Monitoring System for the Characterization of HIRF Effects on a Fault-Tolerant Computer Communication Systems.* NASA-TM-2008-215322, July 2008.

[3] Torres-Pomales, W.: *Characterization of HIRF Susceptibility Threshold for a Prototype Implementation of an Onboard Data Network.* NASA/TM-2012-217754, August 2012.

[4] Belcastro, Celeste M.: *Laboratory Test Methodology for Evaluating the Effects of Electromagnetic Disturbances on Fault-Tolerant Control Systems.* NASA Technical Memorandum 101665, November 1989.

[5] Fuller, Gerald L.: *Understanding HIRF – High Intensity Radiated Fields.* Aviation Communications, Inc., Leesburg, VA, 1995, p. 7-2.

[6] Hess, Richard: *Computing Platform Architectures for Robust Operation in the Presence of Lightning and Other Electromagnetic Threats.* 16th Digital Avionics Systems Conference (DASC), 1997.

[7] Ladbury, J.; Koepke, G.; Camell, D.: "Evaluation of the NASA Langley Research Center Mode-Stirred Chamber Facility", NIST Technical Note 1508, January 1999.

[8] Ely, Jay J.; Nguyen, Truong X.; and Scearce, Stephen A.: *The Influence of Modulated Signal Risetime in Flight Electronics Radiated Immunity Testing with Mode-Stirred Chamber.* NASA/TM-2000-209844, January 2000.

[9] Torres-Pomales, Wilfredo; et al: *ROBUS-2: A Fault-Tolerant Broadcast Communication System.* NASA/TM-2005-213540, March 2005.

[10] Torres-Pomales, Wilfredo; et al: *Design of the Protocol Processor for the ROBUS-2 Communication System.* NASA/TM-2005-213934, November 2005.

[11] Torres-Pomales, Wilfredo: *An Approach for the Assessment of System Upset Resilience.* NASA/TM, 2012, under review.

REPORT DOCUMENTATION PAGE

1. REPORT DATE *(DD-MM-YYYY)*	2. REPORT TYPE	3. DATES COVERED *(From - To)*
01-12-2012	Technical Memorandum	

4. TITLE AND SUBTITLE	5a. CONTRACT NUMBER
Analysis of the Radiated Field in an Electromagnetic Reverberation Chamber as an Upset-Inducing Stimulus for Digital Systems	
	5b. GRANT NUMBER
	5c. PROGRAM ELEMENT NUMBER

6. AUTHOR(S)	5d. PROJECT NUMBER
Torres-Pomales, Wilfredo	
	5e. TASK NUMBER
	5f. WORK UNIT NUMBER
	534723.02.02.07.30

7. PERFORMING ORGANIZATION NAME(S) AND ADDRESS(ES)	8. PERFORMING ORGANIZATION REPORT NUMBER
NASA Langley Research Center Hampton, VA 23681-2199	L-20204

9. SPONSORING/MONITORING AGENCY NAME(S) AND ADDRESS(ES)	10. SPONSOR/MONITOR'S ACRONYM(S)
National Aeronautics and Space Administration Washington, DC 20546-0001	NASA
	11. SPONSOR/MONITOR'S REPORT NUMBER(S)
	NASA/TM-2012-217789

12. DISTRIBUTION/AVAILABILITY STATEMENT
Unclassified - Unlimited
Subject Category 33
Availability: NASA CASI (443) 757-5802

13. SUPPLEMENTARY NOTES

14. ABSTRACT
Preliminary data analysis for a physical fault injection experiment of a digital system exposed to High Intensity Radiated Fields (HIRF) in an electromagnetic reverberation chamber suggests a direct causal relation between the time profile of the field strength amplitude in the chamber and the severity of observed effects at the outputs of the radiated system. This report presents an analysis of the field strength modulation induced by the movement of the field stirrers in the reverberation chamber. The analysis is framed as a characterization of the discrete features of the field strength waveform responsible for the faults experienced by a radiated digital system. The results presented here will serve as a basis to refine the approach for a detailed analysis of HIRF-induced upsets observed during the radiation experiment. This work offers a novel perspective into the use of an electromagnetic reverberation chamber to generate upset-inducing stimili for the study of fault effects in digital systems.

15. SUBJECT TERMS

Avionics; Data network; Electromagnetic field; Resilience; Safety

16. SECURITY CLASSIFICATION OF:			17. LIMITATION OF ABSTRACT	18. NUMBER OF PAGES	19a. NAME OF RESPONSIBLE PERSON
a. REPORT	b. ABSTRACT	c. THIS PAGE			STI Help Desk (email: help@sti.nasa.gov)
U	U	U	UU	76	19b. TELEPHONE NUMBER *(Include area code)* (443) 757-5802